

APPLICATIONS OF TOPOLOGICAL AND PERTURBATION METHODS TO
ANALYSIS OF PERIODIC SOLUTIONS IN DELAY DIFFERENTIAL EQUATIONS:
CLASSIFICATION OF SYMMETRIES, ASYMPTOTIC APPROXIMATION AND
STABILIZATION

by

Pavel Kravets



APPROVED BY SUPERVISORY COMMITTEE:

Dmitry Rachinskiy, Chair

Zalman Balanov

Wiesław Krawcewicz

Oleg Makarenkov

Copyright © 2019

Pavel Kravets

All rights reserved

To My Family

APPLICATIONS OF TOPOLOGICAL AND PERTURBATION METHODS TO
ANALYSIS OF PERIODIC SOLUTIONS IN DELAY DIFFERENTIAL EQUATIONS:
CLASSIFICATION OF SYMMETRIES, ASYMPTOTIC APPROXIMATION AND
STABILIZATION

by

PAVEL KRAVETC, MS

DISSERTATION

Presented to the Faculty of
The University of Texas at Dallas
in Partial Fulfillment
of the Requirements
for the Degree of

DOCTOR OF PHILOSOPHY IN
MATHEMATICS

THE UNIVERSITY OF TEXAS AT DALLAS

August 2019

ACKNOWLEDGMENTS

I would like to thank my advisor, Professor Dmitry Rachinskiy, who is not only an outstanding mentor but also a great friend. It would be impossible for me to obtain the results of my dissertation without his help. I wish to express my deepest appreciation to Professor Zalman Balanov and Professor Wiesław Krawcewicz, who patiently educated me throughout my PhD years and provided a significant contribution to my dissertation. This work could not be done without Professor Andrei Vladimirov who despite the distance was always eager to share his valuable ideas and insights. Also, I am very grateful that I had a chance to work with Professor Qingwen Hu who is an excellent teacher and collaborator. Finally, I would like to thank my family who always supports me in my pursuits, and all the friends I met during my PhD who made my life in Dallas happy and memorable.

May 2019

APPLICATIONS OF TOPOLOGICAL AND PERTURBATION METHODS TO
ANALYSIS OF PERIODIC SOLUTIONS IN DELAY DIFFERENTIAL EQUATIONS:
CLASSIFICATION OF SYMMETRIES, ASYMPTOTIC APPROXIMATION AND
STABILIZATION

Pavel Kravets, PhD
The University of Texas at Dallas, 2019

Supervising Professor: Dmitry Rachinskiy, Chair

The present dissertation contains several interconnected results regarding periodic solutions to delay differential equations (DDEs).

First of all, we formulate and prove a theorem that guarantees the occurrence of the Hopf bifurcation of relative periodic solutions from a relative equilibrium in a general $\Gamma \times S^1$ -equivariant system of functional differential equations (FDEs) using the method based on twisted equivariant degree with one free parameter. This theorem also allows to classify the symmetries of the relative periodic solutions. The theoretical result is illustrated through the series of examples including D_8 - and S_5 -symmetric coupling of identical mode-locked semiconductor lasers and D_8 -symmetric configuration of coupled electro-mechanical oscillators with hysteresis. The latter example shows the possibility to adapt the proposed method for the settings with weakened conditions on the smoothness.

Secondly, we perform the analysis of a rather broad class of slow-fast delayed models of population dynamics, that exhibit the behavior similar to the aforementioned mode-locked

semiconductor lasers. In particular, we study the mechanism of formation of pulsating periodic solutions as well as develop a nonlocal method for their asymptotic approximations. Finally, we develop a noninvasive delay feedback (Pyragas) control to make a neutrally stable periodic orbit of a Hamiltonian system exponentially stable. More specifically, we establish different sufficient conditions for the stabilization of orbits with small and large amplitudes. We also present a discussion of how these conditions agree with each other.

TABLE OF CONTENTS

ACKNOWLEDGMENTS	v
ABSTRACT	vi
LIST OF FIGURES	xi
LIST OF TABLES	xiii
CHAPTER 1 INTRODUCTION	1
1.1 Motivation, Background and Results	1
1.1.1 Delay differential equations	1
1.1.2 DDE models of laser devices	3
1.1.3 Symmetries	5
1.1.4 Hopf bifurcation in equivariant systems	8
1.1.5 Nonlocal asymptotic analysis of DDE population models	11
1.1.6 Stabilization of periodic solutions	14
1.2 Preliminaries	16
1.2.1 Notation	16
1.2.2 Equivariant Jargon	16
1.2.3 Topological Tools	17
1.2.4 Preisach Model	21
1.3 Outline of the Dissertation	22
CHAPTER 2 EQUIVARIANT DEGREE METHOD FOR ANALYSIS OF HOPF BI- FURCATION OF RELATIVE PERIODIC SOLUTIONS	25
2.1 $\Gamma \times S^1$ -Symmetric Systems of FDEs	25
2.1.1 Notation and statement of the problem	25
2.1.2 Symmetric bifurcation of relative equilibria from an equilibrium	27
2.1.3 Hopf bifurcation from a relative equilibrium	35
2.1.4 Proof of Theorem 2.1.14	39
2.2 DDE Model of a Symmetric Configuration of Passively Mode-Locked Semi- conductor Lasers	45
2.2.1 Mathematical model	45

2.2.2	D_n -configuration of identical semiconductor lasers	48
2.2.3	D_8 -configuration: bifurcation of symmetric relative equilibria	48
2.2.4	D_8 -configuration: bifurcation of relative periodic solutions	55
2.2.5	S_n -configuration of identical semiconductor lasers	67
2.2.6	S_5 -configuration: bifurcation of symmetric relative equilibria	71
2.2.7	S_5 -configuration: bifurcation of relative periodic solutions	75
2.3	System with Hysteresis Operators	85
CHAPTER 3 PERIODIC PULSATING DYNAMICS OF SLOW-FAST DELAYED SYSTEMS WITH A PERIOD CLOSE TO THE DELAY		91
3.1	Main prototype model	91
3.2	Bifurcation analysis	93
3.2.1	Bifurcations at the equilibrium with $A = 0$	93
3.2.2	Bifurcations at the positive equilibrium	95
3.2.3	The role of competition	100
3.3	Scaling with γ . Approximate solution	102
3.3.1	Separation of slow and fast stages	102
3.3.2	Area of the pulse	103
3.3.3	Pulse shape	107
3.3.4	Approximation for $\gamma_q \gg 1$	111
3.3.5	Pulses with unstable background	113
3.4	Conclusion	115
CHAPTER 4 SELECTIVE PYRAGAS CONTROL OF HAMILTONIAN SYSTEMS		118
4.1	Stabilization of small periodic orbits	119
4.1.1	Main statement	119
4.1.2	Example: Duffing oscillator	123
4.1.3	Example: Two coupled Duffing oscillators	124
4.2	Stabilization of large periodic orbits	126
4.2.1	Main statement	126
4.2.2	Example	133

4.3	How do stability conditions for small and large cycles agree?	134
4.4	Conclusions	135
APPENDIX A TWISTED SUBGROUPS		137
A.1	Notations used for the twisted subgroups of $\mathcal{K} := D_8 \times S^1$	137
A.2	Notations used for the twisted subgroups of $\mathcal{K} := D_8 \times \{1\} \times S^1$	138
A.3	Notations used for the twisted subgroups of $\mathcal{K} := \mathbb{Z}_8^{t_l} \times S^1, l = 1, 2, 3$	138
A.4	Notations used for the twisted subgroups of $\mathcal{K} := D_8^d \times S^1$	139
A.5	Notations used for selected twisted subgroups of $\mathcal{H} = S_5 \times S^1$	140
A.6	Notations used for selected twisted subgroups of $\mathcal{K} := \mathbb{Z}_5^{t_l} \times S^1$	140
A.7	Notations used for selected twisted subgroups of $\mathcal{K} := D_6^d \times S^1$	141
A.8	Notations used for selected twisted subgroups of $\mathcal{K} := S_4 \times S^1$	141
APPENDIX B COMPUTATION OF THE NORMAL FORM		142
REFERENCES		146
BIOGRAPHICAL SKETCH		159
CURRICULUM VITAE		

LIST OF FIGURES

2.1 S^1 -equivariant electro-mechanical oscillator. 86

2.2 D_8 -symmetric mechanical coupling of 8 identical oscillators (2.122). 87

3.1 Solution of (3.9). The horizontal axis is ω . Every second intersection of the straight line $\eta = \omega/\gamma$ and the function $\eta = -\kappa g_0^* \tan(\omega T)/\alpha$ satisfies the condition (3.10). Here $\gamma = 100, T = 1$ 95

3.2 Panel (a): Spectra of the zero equilibrium for $g_0 = 3.7497$ and $g_0 = 3.7528$. Numerical values of the eigenvalues are shown by circles; lines are obtained from (3.13). Filled circles correspond to unstable eigenvalues. Panel (b): Spectrum of the positive equilibrium of system (3.1)–(3.3) after the first Hopf bifurcation ($g_0 = 3.75003$), i.e., exactly one pair of complex conjugate eigenvalues cross the imaginary axis from left to right. Solid line defined by (3.19) carries the weak spectrum; dashed line (3.18) carries the strong spectrum. Parameters are as follows: $\gamma = 1000, \gamma_q = 10, \kappa = 0.6, \mu = 0.5, \alpha = 1, q_0 = 2.5, \beta = 1, s = 1, k = 0.7, T = 1$ 96

3.3 Bifurcation diagrams obtained with numerical package DDE-BIFTOOL for system (3.1)–(3.3) for two parameter sets. The vertical axis shows the maximum of the A -component of a periodic solution. The PE line corresponds to the positive equilibrium. Branches H_1 – H_7 (H_1 – H_5 on panel (b)) correspond to the periodic solutions born via Hopf bifurcations on the positive equilibrium. Stable branches are shown by solid lines and unstable branches are shown by dashed lines. The branch H_1 on panel (b) exhibits slight hysteresis near the threshold g_0^* . All the branches connect to the branch of the positive equilibrium at Hopf bifurcation points at both ends. 97

3.4 Time trace of the periodic solution of system (3.1)–(3.3). Panel (a): the A -component; Panel (b): the G -component (solid) and the Q -component (dashed). The A -component is almost zero between the pulses. The Q -component almost reaches the equilibrium value $q_0/\beta = 2.5$ between the pulses of the A -component and drops almost to zero during the pulse because $\gamma_q = 10$ is relatively large. The G -component drops fast during the pulse and then recovers slowly between the pulses. The period of the solution is close to the delay $T = 1$. The following parameters were used: $\gamma = 400, \gamma_q = 10, \kappa = 0.6, g_0 = 4, q_0 = 2.5, \alpha = 1, \beta = 1, s = 1, k = 0.7, T = 1$. The threshold value is $g_0^* = 3.75$ 98

3.5 The phase and amplitude of the Fourier coefficients for the A -component $A(t/\tau) = \sum_{n=1}^{\infty} A_n \cos(2\pi n t/\tau + \phi_n)$ of the periodic solution along the branch H_1 shown in Figure 3.3a where τ is the period of solution. 98

3.6 Spectrum of the positive equilibrium and curves (3.19), (3.18) for $g_0 = 3.7509$ (panel (a)) and $g_0 = 3.7648$ (panel(b)). Notation and other parameters are the same as in Figure 3.2b. 99

3.7	Panel (a) shows the solution of (3.32). Panel (b) shows the dependence of the integral of A -component of system (3.1)–(3.3) over one period on γ . The power law fit is shown by the solid line. The horizontal asymptote $p = \hat{p}_*$ coincides with analytic value p_* shown on panel (a). Here $\kappa = 0.6$, $\mu = 0.5$, $\alpha = 1$, $q_0 = 1$, $\beta = 1$, $s = 2$, $k = 1$, $T = 1$, $\gamma_q = 100$, $g_0 = 2.6$	106
3.8	A typical spectrum of equations (3.40) and (3.41) when condition (3.42) is satisfied. The notation is the same as in Figure 3.2.	109
3.9	We adopt the shooting method in order to find parameter c in equation (3.35). The three curves correspond to three trajectories starting near the equilibrium $p_* = 1.486$ with different values of c . Other parameters are $G_b = 2.906$, $Q_b = 2.5$, $k = 0.7$, $\gamma_q = 10$, $s = 1$, $\mu = 0.5$, $\kappa = 0.6$. Note that with this set of parameters equation (3.35) has an additional positive equilibrium $p_{\dagger} = 0.146$ which is an asymptotically stable focus. For one exact value $c = c_*$ ($0.537 < c_* < 0.538$) there exists a heteroclinic orbit of (3.35) connecting the equilibria p_* and 0. This orbit describes the shape of the pulse, and the value c_* defines the period of the pulsating solution. For $c < c_*$, trajectories starting near p_* belong to the basin of attraction of the positive equilibrium p_{\dagger} ; for $c > c_*$, such trajectories become negative and go to negative infinity.	111
3.10	Black solid curve represents a single pulse of the A -component of the periodic pulsating solution of system (3.1)–(3.3) with the following parameters: $g_0 = 4$, $k = 0.7$, $q_0 = 2.5$, $s = 1$, $T = 1$, $\alpha = 1$, $\beta = 1$, $\gamma = 400$, $\kappa = 0.6$, $\mu = 0.5$, $\gamma_q = 100$. Dashed curve is the derivative of the heteroclinic solution of (3.35) satisfying the boundary conditions (3.36). This solution exists for $c = 0.3736$ which was found using the shooting method, see Figure 3.9. gray solid curve is the derivative of the heteroclinic solution of the approximating (3.43) connecting the saddle equilibrium point $\tilde{p} = 1.6968$ and the stable focus at zero. This curve oscillates near the focus and fails to approximate the leading edge of the pulse (left tail).	112
4.1	Panel (A): Bifurcation diagram of the controlled system for $\tilde{\kappa} = (-0.02, 0.012)$. Points A , B and C on the branch correspond to the delays $\tau_A = 7.1857$, $\tau_B = 5.9655$ and $\tau_C = 5.1761$, respectively. Panel (B): The same branch of periodic solutions has different stability properties for $\hat{\kappa} = (-0.02, 0.02)$. Stable and unstable solutions are shown by solid and dashed lines, respectively.	134
4.2	Control parameters plane. Conditions (4.18) of Theorem 4.1.1 are satisfied within the sector O_1OO_2 . Sectors A_1OA_2 , B_1OB_2 , C_1OC_2 are defined by conditions (4.23) and (4.24) for the periodic solutions indicated by points A , B and C , respectively, on Figure 4.1. Point $\tilde{\kappa} = (-0.02, 0.012)$ corresponds to control parameters used in Figure 4.1(A); parameters $\hat{\kappa} = (-0.02, 0.02)$ are used in Figure 4.1(B).	135

LIST OF TABLES

2.1	Maximal twisted orbit types in each isotypical component of the D_8 -representation V	49
2.2	Number of unstable eigenvalues in each isotypical component for the equilibrium $\mathcal{O}(\alpha)$	54
2.3	Maximal twisted orbit types in the isotypical components of the $D_8 \times \{1\}$ -representation V^c	61
2.4	Maximal twisted orbit types in the isotypical components of the $\mathbb{Z}_8^{t_1} \times \{1\}$ -representation V^c	63
2.5	Maximal twisted orbit types in the isotypical components of the D_8^d -representation V^c	64
2.6	Number of unstable eigenvalues for each isotypical component along the branch of the relative equilibrium with (D_8) symmetry (see item (i) on page 53)	68
2.7	Number of unstable eigenvalues for each isotypical component along the branch of the relative equilibrium with $(\mathbb{Z}_8^{t_1})$ symmetry (see item (ii) on page 53)	68
2.8	Number of unstable eigenvalues for each isotypical component along the branch of the relative equilibrium with $(\mathbb{Z}_8^{t_2})$ symmetry (see item (iii) on page 53)	69
2.9	Number of unstable eigenvalues for each isotypical component along the branch of the relative equilibrium with $(\mathbb{Z}_8^{t_3})$ symmetry (see item (iv) on page 53)	69
2.10	Number of unstable eigenvalues for each isotypical component along the branch of the relative equilibrium with (D_8^d) symmetry (see item (vi) on page 53)	70
2.11	Maximal twisted orbit types in each isotypical component of the S_5 -representation V	72
2.12	Number of unstable eigenvalues in each isotypical component for the equilibrium $\mathcal{O}(\alpha)$	76
2.13	Maximal twisted orbit types in the isotypical components of the $S_5 \times \{1\}$ -representation V^c	78
2.14	Maximal twisted orbit types in the isotypical components of the $\mathbb{Z}_5^{t_1}$ -representation V^c	79
2.15	Maximal twisted orbit types in the isotypical components of the D_6^d -representation V^c	80
2.16	Maximal twisted orbit types in the isotypical components of the S_4 -representation V^c	81

2.17	Number of unstable eigenvalues for each isotypical component along the branch of the relative equilibrium with (S_5) symmetry	82
2.18	Number of unstable eigenvalues for each isotypical component along the branch of the relative equilibrium with $(\mathbb{Z}_5^{t_1})$ symmetry	82
2.19	Number of unstable eigenvalues for each isotypical component along the branch of the relative equilibrium with (D_6^d) symmetry	83
2.20	Number of unstable eigenvalues for each isotypical component along the branch of the relative equilibrium with (S_4) symmetry	83
2.21	Number of unstable eigenvalues in each isotypical component along the branch of the relative equilibrium with (D_8) symmetry.	90
3.1	Comparison of the asymptotic and numerical values of δ_n, ω_n for the following set of parameters: $\gamma = 600, \gamma_q = 40, \kappa = 0.6, \mu = 0.5, \alpha = 1, q_0 = 2.5, \beta = 1, s = 1, k = 0.7, T = 1$	100

CHAPTER 1

INTRODUCTION

1.1 Motivation, Background and Results

1.1.1 Delay differential equations

When modeling a certain phenomenon using ordinary differential equations (ODEs), one has to assume that the future state of the system is determined entirely by its present and not by its past states. However, in many applications, this assumption leads to inaccurate or even meaningless models. Of course, the importance of hereditary effects in modeling was known for a long time, still they were often ignored, and were not thoroughly studied until the 20th century. One of the reasons is that they are indubitably difficult to consider. Explicit inclusion of the past states in an ODE turns it into a completely different kind of differential equations called *delay differential equations* (DDEs). Even a single delayed term in the form $x(t - \tau)$ where τ is a real constant, complicates the system immensely as in order to find a future state of the system one has to specify initial data on the whole interval $[-\tau, 0]$ rather than just one value $x(0)$. Thus, similarly to partial differential equations, the phase space of DDEs is infinitely dimensional. DDEs belong to a more general class of equations called *functional differential equations* (FDEs). Along with equations with discrete delays, this class also includes equations where delay is distributed (integro-differential equations), time- or state-dependent, and systems with nonsmooth memory effects such as hysteresis.

In the 20th century the theory of DDEs underwent a remarkable development. Early results on the general theory of linear systems and stability can be found in the works by Myshkis [108], Bellman and Danshkin [20], Bellman and Cooke [19] and Krasovskii [85]. These results laid the foundation for the profound work by Hale [58] who formulated the modern analytic and geometric theory of FDEs. Rapid development of the theory facilitated

new insights in different fields of applications such as population dynamics [89], laser dynamics [109, 68, 93, 156], engineering [91], fluid dynamics [151, 152], economics [18, 23], road traffic [134, 115, 114], climate science [78], etc. A good treatise of DDEs with applications can be found in [39, 140].

Dependence on the past is essential for models of population dynamics. In his groundbreaking works [161, 162], Volterra proposed the first predator-prey model with distributed delay and since then DDEs have been extensively adopted for models of population dynamics. In the predator-prey model, the hereditary terms are present in the form of convolution of the state variables with functions weighting the contribution of the past predation. Other models include discrete delays representing time of the growth to maturity of a corresponding species or its gestation period (see [133, 89] and references therein). Delay is generally believed to be a destabilizing factor in population dynamics [102]. Increasing delay can lead to oscillations where the system with zero or small delay exhibits a globally stable equilibrium.

Control engineering constitutes another prominent example where DDEs arise naturally. In particular, delays almost inevitably appear in any system with feedback control because there is always a time lag between the measurement and the signal received by the controller. This inherent feature becomes a huge problem in systems where the immediate response is required. For example, the delay in the control of an aircraft is responsible for causing the so-called pilot-induced oscillations [9], i.e., sustained or uncontrollable oscillations resulting from efforts of the pilot to control the aircraft¹, which can end tragically. In contrast, for some cases time-delayed feedback control is actually beneficial. For instance, time-delayed control strategy in a container crane can significantly reduce the sway of a heavy cargo [61, 99, 100, 101]. Furthermore, a state-of-the-art application of DDEs for control is Pyragas method for noninvasive stabilization of unstable periodic solutions to ordinary differential systems [127, 44, 66]. This technique uses a delayed feedback control proportional to the

¹As defined by MIL-HDBK-1797A.

difference $x(t - T) - x(t)$ with T close to the period of the targeted periodic solution $x_*(t)$. Notably, Pyragas control method can be used to suppress or enhance synchrony in ensembles of globally coupled oscillators [132]. Another example where the time delay is an intrinsic part of the system is a high-speed milling where, through the variation of the chip thickness, a varying cutting force acts on the tool and this difference in the force depends on the past vibrations of the tool [145, 53, 142, 144, 36].

1.1.2 DDE models of laser devices

DDEs are extensively used in laser dynamics. In particular, a model of a mode-locked semiconductor laser is directly related to the present work. Mode locking of lasers [60] is used to produce periodic sequences of short optical pulses at high repetition rates, which are suitable for various applications including material processing, medical imaging, telecommunications [74, 76], optical sampling, microwave photonics, optical division multiplexing [35], and two-photon imaging [90]. The optical spectrum of a mode-locked laser consists of a set of equally spaced narrow lines corresponding to the longitudinal cavity modes characterized by fixed phase relationships between them². There are two main methods to produce mode-locked optical pulses, active and passive mode-locking, and also a combination thereof called hybrid mode-locking. In particular, a passively mode-locked laser is a self-oscillating system which does not require the use of an external radio frequency modulation³. In the classical theory of a mode-locked laser due to Haus [59], a slow evolution of the shape of the optical pulse circulating in the cavity is described by a complex parabolic master equation of Ginzburg-Landau type. The solution describing a solitary pulse is explicit and has a hyperbolic secant profile. However, the Haus master equation is derived under the assumption

²Achieving such phase relationships can be, at least qualitatively, viewed as a problem of synchronization of many nonlinear coupled oscillators with frequencies close to multiples of a fundamental frequency.

³Passive mode-locking is commonly achieved by including a saturable absorber section into the laser cavity.

of small gain and loss per cavity round trip. An alternative multi-rate functional differential model, which is free from this approximation, has been obtained from the traveling wave model in the case of a ring geometry of the laser cavity in [156]. Under further natural assumptions, such as the Lorentzian profile of the spectral filtering element, the functional differential model simplifies to the delay differential system

$$\begin{aligned}
\dot{g}(t) &= g_0 - \gamma_g g(t) - \frac{1}{E_g} e^{-q(t)} (e^{g(t)} - 1) |a(t)|^2, \\
\dot{q}(t) &= q_0 - \gamma_q q(t) - \frac{1}{E_q} (1 - e^{-q(t)}) |a(t)|^2, \\
\dot{a}(t) &= -\gamma a(t) + \gamma \sqrt{\kappa} \exp \left[\frac{(1 - i\eta_g)g(t - T) - (1 - i\eta_q)q(t - T)}{2} \right] a(t - T),
\end{aligned} \tag{1.1}$$

where the complex-valued variable a is the electric field envelope at the entrance of the absorber section; $|a|^2$ represents the optical power (which is proportional to the density of photons); the real-valued variables q and g represent saturable integral losses and gain, respectively (q and g are functions of the density of the electric charge carriers in the absorber section and the active section of the laser, respectively); the constants γ_g and γ_q are the carrier density relaxation rates in the gain and absorbing sections; E_g and E_q are the saturation energies in the these sections; the ratio $s = E_g/E_q$ is important for laser dynamics. Delay T stands for the cold cavity round-trip time, and $\sqrt{\kappa}$ is the linear nonresonant attenuation factor per pass. The parameter g_0 is proportional to the pump current, which is the physical control parameter. Finally, $\gamma \gg 1$ is the parameter of the Lorentzian profile of spectral filtering. The details of the system are explained in [159, 156, 157]. This delay differential model is suitable for describing mode-locking in a laser with large gain and losses, that is the situation typical of semiconductor laser devices⁴. At the same time, the model is amenable to analytical and numerical bifurcation analysis [155, 112, 160, 7, 8, 5, 71, 120, 56, 124].

⁴In the limit of small gain and losses per cavity round trip, one recovers the Haus hyperbolic secant pulse shape in the delay differential model.

Furthermore, this delay differential system has been extensively applied to analyze instabilities [121, 113] and hysteresis [57, 123] in mode-locked lasers, optically injected lasers [131, 4], hybrid mode locking [6], noise reduction [72], resonance to delayed feedback [3], and Fourier domain mode locking [139].

1.1.3 Symmetries

One can easily notice that system (1.1) has an equilibrium $(\gamma_g/g_0, \gamma_q/q_0, 0)$ corresponding to the regime when the laser doesn't emit any light. Moreover, using the ansatz

$$g(t) = g^*, \quad q(t) = q^*, \quad a(t) = e^{i\omega t} a^* \quad (1.2)$$

where g^* , q^* , ω and $a^* \neq 0$ are some real constants, leads to the system of four algebraic (i.e., nondifferential) equations including the following transcendental equation for ω :

$$-\frac{\omega}{\gamma} = \tan\left(\omega T + \frac{\eta_g g^* - \eta_q q^*}{2}\right). \quad (1.3)$$

Solving these equations yields infinitely many periodic solutions to (1.1) in the form (1.2) called *relative equilibria*, or, in the context of laser dynamics, *continuous wave (cw) solutions*. The structure (1.2) of relative equilibria allows to study such orbits in a fashion similar to usual steady-state solutions and, thus, simplifies the analysis.

In fact, the existence of relative equilibria (1.2) is due to the intrinsic symmetry of system (1.1). In general, symmetries in dynamical systems manifest themselves through the notion of *equivariance*, i.e., if G is a (compact Lie) group and a vector space V is G -representation, then a vector field $f : V \rightarrow V$ is called *G -equivariant* if for every $\gamma \in G$ and $x \in V$, $f(\gamma x) = \gamma f(x)$. Thus, one can easily check that the right-hand side of system (1.1) is equivariant with respect to the circle group $S^1 \simeq \{z \in \mathbb{C} : |z| = 1\}$ where S^1 acts trivially on g and q , and by complex multiplication on a . In fact, this transformation corresponds to the phase shift of the complex valued electric field. Thus, commonly the rate equations of

semiconductor laser systems are S^1 -symmetric (see, for example, [165, 46, 40]). Moreover, they often naturally include delays associated with propagating of light through optical fibers, the classical example being the Lang-Kabayashi model where the light is re-injected into the laser cavity by an external mirror [93, 166].

The existence of relative equilibria is a common feature of dynamical systems that exhibit continuous symmetries. Strictly speaking, if $f : V \rightarrow V$ is equivariant with respect to a Lie group G and $G(x)$ is the group orbit of some $x \in V$, such that $G(x)$ is invariant under the flow of f , then $G(x)$ is called a relative equilibrium of f , i.e., relative equilibrium is an equilibrium modulo the group action. The latter definition justifies the naming.

Similarly, a counterpart of a periodic solution is a *relative periodic solution*. In particular, in S^1 -symmetric systems, the S^1 -equivariant Hopf bifurcation is responsible for branching of relative periodic solutions from a relative equilibrium. This scenario is analogous to the classical Hopf bifurcation of periodic solutions from an equilibrium state in generic systems (without symmetry). Note that S^1 -equivariant Hopf bifurcation is essentially a torus bifurcation, if one disregards the S^1 -equivariance of the system.

An example of relative periodic solution in system (1.1) is the so-called mode-locking regime when the laser emits a periodic sequence of light pulses with the period close to the cold cavity round trip time T . A typical bifurcation scenario associated with formation of this regime is the Hopf bifurcation of a relative equilibrium (1.2) from the “laser off” equilibrium followed by the S^1 -equivariant Hopf bifurcation of a relative periodic solution from the relative equilibrium with the increase of the bifurcation parameter (pump current g_0). As the bifurcation parameter increases further, the relative periodic solution continuously transforms to acquire a pulsating shape. This transformation is simultaneous with a sequence of secondary Hopf bifurcations from the equilibrium and relative equilibrium solutions.

In recent years a lot of attention has been drawn to the dynamics of multiple identical laser devices coupled together [122, 94, 73, 154]. Combining lasers in an array can be used to

amplify the output power and substantially improve the characteristics of the output beam by synchronizing the frequencies of the individual lasers [22]. In particular, an array of n nearest-neighbor coupled systems (1.1) was recently considered in [125]. Forming a regular n -gon, such a configuration naturally respects the dihedral symmetry D_n , i.e., the group generated by two transformations on the indices: shifting by 1 and flipping. Combining it with the S^1 symmetry of each individual laser (1.1), one can see that the whole system is $D_n \times S^1$ -equivariant. Generally speaking, any Γ -symmetric configuration of n identical lasers (1.1) is $\Gamma \times S^1$ -equivariant where Γ is some subgroup of the permutation group S_n which represents the *all-to-all* coupled array. This system also undergoes a bifurcation scenario similar to the case of a single laser, however, the details are by far more intricate. First of all, multiple branches of relative equilibria (resp. relative periodic solutions) bifurcate simultaneously. Secondly, these solutions have an additional structure due to the symmetry of the coupling. For example, there is a fully synchronized relative equilibrium when all the lasers in unison repeat the same dynamics, i.e., its symmetry corresponds to $\Gamma \times S^1$. However, there also can be a τ -periodic relative equilibrium with $\mathbb{Z}_n \times S^1$ symmetry such that $x_i(t) = x_{i-1}(t - \tau/n)$ for all $i \in \mathbb{Z}_n$ where $x_i(t)$ is the state of i -th laser. Therefore, each branch of relative equilibria/relative periodic solutions is born via Hopf bifurcation with a prescribed symmetric properties (*spatio-temporal symmetries*) represented by a subgroup H of the group $\Gamma \times S^1$ for relative equilibria and the group $\Gamma \times S^1 \times S^1$ for relative periodic solutions, respectively, where the second copy of S^1 is associated with time periodicity. This naturally leads to the problem of classification of relative equilibria (relative periodic solutions) according to their spatio-temporal symmetries.

Applications of relative equilibrium states and relative periodic orbits are not limited to equations of laser dynamics. Actually, quite the opposite, such trajectories are abundant in a wide variety of models. Many examples are found in conservative systems related to rigid bodies [98], deformable bodies [31], molecular vibrations [82], celestial mechanics [27, 104]

and vortex theory [116] (see also [163, 50] and references therein). Moreover, in addition to S^1 -symmetry, many of such systems also respect a finite group Γ of spatial symmetries such as, for example, a symmetry of coupling of atoms in molecules [107]. Other examples include dynamics of a deformable body in an ideal irrotational fluid [163], symmetric celestial motions, for instance, central configurations [105, 117], etc. On the other hand, there is a long list of applications described by *nonconservative* systems of ODEs admitting relative equilibria/relative periodic solutions (see, for example, [50], where the Couette-Taylor experiment is discussed in detail).

1.1.4 Hopf bifurcation in equivariant systems

The analysis of Hopf bifurcation of periodic solutions from an equilibrium state (both in nonequivariant and equivariant setting) has been done by many authors using different techniques. Essentially, this analysis includes two main problems: (i) finding the bifurcation points and establishing the occurrence of the bifurcation (in equivariant setting, this problem additionally requires to describe symmetric properties of the bifurcating solutions), and (ii) analysis of stability properties of the bifurcating solutions. Assuming that the system satisfies several regularity and genericity conditions, the main method to study both problems is based on the normal form classification combined with Center Manifold Theorem/averaging method/Lyapunov-Schmidt reduction (see, for example, [96, 51, 50] and references therein). If a (nonequivariant) setting is not regular/generic enough and the stability of bifurcating solutions is not questioned (only problem (i) above), then alternative methods (rooted in homotopy theory) are available: Fuller index [49, 34, 33], (nonequivariant) framed bordism theory [1], parameter functionalization method combined with the Leray-Schauder degree [83], to mention a few.

During the last twenty years the equivariant degree theory emerged in nonlinear analysis (see monographs [16, 70] and surveys [69, 12]). The equivariant degree being the main topological tool used in Chapter 2, is an instrument that allows “counting” orbits of solutions to

symmetric equations in the same way as the usual Brouwer degree does, but according to their symmetry properties. In particular, the equivariant degree theory has all the attributes allowing its application in nonsmooth (differentiability at selected points versus differentiability in a neighborhood) and nongeneric (multiple resonant eigenvalues of linearizations) equivariant settings related to equivariant dynamical systems having, in general, infinite dimensional phase spaces with lack of linear structure (hysteretic nonlinearities). We refer to [16, 69, 12, 70, 13, 63] and references therein for the equivariant degree treatment of the (symmetric) Hopf bifurcation in different environments (see also [81]).

In his pioneering work [88], M. Krupa proposed a general method for analysis of the bifurcation of relative periodic solutions from a relative equilibrium for systems of ordinary differential equations (in general, nonhamiltonian). This elegant method reduces the problem to the analysis of a generic (nonsymmetric) Hopf bifurcation for an explicit differential equation on the normal slice to the relative equilibrium. An extension of Krupa's method to the case of more complicated spatial symmetries (including $\Gamma \times S^1$) has been developed in [150] (see also [32] for the moving frames method and [92] for the hierarchy of secondary bifurcations). Krupa's method allows one both to locate Hopf bifurcation of relative periodic solution, and to establish stability of it, for S^1 -equivariant (or $\Gamma \times S^1$ -equivariant, if an additional group Γ of spatial symmetries is involved) ordinary differential systems using the analysis of the normal forms of the bifurcation for the system on the normal slice.

Also, Krupa's method can be adapted for analysis of *smooth* FDEs, for which the center manifold reduction can be performed. To be more specific, a smooth FDE with continuous symmetry G admits near a relative equilibrium a finite-dimensional G -invariant center-unstable manifold which is at least C^1 -smooth. In addition, the FDE restricted to this manifold turns out to be a G -equivariant ODE with the same spectral properties of the

linearization at the relative equilibrium as the original FDE, so that Krupa’s result can be applied.⁵

The main goal of Chapter 2 is to adapt the equivariant degree method for analysis of the Hopf bifurcation of relative periodic solutions (for both ODEs and FDEs). More specifically, we obtain conditions for the occurrence of the Hopf bifurcation of relative periodic solutions (together with their complete symmetric classification) from a relative equilibrium in general $\Gamma \times S^1$ -equivariant systems of FDEs using the method based on twisted equivariant degree with one free parameter. For a systematic exposition of this method, we refer to [16, 12, 15, 14, 70, 69, 87]. As is well-known, this method is insensitive to violations of genericity assumptions [43, 63] (these assumptions include the simplicity of purely imaginary eigenvalues at the bifurcation point, transversality of the eigenvalue crossing, and nonresonance conditions). Our results are formulated for a general FDE system, which respects a group $\Gamma \times S^1$ of spatial symmetries with an arbitrary finite group Γ , and include the method of classification of symmetries of the relative periodic solutions based on the linearization of the problem.

Using the example of the D_8 -symmetric configuration of laser systems (1.1), we demonstrate with details how one applies the equivariant degree method in a specific setting with a relatively large symmetry group in order to extract the information about symmetries of solutions. Our results complement some findings obtained in [125]. In the second example we extend the application of the same method to S_5 -symmetric configuration of lasers (1.1).

The laser model is smooth and as such could be alternatively treated using the center manifold reduction method, which could also provide further information on dynamics.

In order to reveal the full potential of our result, we present the third example, where the equivariant degree method is applied to a system of symmetrically coupled hysteretic

⁵This scheme is known to the author from personal communication with several colleagues. However, we are not aware of any published work detailing this method.

oscillators. Systems with hysteresis can be viewed as a natural class of *nonsmooth* FDEs [84]. In [13], the equivariant degree was applied to the analysis of symmetric Hopf bifurcations in symmetric networks of electrical circuits with magnetic hysteresis modeled by the so-called Preisach operator (see [103]). In the present work, we set up a model of an electro-mechanical motor system in which the electrical component gives rise to hysteresis while the mechanical component is a source of spacial S^1 -symmetry. The hysteresis operator is differentiable with the zero derivative at the (relative) equilibrium but it is not differentiable in any neighborhood of the (relative) equilibrium (this situation is typical to the systems with hysteresis). To the best of our knowledge, bifurcations of relative periodic solutions in the presence of hysteresis have not been studied until now.

1.1.5 Nonlocal asymptotic analysis of DDE population models

The method proposed in Chapter 2 can be categorized as local. More specifically, one can employ it to determine the dynamics only locally near the bifurcation points. In particular, the main result of Chapter 2 is used to locate those points and to predict the birth of (relative) periodic solutions with the prescribed symmetries. However, the questions regarding the shapes of their profiles and other properties away from the bifurcation points, are beyond the scope of Chapter 2.

For example, the aforementioned mode-locking regime in system (1.1) is a periodic solution characterized by a distinctive pulsating profile and a period close to the delay. In general, appearance of such pulses is typical for laser dynamics, chemical kinetics [39, 48] and population dynamics (including Lotka-Volterra, host-parasite, and susceptible-infective-recovered models). In the context of population dynamics, periodic pulsating solutions are characterized by the alternation of long time intervals of almost complete extinction of some species and very short intervals of outbursts in their number. Further, similarly to (2.60) such dynamics often include processes with different time scales.

In many applications the period of the periodic pulsating solution and the delay time do not correlate. Hutchinson's delayed logistic model is a classical example of this scenario [47]. However, for certain systems, solutions with a period τ , which is close to the delay time T , can play an important role. For instance, the prototype delayed model that was proposed in [119] demonstrates stable periodic regimes with $\tau \approx T$ for certain parameters of the feedback. This model has applications in lasers [30, 118, 41] (including (1.1)), population epidemics [146, 136], and malaria infection [106]. Also, in the framework of the aforementioned Pyragas control, the delay is chosen to be close to the period of the unstable periodic target trajectory. The resulting stabilized periodic solution is close to x_* and therefore has a period $\tau \approx T$.

The subject of Chapter 3 is a case study of a rather broad class of population models, which have a stable periodic pulsating solution with a period close to the delay time. Our goal is to highlight those features of the systems that can support the existence of such periodic solutions. These features are shared by the laser dynamics model (1.1) and the population models considered here. In particular, we are interested in (i) a bifurcation scenario associated with the formation of periodic pulses, and (ii) nonlocal asymptotic analysis of the slow-fast pulsating periodic solution far from the Hopf bifurcation point. We will use singular perturbation analysis as a tool for identifying the conditions, which initialize periodic pulsating dynamics, finding parameter values that can support such dynamics, and obtaining asymptotic approximations for the periodic pulsating solution of period $\tau \approx T$.

More specifically, we consider models involving populations of species which evolve on different time scales. The models include an explicit delay time T which can have different nature and, therefore, can appear in different terms of the equations [133]; the maturity delay is considered as the main example [52, 17, 164]. We are interested in periodic dynamics presented by a limit cycle with the following properties:

- The period of the cycle is close to the delay time T ;

- The time trace of one component (which we call the A -component) of the cycle is a sequence of identical short pulses, typically one pulse per period, separated by intervals where the A -component is close to zero;
- The oscillations are self-excited, i.e., the cycle is either globally stable or has a large basin of attraction, while the equilibrium with the zero A -component is unstable.

These properties will be formalized and quantified in terms of the parameter $\gamma \gg 1$ which measures the ratio of the slow and fast time scales of the population processes involved in the system. In particular, the period of the cycle is $T + O(1/\gamma)$, the duration of the pulse scales as $1/\gamma$, while the pulse amplitude is asymptotically proportional to γ , and the time average of each population tends to a finite positive limit value as γ increases.

In the systems that we consider, periodic solutions with the above properties are formed near a transcritical bifurcation point (threshold) separating the domain where the equilibrium with the zero A -component is stable from the domain where it is unstable and coexists with the positive equilibrium. The cycle branches from the positive equilibrium via a Hopf bifurcation and continuously transforms into periodic pulsations of the amplitude $O(\gamma)$ over a short interval of the parameter values. Therefore, we look at the bifurcations that the equilibrium points undergo near the threshold. An asymptotic analysis of the spectrum shows that there is a sequence of eigenvalues, which have almost the same real part and the imaginary parts close to the multiples of the fundamental frequency $2\pi/T$. Because of this, the positive equilibrium undergoes a cascade of almost simultaneous and almost resonant Hopf bifurcations in an immediate vicinity of the threshold. This cascade is simultaneous with the fast transition from a steady state to the periodic pulsating dynamics with a period $\tau \approx T$.

We take advantage of the pulsating profile of the solution to derive an asymptotic approximation to the pulses and determine their parameters using the method of matched

inner (fast) and outer (slow) expansions [79]. This method was successfully applied to derive fixed-point conditions for the existence of pulsating solutions [146, 118, 55] and their asymptotics [157, 130] for both lasers and population models (however, we do not consider the existence problem here). Further, we obtain the law of scaling of pulses with γ and an equation for the pulse profile by adapting the approach used in [156]. All the asymptotic formulas are compared with numerical simulations. We also note an alternative perturbation technique of the fixed-point analysis based on averaging, which was proposed in [29].

1.1.6 Stabilization of periodic solutions

Finally, we move our attention to the problem of stabilization of periodic solutions. In [128] Pyragas suggested a simple method to stabilize a periodic solution of a system by introducing feedback of the form $K(x(t - T) - x(t))$ where T is the period of the solution that is to be stabilized. An important feature of this control is that it is noninvasive in the sense that it does not change the periodic solution itself but only its stability properties. This method has been implemented in a wide variety of applications, see, e.g., [129, 137, 143, 147, 132].

In most applications Pyragas control is used to stabilize an unstable orbit which is hyperbolic. That is to say that at least one of its Floquet multipliers is outside the unit circle, and the gain matrix K must be sufficiently large to ‘move’ these unstable eigenvalues inside the unit circle. On the other hand, since introducing feedback transforms the system to a delay differential equation, for small K infinitely many eigenvalues appear near zero. However, with the increasing gain these additional eigenvalues may become difficult to control. Therefore a delicate balance must be maintained: too small gain and the original unstable eigenvalues cannot be controlled, too large gain and the the additional eigenvalues may become unstable. For a discussion of sufficient conditions under which small orbits born near a Hopf bifurcation point can be stabilized see [75]. For necessary conditions for stabilization of generic orbits see [67]. In [45, 62, 65, 135] these results were extended to equivariant systems.

In Chapter 4 we extend the Pyragas control scheme to Hamiltonian systems. Due to the additional symmetry inherited from the Hamiltonian structure, Floquet multipliers come in pairs, μ, μ^{-1} . For this reason, periodic solutions are either unstable or neutrally stable. In this work we concentrate on the case of neutrally stable solutions. The multiplier $\mu = 1$ will always have multiplicity at least 2, and it is generic for periodic orbits to foliate a surface in the phase space. However, generically different periodic solutions lying on the same surface have different periods and, hence, proper selection of the parameter T in the Pyragas control scheme can select between them. For convenience we focus our attention to Newton equations of the type $\ddot{x} + \nabla V(x) = 0$. Our goal is to transform a neutrally stable periodic orbit of the uncontrolled system to the exponentially stable orbit by implementing feedback of the form $K(x(t - T) - x(t))$ where T is the period of the targeted orbit to be stabilized and K is an arbitrarily small gain matrix. This is in contrast to the situation which is generic in nonhamiltonian systems where control can never be arbitrarily small. We discuss sufficient conditions from two perspectives.

First of all, we treat the case of small amplitude solutions where sufficient conditions for exponential stability are framed in terms of the asymptotic expansion of $\nabla V(x)$ at the equilibrium $x = 0$ up to the third order. The importance of the third order expansion is motivated by the Lyapunov Center Theorem and the normal form for the Hopf bifurcation. Secondly, we deal with arbitrary periodic solutions, but instead of being framed in terms of the asymptotic expansion of the field $\nabla V(x)$, we use conditions on the Floquet modes of the targeted orbit as a solution of the uncontrolled system. Each section is supplemented with examples. Further, we briefly show how the conditions for the arbitrary periodic solutions agree with the case of small amplitude orbits.

1.2 Preliminaries

1.2.1 Notation

Let \mathbb{R} (\mathbb{C}) be the set of all *real* (*complex*) numbers, \bar{z} the *complex conjugate* of $z \in \mathbb{C}$, \mathbb{R}^N (\mathbb{C}^N) the space of all *real* (*complex*) N -dimensional *column* vectors. When we write $y = (x_1, x_2, \dots, x_k)$ for $x_i \in \mathbb{R}^N$ (\mathbb{C}^N), we mean that vector $y \in \mathbb{R}^{kN}$ (\mathbb{C}^{kN}) is obtained by stacking vectors x_1, x_2, \dots, x_k vertically. This is done in order to avoid cumbersome expressions such as $y = (x_1^T, x_2^T, \dots, x_k^T)^T$. Below $\langle \cdot, \cdot \rangle$ stands for the usual *inner product*, i.e., for any $u, v \in \mathbb{C}^N$, $\langle u, v \rangle = \bar{u}^T v$, and $\|\cdot\|$ is the corresponding Euclidean norm.

1.2.2 Equivariant Jargon

Let G be a compact Lie group. Given (closed) subgroups $H \subset G$, and denote by $N(H)$ the normalizer of H in G , by $W(H) = N(H)/H$ the Weyl group of H in G , and by (H) the conjugacy class of H in G . The set of all conjugacy classes of subgroups in G is denoted by $\Phi(G)$. Clearly, $\Phi(G)$ admits a partial order defined by:

$$(H) \leq (K) \quad \Leftrightarrow \quad \exists_{g \in G} gHg^{-1} \subset K.$$

Let X be a G -space and $x \in X$. We denote by $G_x := \{g \in G : gx = x\}$ the *isotropy* (or *stabilizer*) of x , by $G(x) := \{gx : g \in G\} \simeq G/G_x$ the *orbit* of x . The conjugacy class (G_x) will be called the *orbit type* of x . We will also adopt the following notation: $X^H := \{x \in X : G_x \supset H\}$.

For two G -spaces X and Y , a continuous map $f : X \rightarrow Y$ is said to be *equivariant* if $f(gx) = gf(x)$ for all $x \in X$ and $g \in G$. If the G -action on Y is trivial, then f is called *invariant*. Clearly, for any subgroup $H \subset G$ and equivariant map $f : X \rightarrow Y$, the map $f^H : X^H \rightarrow Y^H$, with $f^H := f|_{X^H}$, is well-defined. Finally, given two orthogonal G -representations W and V and an open bounded subset $\Omega \subset W$, an equivariant map $f : \Omega \rightarrow V$ is called Ω -*admissible* if $f(x) \neq 0$ for all $x \in \partial\Omega$.

If \mathfrak{W} is a G -representation, then for any function $x : S^1 \rightarrow \mathfrak{W}$, the spatio-temporal symmetry of x is a group $\mathfrak{H} < G \times S^1$ such that $g \cdot x(t - \theta) = x(t)$ for any $t \in \mathbb{R}/2\pi\mathbb{Z} \simeq S^1$ and any $(g, e^{i\theta}) \in \mathfrak{H}$. If x is nonconstant, then \mathfrak{H} has the structure of a graph of a homomorphism $\varphi : H \rightarrow S^1$, where H stands some subgroup of G . To emphasize this nature of the group \mathfrak{H} , the following notation is commonly used:

$$H^\varphi := \{(h, \varphi(h)) : h \in H\}.$$

The group H^φ is called a *twisted* symmetry group with twisting homomorphism φ .

Relative periodic solutions of our interest have symmetry groups which are subgroups of $\Gamma \times S^1 \times S^1$. Such a subgroup can be characterized by two twisting homomorphisms $\varphi : K \rightarrow S^1$ and $\psi : K^\varphi \rightarrow S^1$ for some subgroup $K < \Gamma$. Sometimes, in order to simplify our notations, instead of writing $K^{\varphi, \psi}$, we used the bold symbol \mathbf{K}^ψ to distinguish it from the group K^φ used for twisted symmetries of periodic solutions.

For further details of the equivariant jargon used in this dissertation, we refer to [148, 77, 24, 16]; for the representation theory background, see [148, 25].

1.2.3 Topological Tools

Brouwer Degree

The Brouwer degree first introduced in [28] to prove the Brouwer fixed point theorem, is a powerful tool to “count” the solutions to nonlinear equations in a given domain. It can be viewed as a generalization of winding number and the argument principle from complex analysis. For the continuous functions in Euclidean spaces the Brouwer degree can be defined via axiomatic approach as follows.

Let V be a Euclidean space and $\mathcal{M}(V, V)$ be the set of all admissible pairs (f, Ω) in V . Put $\mathcal{M} := \bigcup_V \mathcal{M}(V, V)$. Then there exists a unique function $\deg : \mathcal{M} \rightarrow \mathbb{Z}$ satisfying the following properties (axioms):

(P1) Existence. If $\deg(f, \Omega) \neq 0$ then there exists $z \in \Omega$ such that $f(z) = 0$.

(P2) Additivity. If $\Omega_1, \Omega_2 \subset \Omega$ are two disjoint sets such that pairs $(f, \Omega_1), (f, \Omega_2)$ are admissible and $f^{-1}(0) \cap \Omega \subset \Omega_1 \cup \Omega_2$, then $\deg(f, \Omega) = \deg(f, \Omega_1) + \deg(f, \Omega_2)$.

(P3) Homotopy. If $f_t : \mathbb{R}^n \rightarrow \mathbb{R}^n$, $t \in [0, 1]$ is an Ω -admissible homotopy, then $\deg(f_t, \Omega)$ is constant for all $t \in [0, 1]$.

(P4) Normalization. For some $z_o \in \mathbb{R}^n$, if $(\text{Id} - z_o, \Omega)$ is admissible, then

$$\deg(\text{Id} - z_o, \Omega) = \begin{cases} 1 & z_o \in \Omega, \\ 0 & z_o \notin \Omega. \end{cases}$$

Moreover, one can show that the degree defined above satisfies additional useful properties, e.g.,

(P5) Multiplicativity. For any $(f_1, \Omega_1), (f_2, \Omega_2) \in \mathcal{M}$

$$\deg(f_1 \times f_2, \Omega_1 \times \Omega_2) = \deg(f_1, \Omega_1) \cdot \deg(f_2, \Omega_2).$$

(P6) Suspension. If W is a Euclidean space and U is an open bounded neighborhood of $0 \in W$, then

$$\deg(f \times \text{Id}_W, \Omega \times U) = \deg(f, \Omega).$$

(P7) Regular Value Property. If $(f, \Omega) \in \mathcal{M}$, $f \in C^1$ and 0 is a regular value of f .

Then

$$\deg(f, \Omega) = \sum_{x \in f^{-1}(0) \cap \Omega} \text{sign}(\det Df(x)).$$

(P8) Hopf Property. If B is the unit ball in V and $\deg(f_1, B) = \deg(f_2, B)$ then f_1 and f_2 are B -admissible homotopic.

The suspension property **(P6)** allows one to define the so-called *Leray-Schauder degree* – an extension of the Brouwer degree to infinite dimensions. The regular value property **(P7)** says that the Brouwer degree is not just a mere indicator of the existence of solutions to equations but also an algebraic count.

In general, calculation of Brouwer degree is not an easy problem, however, the homotopy invariance **(P3)** of the degree allows to compute it by deforming the complicated mapping to a nicer one. Moreover, the multiplicativity property **(P5)** can be used to reduce the dimension if the given mapping can be decomposed into a direct product of simpler ones. Furthermore, symmetric properties of the map give restrictions on the possible values of the degree. One of the first such restrictions is the Borsuk-Ulam theorem [21] saying that the degree of an odd map is odd. In a wide variety of later works this result was extended to the maps with more complex symmetry structure [141, 70].

Equivariant Degree

Equivariant degree is a counterpart of the Brouwer degree for symmetric maps which allows to classify and count solutions with respect to their symmetries. The equivariant degree theory is a complicated subject which lies in the intersection of algebra, topology, representation theory and analysis.

Depending on the particular problem there are different kinds of equivariant degree one can employ. The simplest version is the equivariant degree without free parameters which is used in applications to boundary value problem. Trying to merely generalize the Brouwer degree to symmetric settings, i.e. Γ -equivariant mappings where Γ is some compact Lie group, one has to bear in mind certain subtleties that the symmetry brings.

First of all, Γ -equivariant degree should be defined only for Γ -equivariant mappings, thus the notion of admissible pair is replaced with admissible Γ -pair, i.e, assuming V is an orthogonal Γ -representation, $(f, \Omega) \in \mathcal{M}(V, V)$ is an admissible Γ -pair if Ω is Γ -invariant

and f is Γ -equivariant. The set of all admissible Γ -pairs in V is denoted by $\mathcal{M}^\Gamma(V, V)$ and $\mathcal{M}^\Gamma := \bigcup_V \mathcal{M}^\Gamma(V, V)$. Secondly, the solutions of the equation $f(x) = 0$ appear in group orbits, i.e., if $f(x_o) = 0$ then $f(y) = 0$ for every $y \in \Gamma(x)$. Moreover, if $x_1, x_2 \in \Gamma(x)$ then $(\Gamma_{x_1}) = (\Gamma_{x_2}) = (\Gamma_x)$. Thus, the symmetry of any group orbit $\Gamma(x)$ such that $f(x) = 0$ is completely characterized by its conjugacy class (Γ_x) . Thirdly, the equivariant counterpart of the additivity property **(P2)** should take into account independent contributions of each group orbit in the solution set of $f(x) = 0$ separately. Finally, the counterpart of multiplicativity property **(P5)** should incorporate the fact that the product $\Gamma(x_1) \times \Gamma(x_2)$ usually contains several orbit types.

Therefore, instead of the ring \mathbb{Z} the equivariant degree should take values in some algebraic structure that takes into account the observations above. Such structure is the *Burnside ring* of Γ denoted by $A(\Gamma)$. More specifically, $A(\Gamma) := \mathbb{Z}[\Phi_0(\Gamma)]$ is the free \mathbb{Z} -module generated by $(H) \in \Phi_0(\Gamma)$, i.e. $a \in A(\Gamma)$ is $a = n_{H_1}(H_1) + \dots + n_{H_m}(H_m)$ where $n_{H_i} \in \mathbb{Z}$ and $(H_i) \in \Phi_0(\Gamma)$ for all $i = 1, \dots, m$, equipped with a multiplication defined as

$$(H) \cdot (K) = \sum_{(L) \in \Phi_0(\Gamma)} n_L(H, K)(L),$$

where $n_L(H, K)$ is the number of orbits of type (L) in the space $\Gamma/H \times \Gamma/K$, i.e.,

$$n_L(H, K) := \left| (\Gamma/H \times \Gamma/K)_{(L)} / \Gamma \right|.$$

Thus, similarly to the Brouwer degree one can define Γ -equivariant degree $\Gamma\text{-deg} : \mathcal{M}^\Gamma \rightarrow A(\Gamma)$ via the axiomatic approach. The set of axioms is parallel to the properties **(P1)**–**(P8)**.

In order to apply the degree method to detect (symmetric) Hopf bifurcation, we need to introduce the notion of *twisted $\Gamma \times S^1$ -equivariant degree with one free parameter*, or shortly *twisted degree*. The reason is in the fact that periodic functions naturally have S^1 symmetry, i.e., the space $C(S^1; V)$ of all continuous periodic functions is an isometric Banach S^1 -representation with the S^1 action defined as

$$(e^{i\tau} x) (\cdot) = x(\cdot + \tau), \quad e^{i\tau} \in S^1 \quad \text{and} \quad x \in C(S^1; V),$$

and the Leray-Schauder degree totally ignores this symmetry, making itself ineffective to locate nonconstant periodic solutions to autonomous systems. Moreover, twisted degree provides extra information regarding the additional spatial Γ -symmetry of the system. The set of values of twisted degree is $A_1^t(\Gamma \times S^1) = \mathbb{Z}[\Phi_1^t(\Gamma \times S^1)]$, where $\Phi_1^t(\Gamma \times S^1)$ stands for the set of conjugacy classes for all twisted subgroups $H = K^{\theta, l}$ such that $\dim W(H) = 1$. Further, the \mathbb{Z} -module $A_1^t(\Gamma \times S^1)$ has an additional structure of $A(\Gamma)$ -module. Thus, similarly to the equivariant degree without free parameters, one can define twisted degree through the set of corresponding axioms. For the detailed presentation of equivariant degree theory see [16, 12, 15, 14, 70, 69, 87].

1.2.4 Preisach Model

In Chapter 2 we use the following fundamental model of hysteresis phenomena with nonlocal memory.

An elementary building block of the Preisach model of hysteresis is the *nonideal relay* operator also known as a *rectangular hysteresis loop*. This operator maps pairs $(\mu_0, h(\cdot)) \in \{-1, 1\} \times C(t_0, \infty)$ to binary functions $\mu(\cdot) : [t_0, \infty) \rightarrow \{-1, 1\}$, where μ_0 is called the initial state of the relay, $h(\cdot)$ and $\mu(\cdot)$ are input and output, respectively. The output, denoted by

$$\mu(t) = (R_{\alpha, \beta}[\mu_0]h)(t), \quad t \geq t_0, \quad (1.4)$$

is defined by

$$\mu(t) = \begin{cases} -1 & \text{if there is a } t_1 \in [t_0, t] \text{ such that } h(t_1) = \alpha \text{ and } h(s) < \beta \text{ for } s \in (t_1, t], \\ 1 & \text{if there is a } t_1 \in [t_0, t] \text{ such that } h(t_1) = \beta \text{ and } h(s) > \alpha \text{ for } s \in (t_1, t], \\ \mu_0 & \text{if } \alpha < h(s) < \beta \text{ for all } s \in [t_0, t], \end{cases}$$

where the parameters α and β satisfying $\alpha < \beta$ are called switching thresholds. According to this definition, an output has at most finite number of jumps on any finite interval

$t_0 \leq t \leq t_1$. In the context of modeling magnetic materials, a nonideal relay represents dynamics of the magnetic moment of an individual domain in the domain structure created by a one-dimensional magnetic field in the ferromagnetic sample. In this interpretation, the equality $\mu(t) = 1$ (resp. $\mu(t) = -1$) means that the magnetic moment points in the direction of the field (resp. in the opposite direction) at a moment t .

The main premise of the Preisach model is that magnetic moments of individual domains do not affect each other. Hence, the total magnetization $m(\cdot)$ is the weighted sum (integral) of the outputs of the individual relays $R_{\alpha,\beta}$, which respond independently to the variations of the input $h(\cdot)$:

$$m(t) = \int_{\alpha < \beta} \phi(\alpha, \beta) (R_{\alpha,\beta}[\mu_0(\alpha, \beta)]h)(t) d\alpha d\beta, \quad t \geq t_0. \quad (1.5)$$

Here, the integrable weight function $\phi : \mathbb{R}_0^2 \rightarrow \mathbb{R}$ with the domain $\mathbb{R}_0^2 = \{(\alpha, \beta) : \alpha < \beta\}$ is known as the *Preisach density function* and the measurable function $\mu_0 : \mathbb{R}_0^2 \rightarrow \{-1, 1\}$ is the *initial state* of the Preisach model. Formula (1.5), in which the initial state μ_0 is treated as a parameter, defines a continuous mapping of inputs $h(\cdot)$ to outputs $m(\cdot)$ in $C(t_0, \infty)$. This mapping known as the Preisach operator also continuously depends on μ_0 with respect to a natural metric in the functional space \mathcal{M} of initial states. However, as pointed out above, the Preisach operator is not differentiable except at certain points; and, its dependence on $\mu_0 \in \mathcal{M}$ is not smooth either.

We note that dynamics of systems with Preisach operators (2.125) should be considered in the infinite-dimensional phase space.

1.3 Outline of the Dissertation

Chapter 2 presents the material of two publications [10, 11]. The main goal of this chapter is to develop the Equivariant Degree method for studying relative equilibria and relative periodic solutions in the settings with lack of smoothness and/or genericity. More specifically,

we present conditions for the equivariant Hopf bifurcation of relative periodic solutions from relative equilibria in systems of FDEs respecting $\Gamma \times S^1$ -spatial symmetries. The existence of branches of relative periodic solutions together with their symmetric classification is established using the equivariant twisted $\Gamma \times S^1$ -degree with one free parameter. The main results are illustrated through the case study of D_8 and S_5 configurations of coupled mode-locked semiconductor lasers, and a system of electro-mechanical oscillators with hysteresis coupled in the D_8 symmetric fashion. The results of Chapter 2 were obtained in collaboration with Zalman Balanov, Dmitrii Rachinskii, Wiesław Krawcewicz and Hao-Pin Wu.

In Chapter 3 we consider slow-fast delayed systems and discuss pulsating periodic solutions, which are characterized by the specific property that the period of the periodic solution is close to the delay. Such solutions were previously found in the models of mode-locked lasers. Through a case study of population models, this work demonstrates the existence of similar solutions for a rather wide class of delayed systems. The periodic dynamics originates from the Hopf bifurcation on the positive equilibrium. We show that the continuous transformation of the periodic orbit to the pulsating regime is simultaneous with multiple secondary almost resonant Hopf bifurcations, which the equilibrium undergoes over a short interval of parameter values. We derive asymptotic approximations for the pulsating periodic solution close to, and away from, the bifurcations point, and consider scaling of the solution and its period with the small parameter that measures the ratio of the time scales. The role of competition for the realization of the bifurcation scenario is highlighted. The results of Chapter 3 were obtained in collaboration with Andrei Vladimirov and Dmitrii Rachinskii, and first appeared in [86].

Chapter 4 presents the material which was previously published in [64]. In this chapter, we consider a Newtonian system which has a branch (surface) of neutrally stable periodic orbits. We discuss sufficient conditions which allow arbitrarily small delayed Pyragas control to make one selected cycle asymptotically stable. In the case of small amplitude periodic

solutions we give conditions in terms of the asymptotic expansion of the right hand side, while in the case of larger cycles we frame the conditions in terms of the Floquet modes of the target orbit as a solution of the uncontrolled system. This work was done in collaboration with Edward Hooton, Qingwen Hu and Dmitrii Rachinskii.

Appendix A lists a few twisted subgroups, which are used in Sections 2.2 and 2.3 to describe symmetries of solutions. Appendix B contains the derivation of the normal form for the Hopf bifurcation in a delayed system.

CHAPTER 2

EQUIVARIANT DEGREE METHOD FOR ANALYSIS OF HOPF BIFURCATION OF RELATIVE PERIODIC SOLUTIONS¹

The main goal of this chapter is to adapt equivariant degree method to study a Hopf bifurcation of relative periodic solutions from relative equilibria in $\Gamma \times S^1$ -symmetric FDEs.

In Section 2.1, we first classify symmetries of branches of relative equilibria, which bifurcate from a $\Gamma \times S^1$ -fixed equilibrium of an equivariant FDE. Then, the main theorem on classification of symmetries of relative periodic solutions bifurcating from the branches of relative equilibria (Theorem 2.1.14) is presented and proved. In Section 2.2, the results of Section 2.1 are applied to delay rate equations of the $D_8 \times S^1$ - and $S_5 \times S^1$ -symmetric laser system. In both cases, we prove the occurrence of infinitely many branches of relative equilibria with various symmetries from the “laser off” state. Then the analytic method is combined with numerical computations to analyze symmetric properties of relative periodic solutions that branch from the relative equilibrium states. In Section 2.3, an example a nonsmooth system of symmetrically coupled hysteretic oscillators is considered.

2.1 $\Gamma \times S^1$ -Symmetric Systems of FDEs

2.1.1 Notation and statement of the problem

Assume that Γ is a finite group and let $V := \mathbb{R}^n$ be an orthogonal $\Gamma \times S^1$ -representation such that the S^1 -action on V is given by the homomorphism $T : S^1 \rightarrow O(n)$. Assume that J is the infinitesimal operator of the subgroup $T(S^1) \subset O(n)$, i.e.,

$$J = \lim_{\tau \rightarrow 0} \frac{1}{\tau} [T(e^{i\tau}) - \text{Id}].$$

¹The material of this chapter was published in *Journal of Differential Equations* and in *Journal of Nonlinear and Variational Analysis*. Reprinted with permission.

The action of S^1 on V satisfies for all $e^{i\tau} \in S^1$

$$\forall v \in V \quad e^{i\tau} v = e^{\tau J}(v),$$

and we also have $J e^{\tau J} = e^{\tau J} J$.

We will denote $\mathcal{G} := \Gamma \times S^1$ and use the notation $\mathbf{\Gamma} := \Gamma \times \{1\}$ and $\mathbf{S} := \{e\} \times S^1$ where $e \in \Gamma$ is the neutral element.

Let

$$V = V_0 \oplus V_1 \oplus \cdots \oplus V_m \tag{2.1}$$

be the \mathbf{S} -isotypical decomposition of V , where V_k is modeled on the S^1 -irreducible representation $\mathcal{V}_k \simeq \mathbb{C}$ with the S^1 -action given by $e^{i\tau} z := e^{ik\tau} \cdot z$, where ‘ \cdot ’ stands for the complex multiplication. Then, each of the components V_k , $k > 0$, has a natural complex structure such that for $v \in V_k$

$$e^{i\tau} v = e^{ik\tau} \cdot v, \quad Jv = ik \cdot v.$$

Also, for $v \in V_0$, we have $Jv = 0$.

Let $r > 0$ and denote by $C_{-r}(V)$ the Banach space

$$C([-r, 0]; V) := \{x : \text{where } x : [-r, 0] \rightarrow V \text{ is a continuous function}\},$$

equipped with the norm $\|x\|_\infty := \sup\{|x(\theta)| : \theta \in [-r, 0]\}$. Clearly, $C_{-r}(V)$ is an isometric $\Gamma \times S^1$ -representation, with the action given by

$$\forall \theta \in [-r, 0] \quad ((\gamma, e^{i\tau})x)(\theta) = e^{\tau J}(\gamma x(\theta)), \quad x \in C_{-r}(V), \quad (\gamma, e^{i\tau}) \in \Gamma \times S^1.$$

In addition, we have the following \mathbf{S} -isotypical decomposition of $C_{-r}(V)$:

$$C_{-r}(V) = \bigoplus_{k=0}^m C_{-r}(V_k),$$

where each of the components $C_{-r}(V_k)$ with $k > 0$ has a natural complex structure induced from V_k .

For a continuous function $x : \mathbb{R} \rightarrow V$ and $t \in \mathbb{R}$, let $x_t : [-r, 0] \rightarrow V$ be a function defined by

$$x_t(\theta) := x(t + \theta), \quad \theta \in [-r, 0].$$

We make the following assumption:

(A0) $f : \mathbb{R} \times C_{-r}(V) \rightarrow V$ is a continuous \mathcal{G} -equivariant function, i.e., for $(\gamma, e^{i\tau}) \in \mathcal{G}$

$$f\left(\alpha, (\gamma, e^{i\tau})x\right) = e^{\tau J} \gamma f(\alpha, x) \quad \text{for all } x \in C_{-r}(V). \quad (2.2)$$

Consider the parametrized system of FDEs

$$\dot{x}(t) = f(\alpha, x_t), \quad x(t) \in V. \quad (2.3)$$

In what follows, we will study bifurcations of continuous branches of periodic/quasi-periodic solutions to (2.3) of special type and describe their symmetric properties.

Remark 2.1.1. In the case the space $C_{-r}(V)$ is replaced by

$$C([-r, a]; V) := \{x : [-r, a] \rightarrow V : x \text{ is continuous and bounded}\}$$

for some $a > 0$, (2.3) is an FDE with deviated argument. Even under very strong differentiability assumptions on f , the uniqueness of solutions for (2.3) cannot be established making it impossible to use methods based on applications of Center Manifolds. On the other hand, including the case of infinite delay $r = \infty$, the equivariant degree method can be easily extended, using standard setting, to this type of FDEs.

2.1.2 Symmetric bifurcation of relative equilibria from an equilibrium

In this subsection, we are interested in periodic solutions to (2.3) of the type

$$x(t) = e^{wJt}x \quad \text{for some } x \in V \text{ and } w \in \mathbb{R}. \quad (2.4)$$

Relative equilibria. By substituting (2.4) into equation (2.3), we obtain

$$we^{wtJ}Jx(t) = f(\alpha, e^{w(t+\cdot)J}x). \quad (2.5)$$

Then, using the equivariance condition (2.2), we can rewrite (2.5) as

$$wJx = f(\alpha, e^{wJ}x), \quad x \in V. \quad (2.6)$$

Take the orthogonal \mathbf{S} -invariant decomposition (2.1) of the space V , where $V_0 = V^{\mathbf{S}}$, and denote

$$V_* := V_0^\perp = V_1 \oplus \cdots \oplus V_m.$$

For a fixed $\lambda = u + iw \in \mathbb{C}$, define the linear operator $\xi(\lambda) : V \rightarrow C_{-r}(V)$ by

$$\left(\xi(\lambda)x\right)(\theta) = e^{u\theta}e^{wJ\theta}x_* + x_o, \quad \theta \in [-r, 0], \quad (2.7)$$

where $x = x_* + x_o$, $x_* \in V_*$ and $x_o \in V_0$, and consider the function $\tilde{f} : \mathbb{R} \times \mathbb{C} \times V \rightarrow V$ defined by

$$\tilde{f}(\alpha, \lambda, x) := f(\alpha, \xi(\lambda)x). \quad (2.8)$$

With this notation, equation (2.6) can be written as

$$wJx = \tilde{f}(\alpha, iw, x), \quad x \in V. \quad (2.9)$$

Furthermore, assumption (A0) implies \mathcal{G} -equivariance of \tilde{f} :

$$\tilde{f}\left(\alpha, \lambda, (\gamma, e^{\tau i})x\right) = e^{\tau J}\gamma\tilde{f}(\alpha, \lambda, x) \quad \text{for all } x \in V, \lambda \in \mathbb{C}.$$

Hence, solutions to (2.9) come in \mathbf{S} -orbits. It is clear that any \mathbf{S} -orbit, which is a solution to (2.9), satisfies the standard definition of relative equilibrium (see, for example, [50]). In what follows, we refine this concept to the setting relevant to our discussion.

Assume that $x \in V^{\mathbf{S}} = V_0$. Then, one has $\tilde{f}(\alpha, iw, x) = \tilde{f}(\alpha, 0, x)$ for all ω . Hence, any solution $x \in V^{\mathbf{S}}$ of (2.9) is an equilibrium for equation (2.3) with $\mathbf{S}(x) = \{x\}$. On the other hand, solutions of (2.9) that satisfy $x \notin V^{\mathbf{S}}$ form one-dimensional orbits.

Definition 2.1.2. Suppose that (2.9) holds for some $\alpha_o, \omega_o \in \mathbb{R}$ and $x_o \notin V^{\mathbf{S}}$. Then, the orbit $\mathbf{S}(x_o)$ is a one-dimensional curve in V called a *relative equilibrium* of equation (2.3).

- (i) For $\omega_o \neq 0$, this orbit is a trajectory of time-periodic solutions $x(\cdot) = e^{(\omega_o + \tau)J}x_o$, $e^{i\tau} \in S^1$, to equation (2.3) called a *rotating wave*.
- (ii) For $\omega_o = 0$, the relative equilibrium consists of equilibrium points $e^{\tau J}x_o$, $e^{i\tau} \in S^1$, of (2.3) (the so-called *frozen wave*).

Characteristic quasi-polynomials. In what follows, we will require from f to satisfy *minimal* differentiability properties, i.e., it will be assumed that once we use the symbols of derivatives of f , it is well-defined on a specified set.

Let $\alpha_o \in \mathbb{R}$ be given and let $x_o \in V^{\mathcal{G}}$ be an equilibrium for (2.3). We will also call the pair (α_o, x_o) an *equilibrium*, or a *stationary solution*, in this case.

Let us consider the bifurcation of relative equilibria from this equilibrium. Denote by

$$D_{\mathbf{x}}f(\alpha, \mathbf{x}) : \mathbb{R} \times C_{-r}(V) \rightarrow V \quad (2.10)$$

the derivative of the functional f with respect to $\mathbf{x} \in C_{-r}(V)$ (provided that this derivative exists). If $x_o \in V_0$, then the Jacobi matrix $D_x \tilde{f}(\alpha, \lambda, x_o) : V \rightarrow V$, which is given by

$$D_x \tilde{f}(\alpha, \lambda, x_o) = D_{\mathbf{x}}f(\alpha, \xi(\lambda)x_o)\xi(\lambda) \quad (2.11)$$

is \mathbf{S} -equivariant (cf. (2.7) and (2.8)). Therefore, the subspaces V_0 and V_* are \mathbf{S} -invariant for this matrix. Consider the restrictions $D_x \tilde{f}(\alpha, \lambda, x_o)|_{V_0}$ and $D_x \tilde{f}(\alpha, \lambda, x_o)|_{V_*}$ and define the *characteristic quasi-polynomials* for $x_o \in V_0$ and $\lambda \in \mathbb{C}$:

$$\begin{aligned} \mathcal{P}_0(\alpha, \lambda, x_o) &:= \det \left(D_x \tilde{f}(\alpha, \lambda, x_o)|_{V_0} - \lambda \text{Id} \right), \\ \mathcal{P}_*(\alpha, \lambda, x_o) &:= \det \left(D_x \tilde{f}(\alpha, \lambda, x_o)|_{V_*} - \lambda \text{Id} \right). \end{aligned} \quad (2.12)$$

We make the following assumption.

- (A1) (a) There exists a continuous function $x : (\alpha_o - \varepsilon, \alpha_o + \varepsilon) \rightarrow V_0$ (for some $\varepsilon > 0$) such that: $x(\alpha_o) = x_o \in V^{\mathcal{G}}$ and $\{(\alpha, x(\alpha)) : \alpha \in (\alpha_o - \varepsilon, \alpha_o + \varepsilon)\}$ consists of equilibria for (2.3);
- (b) $D_{\mathbf{x}}f(\alpha, x(\alpha))$ exists for $\alpha \in (\alpha_o - \varepsilon, \alpha_o + \varepsilon)$ and depends continuously on α ;
- (c) the characteristic quasi-polynomial $\mathcal{P}_0(\alpha, \cdot, x(\alpha))$ has no zero roots, i.e., $\mathcal{P}_0(\alpha, 0, x(\alpha)) \neq 0$.

Remark 2.1.3. (i) By formula (2.7), $\xi(\lambda)$ acts trivially on $x \in V_0$, hence the restrictions of \tilde{f} and f on V_0 coincide.

- (ii) By equivariance of \tilde{f} , and due to $x_o \in V^{\mathcal{G}}$, it follows that $x(\alpha) \in V^{\mathcal{G}}$, consequently the set $M \subset \mathbb{R}^2 \times V^{\mathcal{G}}$ given by

$$M := \{(\alpha, w, x(\alpha)) : \alpha \in (\alpha_o - \varepsilon, \alpha_o + \varepsilon), w \in \mathbb{R}\} \quad (2.13)$$

is composed of solutions to (2.9), which can be called *trivial*.

Assume that:

- (A2) The quasi-polynomial $\mathcal{P}_*(\alpha_o, \cdot, x_o)$ has a characteristic root $\lambda = i\omega_o$ for some $\omega_o \in \mathbb{R}$ at the equilibrium point (α_o, x_o) , but for any other equilibrium (α, x) from a neighborhood of (α_o, x_o) in $\mathbb{R} \times V_0$, the corresponding characteristic polynomial has no roots of the form $\lambda = i\omega$, $\omega \in \mathbb{R}$.

In order to find *nontrivial* solutions to (2.9) bifurcating from M , consider the equation

$$\Phi(\alpha, \omega, x) := \tilde{f}(\alpha, i\omega, x) - \omega Jx = 0 \quad (2.14)$$

as a \mathcal{G} -symmetric bifurcation problem with two free parameters α and ω .

By applying the standard terminology (see [16]), if $D_x \tilde{f}(\alpha, i\omega, x) - \omega J : V \rightarrow V$ is not an isomorphism for some point $(\alpha, \omega, x) \in M$, we call it an *M-singular* point of Φ . A necessary

condition for a point $(\alpha', \omega', x') \in M$ to be a bifurcation point for equation (2.9) is that it is an M -singular point. Assumption (A2) implies that the point $(\alpha_o, \omega_o, x_o)$ satisfies this necessary condition.

Remark 2.1.4. Take $C_{-r}(V) = C_{-r}(V_0) \oplus C_{-r}(V_*)$. Assumption (A1) means that $\lambda = 0$ is not an eigenvalue for the restriction of the linearization to $C_{-r}(V_0)$ for α close to α_o . Assumption (A2) means that the restriction of the linearization to $C_{-r}(V_*)$ has a pair of eigenvalues $\lambda = \pm i\omega_o$ for $\alpha = \alpha_o$ and has no eigenvalues of the form $i\omega$, $\omega \in \mathbb{R}$, for $\alpha \neq \alpha_o$ sufficiently close to α_o .

Sufficient condition for bifurcation of relative equilibria. In order to provide a sufficient condition for the bifurcation of relative equilibria from the point $(\alpha_o, \omega_o, x_o)$ and an equivariant topological classification of the bifurcating branches, we apply the twisted \mathcal{G} -equivariant degree with one free parameter (for more details, see [16]). To be more precise, consider the \mathcal{G} -isotypical decomposition of V (see (2.1)):

$$V = V_0 \oplus V_* = \bigoplus_{i=0}^r V_i^0 \oplus \bigoplus_{j=0}^s \bigoplus_{k=1}^m V_{j,k}, \quad (2.15)$$

where $V_{j,k}$ is the isotypical component modeled on the irreducible \mathcal{G} -representation $\mathcal{V}_{j,k}$ and V_i^0 can be identified with the Γ -representation modeled on an irreducible Γ -representation \mathcal{V}_i .

Remark 2.1.5. Let (H_o) be a maximal twisted orbit type in V . Then, (H_0) is also a maximal twisted orbit type for some V_{j_o, k_o} in (2.15), $k_o > 0$. In fact, if U is a direct sum of two \mathcal{G} -representations U_1 and U_2 , then $\mathcal{G}_{(x,y)} = \mathcal{G}_x \cap \mathcal{G}_y$ for any $(x, y) \in U$, $x \in U_1$, $y \in U_2$.

For any $j = 0, \dots, s$ and $k = 1, \dots, m$, put

$$\mathcal{P}_{j,k}(\alpha, \lambda) := \det \left(D_x \tilde{f}(\alpha, \lambda, x(\alpha)) \Big|_{V_{j,k}} - \lambda \text{Id} \right), \quad \lambda \in \mathbb{C}.$$

Notice that the characteristic equation at $(\alpha, x(\alpha))$ can be written as

$$\mathcal{P}_*(\alpha, \lambda) := \mathcal{P}_*(\alpha, \lambda, x(\alpha)) = \prod_{k>0} \prod_{j=0}^s \mathcal{P}_{j,k}(\alpha, \lambda) = 0. \quad (2.16)$$

This implies that λ is a characteristic root for $(\alpha, x(\alpha))$ if it is a root of $P_{j,k}(\alpha, \lambda) = 0$ for some $k > 0$ and $j \geq 0$.

To formulate our first bifurcation result, we need two additional concepts. Observe that using (A2), one can choose a small neighborhood Q of the point $i\omega_o$ in the right half-plane $\operatorname{Re} \lambda > 0$ of \mathbb{C} and a sufficiently small real $\delta = \delta(Q) > 0$ such that, as α varies over the interval $|\alpha - \alpha_o| \leq \delta$, the roots $\lambda(\alpha)$ of $\mathcal{P}_{j,k}(\alpha, \cdot)$ can only leave Q through the ‘exit’ at the point $i\omega_o$ and only when $\alpha = \alpha_o$.

Definition 2.1.6. Define the $V_{j,k}$ -isotypical *crossing number* at (α_o, ω_o) by the formula

$$\mathfrak{t}_{j,k}(\alpha_o, \omega_o) := \mathfrak{t}_{j,k}^-(\alpha_o, \omega_o) - \mathfrak{t}_{j,k}^+(\alpha_o, \omega_o), \quad (2.17)$$

where $\mathfrak{t}_{j,k}^-(\alpha_o, \omega_o)$ is the number of roots $\lambda(\alpha)$ of $\mathcal{P}_{j,k}(\alpha, \cdot)$ (counted according to their $\mathcal{V}_{j,k}$ -isotypical multiplicity) in the set Q for $\alpha < \alpha_o$, and $\mathfrak{t}_{j,k}^+(\alpha_o, \omega_o)$ is the number of roots of $\mathcal{P}_{j,k}(\alpha, \cdot)$ in Q for $\alpha > \alpha_o$.

Definition 2.1.7. A set K of solutions (α, w, x) to equation (2.9) is called a *continuous branch of relative equilibria* bifurcating from the equilibrium (α_o, x_o) of equation (2.3) if:

- (i) $x \notin V^{\mathbf{S}}$ for all $(\alpha, w, x) \in K$;
- (ii) \overline{K} contains a connected component K_o such that $K_o \cap M \neq \emptyset$ (cf. (2.13));
- (iii) For any $\varepsilon > 0$ there is a $\delta > 0$ such that if $(\alpha, w, x) \in K \cap K_o$ and $\|x\| < \delta$, then $|\alpha - \alpha_o| < \varepsilon$ and $|w - \omega_o| < \varepsilon$.

A sufficient condition for the bifurcation of relative equilibria from the equilibrium (α_o, x_o) , which provides an estimate for the number of possible branches of relative equilibria with their symmetric properties, can be formulated as follows.

Proposition 2.1.8. *Given system (2.3), assume conditions (A0)–(A2) are satisfied. Let (\mathcal{H}_o) be a maximal twisted orbit type in V . Take decomposition (2.15) and denote by \mathfrak{M} the set of all \mathcal{G} -isotypical components in which (\mathcal{H}_o) is an orbit type (cf. Remark 2.1.5). Assume there exists $V_{j_o, k_o} \in \mathfrak{M}$ such that:*

(i) (\mathcal{H}_o) is a maximal twisted type in V_{j_o, k_o} ;

(ii) $\mathfrak{t}_{j_o, k_o}(\alpha_o, \omega_o) \neq 0$;

(iii) $\mathfrak{t}_{j, k}(\alpha_o, \omega_o) \cdot \mathfrak{t}_{j', k'}(\alpha_o, \omega_o) \geq 0$ for all $V_{j, k}, V_{j', k'} \in \mathfrak{M}$.

Then, there exist at least $|\mathcal{G}/\mathcal{H}_o|_{\mathbf{S}}$ continuous branches of relative equilibria of equation (2.3) bifurcating from the equilibrium (α_o, x_o) with the minimal symmetry (\mathcal{H}_o) (here $|\cdot|_{\mathbf{S}}$ stands for the number of \mathbf{S} -orbits).

The proof literally follows the argument presented in [16]. For completeness, here we give a brief sketch of the proof. Under extra transversality/genericity conditions, this statement is well-known, see for example [50, 51].

Sketch of the proof of Proposition 2.1.8. The proof splits into three steps.

(a) *Auxiliary function and admissibility.* Take \mathbb{R}^2 with the trivial \mathcal{G} -action and define a sufficiently small \mathcal{G} -invariant neighborhood of the point $(\alpha_o, \omega_o, x_o)$ in $\mathbb{R}^2 \oplus V$ of the form

$$\Omega := \{(\alpha, w, x) : |\alpha - \alpha_o| < \varepsilon, |w - \omega_o| < \varepsilon, \|\hat{x} - x_o\| < \varepsilon, \|x_*\| < \delta\},$$

where $(\alpha, w, x) = (\alpha, w, \hat{x} + x_*)$, $(\alpha, w, \hat{x}) \in M$, $x_* \perp \hat{x}$, and a G -invariant continuous function $\zeta : \bar{\Omega} \rightarrow \mathbb{R}$ satisfying

$$\begin{aligned} \zeta(\alpha, w, x) &< 0 && \text{if } (\alpha, w, x) \in M \cap \bar{\Omega}, \\ \zeta(\alpha, w, x) &> 0 && \text{if } (\alpha, w, x) \in \bar{\Omega} \text{ and } \|x_*\| = \delta \end{aligned}$$

(recall that ζ is called an *auxiliary function*). By condition (A0), the map $\Phi_\zeta : \mathbb{R}^2 \times V \rightarrow \mathbb{R} \times V$ defined by

$$\Phi_\zeta(\alpha, w, x) = (\zeta(\alpha, w, x), \Phi(\alpha, w, x)), \quad (\alpha, w, x) \in \overline{\Omega},$$

is \mathcal{G} -equivariant. Moreover, conditions (A1) and (A2) allow us to choose the parameters $\varepsilon, \delta > 0$ of the set Ω to be sufficiently small to ensure that the map Φ_ζ is Ω -admissible (i.e., Φ_ζ does not have zeroes on $\partial\Omega$).

(b) *Twisted degree and a sufficient condition for the bifurcation of relative equilibria.* Since Φ_ζ is \mathcal{G} -equivariant and Ω -admissible, the twisted degree

$$\mathcal{G}\text{-deg}(\Phi_\zeta, \Omega) = \sum_{(\mathcal{H})} n_{\mathcal{H}}(\mathcal{H}) \quad (2.18)$$

is correctly defined (here, $n_{\mathcal{H}} \in \mathbb{Z}$ and the summation is going over all twisted orbit types occurring in V). The following statement is parallel to Theorem 9.28 from [16].

Proposition 2.1.9. *Given (2.18), assume that $n_{\mathcal{H}_o} \neq 0$ for some maximal twisted orbit type (\mathcal{H}_o) in V . Then, the conclusion of Proposition 2.1.8 holds.*

(c) *Twisted degree and crossing numbers.* To effectively apply Proposition 2.1.9 for proving Proposition 2.1.8, one needs to link the twisted degree (2.18) to (isotypical) crossing numbers (2.17). To this end, one can use the following standard computational formula²:

$$\mathcal{G}\text{-deg}(\Phi_\zeta, \Omega) = \prod_{\mu \in \sigma_-} \prod_{i=0}^r \left(\deg_{\mathcal{V}_i} \right)^{m_i(\mu)} \bullet \sum_{j,k} \mathfrak{t}_{j,k}(\alpha_o, \omega_o) \deg_{\mathcal{V}_{j,k}}, \quad (2.19)$$

where $j = 0, 1, \dots, s$, $k = 1, \dots, m$; σ_- denotes the set of all (real) negative roots μ of the quasi-polynomial $\mathcal{P}(\alpha_o, \lambda)$ at x_o ; $m_i(\mu)$ stands for the \mathcal{V}_i -isotypical multiplicity of μ ; $\deg_{\mathcal{V}_i}$ (resp. $\deg_{\mathcal{V}_{j,k}}$) denote the so-called basic degrees related to irreducible Γ -representations (resp. \mathcal{G} -representations); and, “ \bullet ” stands for the multiplication in the Euler ring $U(\mathcal{G})$

²The details can be found in [16]

(see [148] for more details). Take (\mathcal{H}_o) and V_{j_o, k_o} satisfying (i)–(iii). Then (see conditions (i)–(ii)), (\mathcal{H}_o) appears with nonzero coefficient in $\mathfrak{t}_{j_o, k_o}(\alpha_o, \omega_o) \deg_{V_{j_o, k_o}}$. Condition (iii) implies that (\mathcal{H}_o) “survives” in the sum given in the right hand side of (2.19). Finally, since any \deg_{V_i} is an invertible element of the Burnside ring $A(\mathcal{G}) \subset U(\mathcal{G})$, the result follows.

2.1.3 Hopf bifurcation from a relative equilibrium

Regular relative equilibria. Suppose that for some $\alpha = \hat{\alpha}$ and $\hat{x} \in V \setminus V^{\mathbf{S}}$, equation (2.3) has a relative equilibrium $\mathbf{S}(\hat{x})$ (see Definition 2.1.2). Then, equation (2.9) is satisfied for some $\hat{\omega} \in \mathbb{R}$:

$$\Phi(\hat{\alpha}, \hat{\omega}, \hat{x}) = \tilde{f}(\hat{\alpha}, i\hat{\omega}, \hat{x}) - \hat{\omega}J\hat{x} = 0, \quad (2.20)$$

where $\hat{x} = (\hat{q}, \hat{v}) \in V^{\mathbf{S}} \oplus V_*$ with $\hat{v} \neq 0$. Moreover,

$$\left. \frac{d}{d\tau} \Phi(\hat{\alpha}, \hat{\omega}, e^{\tau J} \hat{x}) \right|_{\tau=0} = D_x \Phi(\hat{\alpha}, \hat{\omega}, e^{\tau J} \hat{x}) J e^{\tau J} \hat{x} \Big|_{\tau=0} = D_x \Phi(\hat{\alpha}, \hat{\omega}, \hat{x}) J \hat{x}, \quad (2.21)$$

provided that the derivatives in (2.21) exist. Hence, relation (2.20) and the \mathbf{S} -equivariance of Φ imply that the directional derivative of Φ at the point \hat{x} in the direction of the orbit $\mathbf{S}(\hat{x})$ is zero:

$$D_x \Phi(\hat{\alpha}, \hat{\omega}, \hat{x}) J \hat{x} = 0. \quad (2.22)$$

That is, the map $D_x \Phi(\hat{\alpha}, \hat{\omega}, \hat{x})$ has a nonzero kernel.

Definition 2.1.10. A relative equilibrium $\mathbf{S}(\hat{x})$ will be called *regular* if the kernel of the map given by the following block-matrix

$$\left[D_w \Phi(\hat{\alpha}, \hat{\omega}, \hat{x}) \mid D_x \Phi(\hat{\alpha}, \hat{\omega}, \hat{x}) \right] : \mathbb{R} \times V \rightarrow V \quad (2.23)$$

is *one-dimensional*, provided that the derivatives in (2.23) exist.

We make the following assumption parallel to (A1):

(A3) (a) Given $(\hat{\alpha}, \hat{\omega}, \hat{x})$ satisfying (2.20), assume that there exist a neighborhood \mathcal{U} of $\hat{\alpha}$ in \mathbb{R} and continuous functions $\omega : \mathcal{U} \rightarrow \mathbb{R}$, $\omega(\hat{\alpha}) = \hat{\omega}$, and $u : \mathcal{U} \rightarrow S := \{x \in V : \langle x, J\hat{x} \rangle = 0\}$, $u(\hat{\alpha}) = 0$, such that

$$\Phi(\alpha, \omega(\alpha), \hat{x} + u(\alpha)) = 0, \quad \alpha \in \mathcal{U}, \quad (2.24)$$

i.e., formula

$$x_\alpha(t) := e^{(\omega(\alpha)t + \tau)J} x(\alpha) \quad (2.25)$$

defines a branch of relative equilibria $\mathbf{S}(x(\alpha))$ parametrized by $\alpha \in \mathcal{U}$ (here $x(\alpha) = \hat{x} + u(\alpha)$);

(b) $D_{\mathbf{x}}f(\alpha, x_\alpha(\cdot))$ exists for $\alpha \in (\alpha_o - \varepsilon, \alpha_o + \varepsilon)$ and depends continuously on α ;

(c) $\mathbf{S}(x(\alpha))$ is a regular relative equilibrium for (2.3) for all $\alpha \in \mathcal{U}$.

Remark 2.1.11. By condition (A3)(b), partial derivatives required in (2.23) are correctly defined so that assumption (A3)(c) makes sense.

It will be assumed that the branch $\mathbf{S}(x(\alpha))$ has symmetric properties (cf. Proposition 2.1.8):

(A4) The regular relative equilibrium $\mathbf{S}(\hat{x})$, $\alpha \in \mathcal{U}$, admits a twisted group symmetry $\mathcal{H} < \mathcal{G}$.

Remark 2.1.12. Due to the equivariance, the twisted symmetry group \mathcal{H} is the same for all relative equilibria $\mathbf{S}(x(\alpha))$, $\alpha \in \mathcal{U}$.

For a given $\alpha \in \mathcal{U}$, put

$$\mathcal{B}_\alpha := D_{\mathbf{x}}f(\alpha, e^{\omega(\alpha)J} x(\alpha)) = D_{\mathbf{x}}f(\alpha, \xi(i\omega(\alpha))x(\alpha)) : C_{-r}(V) \rightarrow V. \quad (2.26)$$

For $\alpha \in \mathcal{U}$ and $\lambda \in \mathbb{C}$, define the linear map $\mathcal{R}_\alpha : V^c \rightarrow V^c$ in the complexification V^c of V by the formula

$$\mathcal{R}_\alpha(\lambda)y := \mathcal{B}_\alpha(e^{(\omega(\alpha)J + \lambda \text{Id}) \cdot} y), \quad y \in V^c. \quad (2.27)$$

Then,

$$\det(\mathcal{R}_\alpha(\lambda) - \omega(\alpha)J - \lambda \text{Id}) = 0 \quad (2.28)$$

is the characteristic equation for the linearization of system (2.3) on the relative equilibrium $\mathbf{S}(x(\alpha))$. Since

$$\mathcal{R}_\alpha(0) - \omega(\alpha)J = D_x\Phi(\alpha, \omega(\alpha), x(\alpha)), \quad (2.29)$$

conditions (A3)(a,b) imply that the characteristic equation (2.28) has a zero root $\lambda = 0$ corresponding to the eigenvector $Jx(\alpha)$; furthermore, due to (A3)(c), this root is simple.

Hopf bifurcation of relative periodic solutions. We are interested in finding solutions to (2.3) of the form

$$x(t) = e^{(\omega(\alpha)+\phi)tJ}(x(\alpha) + y(t)), \quad (2.30)$$

where $y(t)$ is a nonstationary p -periodic function with $p = 2\pi/\beta$ for some $\beta > 0$, and in symmetric properties of these solutions. Here $y(t)$ and $\beta, \phi \in \mathbb{R}$ are unknown. Periodic and quasi-periodic solutions of type (2.30) are called *relative periodic* solutions.

To be more precise, let us define the so-called *equivariant Hopf bifurcation* of small amplitude *relative periodic* solutions of type (2.30) from the family of relative equilibria (2.25).

The following definition is similar to Definition 2.1.7.

Definition 2.1.13. A set K of quadruplets (α, β, ϕ, x) , where x is a solution to equation (2.3) of the form (2.30), is called a *continuous branch of relative periodic solutions* bifurcating (via the *equivariant* Hopf bifurcation) from the relative equilibrium $(\hat{\alpha}, \hat{\omega}, \mathbf{S}(\hat{x}))$ if there exists a $\beta_o > 0$ such that:

- (i) \overline{K} contains a connected component K_o such that $(\hat{\alpha}, \beta_o, 0, \hat{x}) \in K_o$;
- (ii) For any $\varepsilon > 0$ there is a $\delta > 0$ such that if $(\alpha, \beta, \phi, x) \in K \cap K_o$ and $\|y\| < \delta$, then $|\alpha - \hat{\alpha}| < \varepsilon$, $|\phi| < \delta$, and $|\beta - \beta_o| < \varepsilon$.

A necessary condition for the Hopf bifurcation is that characteristic equation (2.28) has a pair of purely imaginary roots $\lambda = \pm i\beta_o$, $\beta_o > 0$, for $\alpha = \hat{\alpha}$. We make a stronger assumption:

(A5) Characteristic equation (2.28) has a pair of purely imaginary roots $\lambda = \pm i\beta_o$, $\beta_o > 0$, for $\alpha = \hat{\alpha}$, and has no roots of the form $\lambda = i\beta$, $\beta \geq 0$, for $\alpha \neq \hat{\alpha}$, $\alpha \in \mathcal{U}$.

Put $\mathcal{K} := \mathcal{H} \times S^1$ and consider the \mathcal{K} -isotypical decomposition of V^c :

$$V^c = U_{0,1} \oplus U_{1,1} \oplus \cdots \oplus U_{p,1}, \quad (2.31)$$

where S^1 -action is given by complex multiplication. Due to the equivariance, each isotypical component $U_{j,1}$ is invariant for the map $\mathcal{R}_\alpha(\lambda)$ and for J . Therefore, we can introduce the characteristic polynomial

$$\hat{\mathcal{P}}_{j,1}(\alpha, \lambda) := \det \left((\mathcal{R}_\alpha(\lambda) - \omega(\alpha)J - \lambda \text{Id})|_{U_{j,1}} \right), \quad \lambda \in \mathbb{C}, \quad (2.32)$$

associated with each isotypical component $U_{j,1}$, and define the $U_{j,1}$ -isotypical crossing numbers

$$\hat{\mathbf{t}}_{j,1}(\hat{\alpha}, \beta_o) = \hat{\mathbf{t}}_{j,1}^-(\hat{\alpha}, \beta_o) - \hat{\mathbf{t}}_{j,1}^+(\hat{\alpha}, \beta_o) \quad (2.33)$$

at the point $(\hat{\alpha}, \beta_o)$ in the same way as we did in Subsection 2.1.2 (cf. (2.17)).

Theorem 2.1.14. *Given system (2.3), assume conditions (A0) and (A3)–(A5) are satisfied. Take decomposition (2.31) and let (\mathcal{L}_o) be a maximal twisted orbit type in V^c . Denote by \mathfrak{N} the set of all \mathcal{K} -isotypical components in (2.31) in which (\mathcal{L}_o) is an orbit type. Assume there exists $U_{j_o,1} \in \mathfrak{N}$ such that:*

- (i) (\mathcal{L}_o) is a maximal twisted orbit type in $U_{j_o,1}$ (cf. Remark 2.1.5);
- (ii) $\hat{\mathbf{t}}_{j_o,1}(\hat{\alpha}, \beta_o) \neq 0$;
- (iii) $\hat{\mathbf{t}}_{j,1}(\hat{\alpha}, \beta_o) \cdot \hat{\mathbf{t}}_{j',1}(\hat{\alpha}, \beta_o) \geq 0$ for all $U_{j,1}, U_{j',1} \in \mathfrak{N}$.

Then, there exist at least $|\mathcal{H}/\mathcal{L}_o|_{S^1}$ continuous branches of relative periodic solutions (2.30) bifurcating via the Hopf bifurcation from the relative equilibrium $(\hat{\alpha}, \hat{\omega}, \mathbf{S}(\hat{x}))$ and having the minimal symmetry (\mathcal{L}_o) .

2.1.4 Proof of Theorem 2.1.14

For the proof, which splits into several steps, we modify the twisted equivariant degree approach described in Sections 10.1-2 of [16] (see also the sketch of the proof of Proposition 2.1.8).

(a) *Rescaling time.* Substituting (2.30) in (2.3) (see also (2.24) and (2.25)) leads to equations

$$\begin{aligned} \dot{y}(t) &= f(\alpha, \tilde{x} + \tilde{y}_t) - (\omega(\alpha) + \phi)J(x(\alpha) + y(t)), \\ y(t) &= y(t + p), \end{aligned} \tag{2.34}$$

where $p > 0$ is an unknown period of y and

$$\tilde{x}(\theta) := e^{(\omega(\alpha) + \phi)\theta J} x(\alpha), \quad \tilde{y}_t(\theta) := e^{(\omega(\alpha) + \phi)\theta J} y(t + \theta). \tag{2.35}$$

By normalizing the period $p = 2\pi/\beta$ of y , we obtain the system

$$\begin{aligned} \dot{y}(t) &= \frac{1}{\beta} \left(f(\alpha, \tilde{x} + \tilde{y}_t^\beta) - (\omega(\alpha) + \phi)J(x(\alpha) + y(t)) \right), \\ y(t) &= y(t + 2\pi) \end{aligned} \tag{2.36}$$

with

$$\tilde{y}_t^\beta(\theta) := e^{(\omega(\alpha) + \phi)\theta J} y(t + \beta\theta). \tag{2.37}$$

(b) *Constraint.* This step reflects the specifics of the Hopf bifurcation of *relative* periodic solutions from a *relative* equilibrium. Namely, in order to ensure that the unknown function $y(t)$ is determined uniquely (up to shifting the argument), we will assume that this function satisfies an additional constraint. From assumption (A3) and (2.22)–(2.24), it follows that for any $\alpha \in \mathcal{U}$, the map given by the matrix $D_x\Phi(\alpha, \omega(\alpha), x(\alpha))$ has the one-dimensional kernel span $\{Jx(\alpha)\}$. Denote by $g^\dagger(\alpha)$ the adjoint eigenvector of the transpose matrix $D_x\Phi(\alpha, \omega(\alpha), x(\alpha))^T$ corresponding to the zero eigenvalue:

$$D_x\Phi(\alpha, \omega(\alpha), x(\alpha))^T g^\dagger(\alpha) = 0, \quad \langle g^\dagger(\alpha), Jx(\alpha) \rangle = 1, \quad \alpha \in \mathcal{U}.$$

We will look for a solution to (2.36) with the y -component satisfying the constraint

$$\mathcal{J}_\alpha(y) := \left\langle g^\dagger(\alpha), \int_0^{2\pi} y(t) dt \right\rangle = 0. \quad (2.38)$$

(c) *Setting system (2.36) in functional spaces.* Using the standard identification of a 2π -periodic V -valued function with the V -valued function on S^1 , we reformulate system (2.36) with constraint (2.38) as a \mathcal{K} -equivariant operator equation in the space $\mathbb{R}_+^2 \times \mathscr{W}$, where \mathcal{K} acts trivially on $\mathbb{R}_+^2 := \mathbb{R} \times \mathbb{R}_+$ and $\mathscr{W} := H^1(S^1; V)$ stands for the first Sobolev space equipped with the \mathcal{K} -action given by

$$(h, e^{i\tau})(u)(t) := hu(t + \tau) \quad ((h, e^{i\tau}) \in \mathcal{H} \times S^1 =: \mathcal{K}, u \in \mathscr{W}). \quad (2.39)$$

To this end, denote

$$v_\alpha := D_\omega \Phi(\alpha, \omega(\alpha), x(\alpha)) \in V \quad (2.40)$$

and observe that

$$v_\alpha \in V^{\mathcal{H}}. \quad (2.41)$$

Indeed, the \mathcal{H} -action on V induces the \mathcal{H} -action on $\mathbb{R} \times V$, where \mathcal{H} acts trivially on \mathbb{R} . Since the map $\Phi(\alpha, \cdot, \cdot) : \mathbb{R} \times V \rightarrow V$ is \mathcal{H} -equivariant and $(\omega(\alpha), x(\alpha)) \in (\mathbb{R} \oplus V)^{\mathcal{H}}$, one has that $D\Phi(\alpha, \omega(\alpha), x(\alpha)) : \mathbb{R} \times V \rightarrow V$ is \mathcal{H} -equivariant as well, which implies (2.41).

Next, given an $\alpha \in \mathscr{U}$, we identify a function $z \in \mathscr{W}$ with the pair (y, ϕ) , where $y \in \mathscr{W}$ satisfies (2.38) and $\phi \in \mathbb{R}$, by the relationships

$$z = \phi v_\alpha + y, \quad \mathcal{J}_\alpha(y) = 0, \quad (2.42)$$

and define the corresponding projections

$$\phi = \hat{\pi}_\alpha(z), \quad y = z - \hat{\pi}_\alpha(z)v_\alpha. \quad (2.43)$$

Let us introduce the following operators:

$$\begin{aligned} L : \mathscr{W} &\rightarrow L^2(S^1; V), & L(z) &= \dot{z}, \\ j : \mathscr{W} &\rightarrow C(S^1; V), & j(z) &= z, \end{aligned}$$

where $C(S^1; V)$ is the space of continuous periodic functions equipped with the usual sup-norm. Furthermore, define $F : \mathbb{R}_+^2 \times C(S^1; V) \rightarrow V$ by

$$F(\alpha, \beta, z(t)) := \frac{1}{\beta} \left(f(\alpha, \tilde{x} + \tilde{y}_t^\beta) - (\omega(\alpha) + \phi)J(x(\alpha) + y(t)) \right), \quad t \in \mathbb{R}, \quad (2.44)$$

with $(\alpha, \beta, z) \in \mathbb{R}_+^2 \times C(S^1; V)$, where the function $y \in C(S^1; V)$ and the scalar ϕ are defined by (2.42) and (2.43); $\tilde{x}, \tilde{y}_t^\beta$ are defined in (2.35), (2.37). Next, denote by $\mathcal{N}_F : \mathbb{R}_+^2 \times C(S^1; V) \rightarrow L^2(S^1; V)$ the Nemytsky operator associated with the map F , i.e.,

$$\left(\mathcal{N}_F(\alpha, \beta, z) \right)(t) := F(\alpha, \beta, z(t)), \quad z \in C(S^1; V). \quad (2.45)$$

Since $Lz = Ly$, system (2.36) with constraint (2.38) is equivalent to the following operator equation:

$$Lz = \mathcal{N}_F(\alpha, \beta, j(z)), \quad (\alpha, \beta) \in \mathbb{R}_+^2, \quad z \in \mathscr{W}. \quad (2.46)$$

Using the formulas similar to (2.39), one can define the \mathcal{H} -actions on an $C(S^1, V)$ and $L^2(S^1; V)$. Clearly, all the operators involved in formula (2.46) are \mathcal{K} -equivariant, therefore equation (2.46) can be transformed to a \mathcal{K} -equivariant fixed-point problem in $\mathbb{R}_+^2 \times \mathscr{W}$ as follows. Define the operator $K : \mathscr{W} \rightarrow L^2(S^1; V)$ by

$$K(z) := \frac{1}{2\pi} \int_0^{2\pi} z(t) dt, \quad (2.47)$$

which is simply a projection on the subspace V of constant functions. Then, the operator $L + K : \mathscr{W} \rightarrow L^2(S^1; V)$ is an isomorphism. Put

$$\mathcal{F}(\alpha, \beta, z) := (L + K)^{-1} [\mathcal{N}_F(\alpha, \beta, j(z)) + K(z)], \quad (2.48)$$

$$\mathfrak{F}(\alpha, \beta, z) := z - \mathcal{F}(\alpha, \beta, z). \quad (2.49)$$

In this way, the following equation is equivalent to (2.46):

$$\mathfrak{F}(\alpha, \beta, z) = 0, \quad (\alpha, \beta, z) \in \mathbb{R}_+^2 \times \mathcal{W}. \quad (2.50)$$

(d) *Reduction to twisted degree.* Take $\hat{\alpha}, \mathcal{U}$ and $\mathbf{S}(x(\alpha))$ provided by condition (A3) (see also (2.24)) and β_o provided by (A5). Put

$$M := \{(\alpha, \beta, z) : \alpha \in \mathcal{U}, \beta \in \mathbb{R}_+, z \in \mathbf{S}(x(\alpha))\} \subset \mathbb{R}_+^2 \times \mathcal{W},$$

where

$$\mathcal{W} = V \oplus \overline{\bigoplus_{l=1}^{\infty} \mathcal{W}_l}, \quad \mathcal{W}_l = \{e^{ilt} \cdot y_l : y_l \in V^c\}, \quad (2.51)$$

and the subspace of constant functions is identified with the space V . For any small $\varepsilon > 0$, define a three-dimensional \mathcal{K} -invariant submanifold

$$M_\varepsilon := \{(\alpha, \beta, z) \in M : |\alpha - \hat{\alpha}| < \varepsilon, |\beta - \beta_o| < \varepsilon\} \subset \mathbb{R}_+^2 \times V \subset \mathbb{R}_+^2 \times \mathcal{W}$$

of M . Take a small $r > 0$, define a normal \mathcal{K} -invariant neighborhood of M_ε by

$$\mathcal{N}_{\varepsilon, r} := \{u + v \in \mathbb{R}_+^2 \times \mathcal{W} : u \in M_\varepsilon, v \perp \tau_u(M_\varepsilon), \|v\| < r\}$$

and denote

$$\partial_M^{\mathcal{N}} := \partial(\mathcal{N}_{\varepsilon, r}) \cap M, \quad \partial_r^{\mathcal{N}} := \{u + v \in \mathcal{N}_{\varepsilon, r} : \|v\| = r\}.$$

By condition (A5), one can choose ε and r to be so small that

$$\mathfrak{F}^{-1}(0) \cap \partial(\mathcal{N}_{\varepsilon, r}) \subset \partial_M^{\mathcal{N}} \cup \partial_r^{\mathcal{N}}.$$

Let $\xi : \overline{\mathcal{N}_{\varepsilon, r}} \rightarrow \mathbb{R}$ be a \mathcal{K} -invariant Urysohn function which is positive on $\partial_r^{\mathcal{N}}$ and negative on $\partial_M^{\mathcal{N}}$. Then, the map $\mathfrak{F}_\xi : \overline{\mathcal{N}_{\varepsilon, r}} \subset \mathbb{R}_+^2 \times \mathcal{W} \rightarrow \mathbb{R} \times \mathcal{W}$ given by

$$\mathfrak{F}_\xi(\alpha, \beta, z) := (\xi(\alpha, \beta, z), \mathfrak{F}(\alpha, \beta, z))$$

is \mathcal{K} -equivariant and $\mathcal{N}_{\varepsilon, r}$ -admissible, therefore the \mathcal{K} -equivariant twisted degree

$$\mathcal{K}\text{-deg}(\mathfrak{F}_\xi, \mathcal{N}_{\varepsilon, r}) = \sum_{(\mathcal{L})} n_{\mathcal{L}}(\mathcal{L}) \quad (2.52)$$

is correctly defined.

Proposition 2.1.15. *Let (\mathcal{L}_o) and $(\hat{\alpha}, \hat{\omega}, \mathbf{S}(\hat{x}))$ be as in Theorem 2.1.14 and assume that $n_{\mathcal{L}_o} \neq 0$ in (2.52). Then, the conclusion of Theorem 2.1.14 holds.*

Proof. Following the same argument as in the proof of Theorem 9.28 from [16], one can establish the existence of a continuous branch of solutions (α, β, z) to equation (2.50) bifurcating from $(\hat{\alpha}, \beta_o, \hat{x})$ with symmetry (\mathcal{L}_o) . For any solution (α, β, z) belonging to this branch, take v_α given by (2.40) and identify ϕ and y using (2.42) and (2.43). Then, the quadruplets (α, β, ϕ, y) constitute a continuous branch required in the conclusion of Theorem 2.1.14. Symmetric properties of this branch are guaranteed by condition (2.41) and assumption $n_{\mathcal{L}_o} \neq 0$. \square

(e) *Computation of twisted degree.* To effectively apply Proposition 2.1.15 to proving Theorem 2.1.14, one needs to prove that the hypotheses of Theorem 2.1.14 indeed guarantee a nonzero summand $n_{\mathcal{L}_o}(\mathcal{L}_o)$ in twisted degree (2.52). To estimate (2.52), one can use a computational product formula similar to (2.19) (cf. [16]). To this end, one needs:

- (i) to show that the restriction of $D_z \mathfrak{F}(\alpha, \beta, \hat{x})$ to V is invertible;
- (ii) to link the restriction of $D_z \mathfrak{F}(\alpha, \beta, \hat{x})$ to $\overline{\bigoplus_{l=1}^{\infty} \mathcal{W}_l}$ to crossing numbers.

Both problems require to evaluate the linearization of F (cf. (2.34)–(2.37) and (2.44)–(2.49)). Assuming in (2.44) ϕ and y to be small, one obtains for the first summand (up to the *higher order terms*):

$$\begin{aligned}
 f(\alpha, \tilde{x} + \tilde{y}_t^\beta) &= f(e^{(\omega(\alpha)+\phi)\theta J}(x(\alpha) + y(t + \beta\theta))) = f(e^{(\omega(\alpha)\theta J}x(\alpha)) \\
 &\quad + D_x f(e^{\omega(\alpha)J\theta}x(\alpha)) \left[e^{(\omega(\alpha)+\phi)\theta J}(x(\alpha) + y(t + \beta\theta)) - e^{\omega(\alpha)\theta J}x(\alpha) \right] \quad (2.53) \\
 &\quad + h.o.t.
 \end{aligned}$$

The expression in square brackets reads:

$$\begin{aligned}
& e^{\omega(\alpha)\theta J} e^{\phi\theta J} x(\alpha) + e^{(\omega(\alpha)+\phi)\theta J} y(t + \beta\theta) - e^{\omega(\alpha)\theta J} x(\alpha) \\
&= e^{\omega(\alpha)\theta J} (e^{\phi\theta J} - \text{Id})x(\alpha) + e^{(\omega(\alpha)+\phi)\theta J} y(t + \beta\theta) \\
&= \phi\theta J e^{\omega(\alpha)\theta J} x(\alpha) + e^{\omega(\alpha)\theta J} (\text{Id} + \phi\theta J)y(t + \beta\theta) \\
&= \phi\theta J e^{\omega(\alpha)\theta J} x(\alpha) + e^{\omega(\alpha)\theta J} y(t + \beta\theta).
\end{aligned} \tag{2.54}$$

Combining (2.53) and (2.54) yields

$$\begin{aligned}
f(\alpha, \tilde{x} + \tilde{y}_t^\beta) &= f(e^{\omega(\alpha)\theta J} x(\alpha)) \\
&+ D_x f(e^{\omega(\alpha)\theta J} x(\alpha)) (\phi\theta J e^{\omega(\alpha)\theta J} x(\alpha) + e^{\omega(\alpha)\theta J} y(t + \beta\theta)) + h.o.t.
\end{aligned} \tag{2.55}$$

The linearization of other summands in (2.44) gives:

$$- (\omega(\alpha) + \phi)J(x(\alpha) + y(t)) = -\omega(\alpha)Jy - \phi Jx(\alpha) + h.o.t. \tag{2.56}$$

Combining now (2.55), (2.56), (2.44) with (2.40) and (2.14) yields the following formula for the linearization of F :

$$D_z F(\alpha, \beta, e^{\omega(\alpha)\theta J} x(\alpha)) = \frac{1}{\beta} (\phi v_\alpha + D_x f(\alpha, e^{\omega(\alpha)\theta J} x(\alpha)) e^{\omega(\alpha)\theta J} y(t + \beta\theta) - \omega(\alpha)Jy(t)), \tag{2.57}$$

where y and ϕ are defined by (2.43). Therefore, $D_z \mathfrak{F}(\alpha, \beta, \hat{x})|_V$ has the form

$$D_z \mathfrak{F}(\alpha, \beta, \hat{x})z = \phi D_w \Phi(\alpha, \omega(\alpha), x(\alpha)) + D_x \Phi(\alpha, \omega(\alpha), x(\alpha))y_0, \tag{2.58}$$

where $\phi = \hat{\pi}_\alpha(z) \in \mathbb{R}$ and $y_0 = K(z) \in V$ satisfies $\langle g^\dagger(\alpha), y_0 \rangle = 0$. Due to (2.58), from assumption (A3) (see (2.23)), one obtains that $D_z \mathfrak{F}(\alpha, \beta, \hat{x})|_V$ is invertible in a neighborhood of the point $\alpha = \hat{\alpha}$. Therefore (cf. Step (c) of the proof of Proposition 2.1.8), $D_z \mathfrak{F}(\alpha, \beta, \hat{x})|_V$ does not affect the existence of maximal twisted orbit types in (2.52) and, therefore, is of no consequence for the analysis of maximal twisted orbit types of relative periodic solutions.

On the other hand, $D_z \mathfrak{F}(\alpha, \beta, \hat{x})|_{\mathcal{Y}_l}$ acts as follows (cf. (2.51)):

$$D_z \mathfrak{F}(\alpha, \beta, \hat{x})y_l = D_x f(\alpha, e^{\omega(\alpha)\theta J} x(\alpha)) e^{(\omega(\alpha)J + i\beta l \text{Id})\theta} y_l - (\omega(\alpha)J + i\beta l \text{Id}) y_l. \tag{2.59}$$

Also, since $D_z\mathfrak{F}(\alpha, \beta, \hat{x})$ is \mathcal{K} -equivariant, it preserves \mathcal{K} -isotypical decompositions of \mathscr{W}_l for all l . Take $l = 1$ and consider decomposition (2.31). For the restriction $D_z\mathfrak{F}(\alpha, \beta, \hat{x})|_{U_{j,1}}$, one has:

$$\Delta_j(\alpha, \beta) := \det \left(D_z\mathfrak{F}(\alpha, \beta, \hat{x})|_{U_{j,1}} \right) = \hat{\mathcal{P}}_{j,1}(\alpha, i\beta).$$

Therefore, the degree of the planar vector field Δ_j equals the crossing number (2.33).

Applying the same argument as in Step (c) of the proof of Proposition 2.1.8 completes the proof of Theorem 2.1.14. \square

2.2 DDE Model of a Symmetric Configuration of Passively Mode-Locked Semiconductor Lasers

2.2.1 Mathematical model

In [158], a model for a mode-locked semiconductor laser with gain and absorber sections was introduced as a system of the following delay differential equations:

$$\begin{aligned} \dot{g}(t) &= g_0 - \gamma_g g(t) - \frac{1}{E_g} e^{-q(t)} (e^{g(t)} - 1) |a(t)|^2, \\ \dot{q}(t) &= q_0 - \gamma_q q(t) - \frac{1}{E_q} (1 - e^{-q(t)}) |a(t)|^2, \\ \dot{a}(t) &= -\gamma a(t) + \gamma \sqrt{\kappa} \exp \left[\frac{(1 - i\eta_g)g(t - T) - (1 - i\eta_q)q(t - T)}{2} \right] a(t - T). \end{aligned} \tag{2.60}$$

The complex-valued function $a(t)$ is the field amplitude at the entrance of the absorber section with $|a(t)|^2$ representing the optical power. The real-valued functions $g(t)$ and $q(t)$ represent saturable gain and losses, respectively, and η_g, η_q are the linewidth enhancement factors corresponding to self-phase modulation. The constants g_0 and q_0 stand for unsaturated gain and absorption. The constants γ_g and γ_q are the carrier density relaxation rates in the gain and absorbing sections; E_g and E_q are the saturation energies in these sections; the ratio $s = E_g/E_q$ is important for laser dynamics. Finally, T stands for the cold

cavity round-trip time, and $\sqrt{\kappa}$ is the linear nonresonant attenuation factor per pass. The parameter g_0 is proportional to the pump current, which is the physical control parameter.

Assume $(g(t), q(t), a(t))^T \in \mathbb{R} \oplus \mathbb{R} \oplus \mathbb{C} \simeq \mathbb{R}^4 =: \mathcal{V}$ and equip \mathcal{V} with the natural S^1 -representation (trivial on (g, q) -components and complex multiplication on a -component). Clearly, system (2.60) is S^1 -equivariant. In what follows, assuming the value $\alpha := g_0$ to be the bifurcation parameter, we will show how Proposition 2.1.8 (resp. Theorem 2.1.14) can be used to study bifurcations of relative equilibria (resp. relative periodic solutions) for the network of identical oscillators (2.60) coupled in a symmetric fashion.

Let $\mathfrak{f} : \mathbb{R} \times C_{-T}(\mathcal{V}) \rightarrow \mathcal{V}$ be the map induced by the right-hand side of system (2.60). Put $V := \mathcal{V}^n$ and define the map $f_o : \mathbb{R} \times C_{-T}(V) \rightarrow V$ by

$$f_o(\alpha, x_t) = \left(\mathfrak{f}(\alpha, x_t^1), \mathfrak{f}(\alpha, x_t^2), \dots, \mathfrak{f}(\alpha, x_t^n) \right), \quad (2.61)$$

where $x = (x^1, x^2, \dots, x^n) \in V$. In general, the network dynamics of x is given by the following equation:

$$\dot{x} = f_o(\alpha, x_t) + g(x_t), \quad x \in V, \quad (2.62)$$

where function $g : C_{-T}(V) \rightarrow V$ describes the interaction between components x^j for $j = 1, \dots, n$. For our considerations, we assume that

- (i) g is linear,
- (ii) g depends only on $x(t)$, i.e., the delayed terms are not present in the coupling,
- (iii) coupling is symmetric with respect to some finite group Γ ,
- (iv) coupling terms appear only in the equation for the a -component of each x^j , $j = 1, \dots, n$.

The latter assumption corresponds to the physically meaningful situation when the lasers are coupled via evanescent fields. We note that the form of coupling terms depends on

the system configuration as well as on the model setting and simplifying assumptions. For example, delayed coupling of the same equations (2.60) was considered in [138].

Let $C : \mathcal{V} \rightarrow \mathcal{V}$ be a linear operator with the matrix

$$C := \begin{bmatrix} 0 & 0 & 0 \\ 0 & 0 & 0 \\ 0 & 0 & e^{i\psi} \end{bmatrix}. \quad (2.63)$$

Then, using the assumptions above, one can rewrite equation (2.62) as follows:

$$\dot{x} = f(\alpha, x, x_t) := f_o(\alpha, x_t) + \eta \mathcal{C} x, \quad x \in V. \quad (2.64)$$

Here \mathcal{C} is the coupling matrix given by

$$\mathcal{C} := \mathcal{K} \otimes C, \quad (2.65)$$

where \mathcal{K} is a symmetric $\{0, 1\}$ -valued adjacency matrix of the network and “ \otimes ” stands for the Kronecker product of the matrices. Parameters $\eta, \psi \in \mathbb{R}$ correspond to the strength and the phase of coupling, respectively.

Remark 2.2.1. Recall, if $\mathbf{S}(\hat{x})$ is a relative equilibrium for system (2.64), then symmetries of $\mathbf{S}(\hat{x})$ are completely determined by a (twisted) isotropy subgroup $\mathcal{G}_{\hat{x}}$ with respect to the $\mathcal{G} := \Gamma \times S^1$ -action.

Note that $x_o(\alpha) := (\alpha/\gamma_g, q_0/\gamma_q, 0)^T \in \mathcal{V}$ is an equilibrium of system (2.60) for any α , hence

$$\mathcal{O}(\alpha) := (x_o(\alpha), x_o(\alpha), \dots, x_o(\alpha)) \in V$$

is an equilibrium of system (2.64) for any α . Also

$$D_{\mathbf{x}}f(\alpha, x_o(\alpha))|_{\mathcal{V}} = \begin{bmatrix} -\gamma_g & 0 & 0 \\ 0 & -\gamma_q & 0 \\ 0 & 0 & \left(\sqrt{\kappa} \exp \left[\frac{(1-i\eta_g)\frac{\alpha}{\gamma_g} - (1-i\eta_q)\frac{q_0}{\gamma_q}}{2} \right] - 1 \right) \gamma \end{bmatrix}. \quad (2.66)$$

2.2.2 D_n -configuration of identical semiconductor lasers

In this subsection, we consider equation (2.64) for the D_n -symmetric network, i.e., the adjacency matrix \mathcal{K} in (2.65) is

$$\mathcal{K} := \begin{bmatrix} 0 & 1 & 0 & \dots & 0 & 1 \\ 1 & 0 & 1 & \dots & 0 & 0 \\ 0 & 1 & 0 & \dots & 0 & 0 \\ \vdots & \vdots & \vdots & \ddots & \vdots & \vdots \\ 0 & 0 & 0 & \dots & 0 & 1 \\ 1 & 0 & 0 & \dots & 1 & 0 \end{bmatrix}.$$

This system was recently studied in [125] as a model of an array of mode-locked lasers coupled via evanescent fields in a ring geometry.

Clearly, the space V is an orthogonal $D_n \times S^1$ -representation, where D_n -action on V is defined by permutation of the coordinates of the vector $x \in V$. More precisely, D_n stands for the dihedral group being the group of symmetries of a regular n -gon, i.e., one can consider it to be a subgroup of the symmetric group S_n on the set $\{1, 2, \dots, n\}$ labeling the vertices of a regular n -gon. This group is generated by the “rotation” $\xi := (1, n, n-1, \dots, 2)$ and the “reflection” $\kappa := (2, n)(3, n-1) \dots (m, n-m)$, where $m = \lfloor n/2 \rfloor$. Then, the $D_n \times S^1$ -action on V is given by

$$(h, e^{i\tau})x = (e^{i\tau}x^{h(1)}, e^{i\tau}x^{h(2)}, \dots, e^{i\tau}x^{h(n)}), \quad h \in D_n, \quad e^{i\tau} \in S^1, \quad (2.67)$$

where $x = (x^1, x^2, \dots, x^n) \in V$ and $e^{i\tau}$ acts on $x^j \in \mathcal{V} \simeq \mathbb{R} \oplus \mathbb{R} \oplus \mathbb{C}$ trivially on the first two components and by complex multiplication on the \mathbb{C} -component for all $j = 1, \dots, n$. Obviously, system (2.64) satisfies condition (A0).

2.2.3 D_8 -configuration: bifurcation of symmetric relative equilibria

Hereafter, we will restrict ourselves to the case $n = 8$.

Isotypical decomposition and maximal twisted orbit types. To apply Proposition 2.1.8 for studying relative equilibria bifurcating from the equilibrium $\mathcal{O}(\alpha)$, observe that V admits the isotypical D_8 -decomposition:

$$V = \bigoplus_{j=0}^4 W_j, \quad (2.68)$$

where W_j is modeled on \mathcal{V}_j , \mathcal{V}_1 is a one-dimensional trivial representation, \mathcal{V}_4 is a one-dimensional D_8/D_4 -representation and $\{\mathcal{V}_j\}_{j=1}^3$ are three two-dimensional nonequivalent irreducible representations with different actions of the rotational generator (for more details, see [16]). Observe also (see (2.15)) that decomposition (2.68) can be refined to the $D_8 \times S^1$ -decomposition: $W_j = V_j^0 \oplus V_{j,1}$, $j = 0, \dots, 4$, where V_j^0 is modeled on $\mathcal{V}_j \simeq \mathbb{R}^2$ and S^1 acts trivially, while $V_{j,1}$ is modeled on $\mathcal{V}_{j,1} \simeq \mathbb{C}^2$ and S^1 acts by complex multiplication (see [16]). Clearly, $\dim W_0 = \dim W_4 = 4$, while $\dim W_1 = \dim W_2 = \dim W_3 = 8$.

Table 2.1: Maximal twisted orbit types in each isotypical component of the D_8 -representation V .

Isotypical component	Maximal twisted orbit types
$V_{0,1}$	$(D_8 \times \{1\}) \simeq (D_8)$
$V_{1,1}$	$(\mathbb{Z}_8^{t_1}), (D_2^d), (\tilde{D}_2^d)$
$V_{2,1}$	$(\mathbb{Z}_8^{t_2}), (D_4^d), (\tilde{D}_4^d)$
$V_{3,1}$	$(\mathbb{Z}_8^{t_3}), (D_2^d), (\tilde{D}_2^d)$
$V_{4,1}$	(D_8^d)

Let us now describe maximal twisted orbit types in V . By inspection, for any $j = 0, 1, 2, 3, 4$, if (\mathcal{H}_o) is a maximal orbit type in $V_{j,1}$, then (\mathcal{H}_o) is a maximal twisted type in V (see Proposition 2.1.8, assumption (i)). In turn, the list of maximal twisted orbit types in any $V_{j,1}$ is given in Table 2.1. We refer to Appendix A.1 for the explicit description of all these subgroups, see also Remark 2.2.1.

Equivariant spectral reduction and condition (A1). The linearization $D_{\mathbf{x}}f_o(\alpha, \mathbf{x}) : \mathbb{R} \times C_{-r}(V) \rightarrow V$ of system (2.64) at $\mathcal{O}(\alpha)$ respects isotypical decomposition (2.68). To describe its action on isotypical components, define a (real) 4×4 -matrix ξ by

$$\xi := \begin{bmatrix} 1 & 0 & 0 \\ 0 & 1 & 0 \\ 0 & 0 & e^{i\frac{2\pi}{8}} \end{bmatrix} \quad (2.69)$$

and put

$$A_j := D_{\mathbf{x}}f(\alpha, x_o(\alpha))|_V + \eta C(\xi^j + \xi^{-j}), \quad j = 0, 1, 2, 3, 4 \quad (2.70)$$

Then,

$$D_{\mathbf{x}}f_o(\alpha, \mathcal{O}(\alpha))|_{W_j} = \begin{cases} A_j & \text{if } j = 0, 4, \\ \begin{bmatrix} A_j & 0 \\ 0 & A_j \end{bmatrix} & \text{if } j = 1, 2, 3. \end{cases} \quad (2.71)$$

Since the action of S^1 on (g, q) -components of (2.60) is trivial, it follows from (2.66) and (2.69)–(2.71) that $\det(D_{\mathbf{x}}f_o(\alpha, \mathcal{O}(\alpha))|_{V^{S^1}}) = (\gamma_g \gamma_q)^8 \neq 0$, hence (see (2.12)), $\mathcal{P}_0(\alpha, 0, \mathcal{O}(\alpha)) \neq 0$ so that system (2.64) satisfies condition (A1).

Characteristic quasi-polynomial. Next, let us consider the characteristic quasi-polynomial $\mathcal{P}_*(\alpha, \lambda, \mathcal{O}(\alpha))$ (see (2.12)). For any $j = 0, 1, 2, 3, 4$, put

$$\widetilde{\mathcal{P}}_j := \lambda + \gamma - \gamma\sqrt{\kappa} \exp \left[\left(\frac{\alpha}{2\gamma_g} - \frac{q_0}{2\gamma_q} \right) + i \left(\frac{\eta_q q_0}{2\gamma_q} - \frac{\eta_g \alpha}{2\gamma_g} \right) \right] e^{-\lambda T} + 2\eta \cos \left(\frac{2\pi j}{8} \right) e^{i\psi}. \quad (2.72)$$

Then, the restriction of the characteristic quasi-polynomial to $V_{j,1}$ reads

$$\mathcal{P}_{j,1}(\alpha, \lambda, \mathcal{O}(\alpha)) = \begin{cases} \widetilde{\mathcal{P}}_j & \text{if } j = 0, 4, \\ (\widetilde{\mathcal{P}}_j)^2 & \text{if } j = 1, 2, 3, \end{cases} \quad (2.73)$$

so that

$$\mathcal{P}_*(\alpha, \lambda, \mathcal{O}(\alpha)) = \prod_{j=0}^4 \mathcal{P}_{j,1}(\alpha, \lambda, \mathcal{O}(\alpha)). \quad (2.74)$$

Condition (A2): existence of centers. In order to simplify the notations, put

$$x(\alpha) := \frac{\alpha}{2\gamma_g} - \frac{q_o}{2\gamma_q}, \quad y(\alpha) := \frac{\eta_q q_o}{2\gamma_q} - \frac{\eta_g \alpha}{2\gamma_g}, \quad (2.75)$$

and

$$a_j + ib_j := 2\eta e^{i\psi} \cos\left(\frac{2\pi j}{8}\right). \quad (2.76)$$

Let us identify the values of α for which $\mathcal{O}(\alpha)$ is a center, i.e., we are looking for those values of α for which there exists $\omega > 0$ such that $\mathcal{P}_*(\alpha, i\omega, \mathcal{O}(\alpha)) = 0$. Equivalently,

$$i\omega = -\gamma + \gamma\sqrt{\kappa} \exp(x(\alpha) + i(y(\alpha) - \omega T)) + a_j + ib_j, \quad j = 0, 1, 2, 3, 4.$$

This complex equation can be reduced to the real equation

$$\tan(y(\alpha) - \omega(\alpha)T) = \frac{\omega(\alpha) - b_j}{\gamma - a_j}, \quad j = 0, 1, 2, 3, 4, \quad (2.77)$$

with

$$\omega(\alpha) := \gamma\sqrt{\kappa} e^{x(\alpha)} \sqrt{1 - \frac{(\gamma - a_j)^2}{\gamma^2 \kappa e^{2x(\alpha)}}} + b_j. \quad (2.78)$$

From (2.75) and (2.78), it follows that for α large enough, the right-hand side of (2.77) is close to

$$\frac{\gamma\sqrt{\kappa}}{\gamma - a_j} \exp\left(\frac{\alpha}{2\gamma_g} - \frac{q_o}{2\gamma_q}\right).$$

Combining this with periodicity of the tangent function, one concludes that (2.77) has infinitely many solutions α together with the corresponding limit frequencies $\omega(\alpha)$.

Proposition 2.2.2. *Suppose $\alpha = \alpha_o^j$ is a root of (2.77), (2.78) for some $j = 0, 1, 2, 3, 4$ and*

$$\gamma > 2\eta \cos(\psi) \cos\left(\frac{2\pi j}{8}\right) \quad \text{and} \quad \omega(\alpha_o^j) > 2\eta \cos(\psi) \sin\left(\frac{2\pi j}{8}\right). \quad (2.79)$$

Then, the following continuous branches of relative equilibria bifurcate from the equilibrium $(\alpha_o^j, \mathcal{O}(\alpha_o^j))$ of equation (2.64):

- for $j = 0$, a branch with symmetry (D_8) ;

- for $j = 1$, two branches with symmetry $(\mathbb{Z}_8^{t_1})$, four branches with symmetry (D_2^d) and four branches with symmetry (\tilde{D}_2^d) ;
- for $j = 2$, two branches with symmetry $(\mathbb{Z}_8^{t_2})$, two branches with symmetry (D_4^d) and two branches with symmetry (\tilde{D}_4^d) ;
- for $j = 3$, two branches with symmetry $(\mathbb{Z}_8^{t_3})$, four branches with symmetry (D_2^d) and four branches with symmetry (\tilde{D}_2^d) ;
- for $j = 4$, a branch with symmetry (D_8^d) .

Proof. Let us show that the center $\mathcal{O}(\alpha_o^j)$ is isolated (cf. condition (A2)). Put $\lambda(\alpha) := \mathbf{r}(\alpha) + i\omega(\alpha)$ and rewrite the characteristic equation as follows (cf. (2.72)–(2.76)):

$$\begin{aligned}\mathbf{r}(\alpha) &= -\gamma + \gamma\sqrt{\kappa} e^{x(\alpha) - \mathbf{r}(\alpha)T} \cos(y(\alpha) - \omega(\alpha)T) + a_j, \\ \omega(\alpha) &= \gamma\sqrt{\kappa} e^{x(\alpha) - \mathbf{r}(\alpha)T} \sin(y(\alpha) - \omega(\alpha)T) + b_j,\end{aligned}\tag{2.80}$$

where $j = 0, \dots, 4$. Assume that for $\alpha = \alpha_o$, the equilibrium $\mathcal{O}(\alpha_o)$ is a center with the limit frequency $\omega(\alpha_o) = \omega_o$ and put

$$x_o := x(\alpha_o^j), \quad y_o := y(\alpha_o^j), \quad x'_o := x'(\alpha_o^j) = \frac{1}{2\gamma_g}, \quad y'_o := y'(\alpha_o^j) = -\frac{\eta_g}{2\gamma_q}.\tag{2.81}$$

Differentiating (2.80) with respect to α , one obtains

$$\begin{aligned}\mathbf{r}'(\alpha_o^j) &= (\gamma - a_j)(x'_o - \mathbf{r}'(\alpha_o^j)T) - (\omega_o - b_j)(y'_o - \omega'(\alpha_o^j)T), \\ \omega'(\alpha_o^j) &= (\omega_o - b_j)(x'_o - \mathbf{r}'(\alpha_o^j)T) + (\gamma - a_j)(y'_o - \omega'(\alpha_o^j)T),\end{aligned}$$

which leads to

$$\mathbf{r}'(\alpha_o^j) = \frac{[(\gamma - a_j)^2 x'_o + (\omega_o - b_j)^2 y'_o]T + (\gamma - a_j)x'_o - (\omega_o - b_j)y'_o}{(1 + (\gamma - a_j)T)^2 + (\omega_o - b_j)^2 T^2}.\tag{2.82}$$

Formulas (2.81), (2.82) show that $\mathbf{r}'(\alpha_o^j) > 0$ provided that relations (2.79) are satisfied. Hence, relations (2.79) guarantee that the transversality condition for $\lambda(\alpha_o^j)$ is satisfied at

$\alpha = \alpha_o^j$, in which case the center $\mathcal{O}(\alpha_o^j)$ is isolated. Moreover, relations (2.79) imply that condition (iii) from Proposition 2.1.8 is satisfied. Since the other conditions have been verified, the result follows. \square

Recall that η stands for the coupling strength. In particular, conditions (2.79) are satisfied for all j for any relatively weak coupling.

Table 2.2 illustrates Proposition 2.2.2. Assume that $\eta = 2$, $\alpha_g = 1$, $\alpha_q = 1$, $\gamma_g = 10^{-2}$, $\gamma_q = 1$, $\gamma = 15$, $\kappa = \sqrt{0.2}$, $q_0 = 2$, $E_g = 1$, $E_q = 0.1$, $T = 2.5$. For this set of parameters conditions (2.79) are fulfilled for all $(\alpha, \omega(\alpha))$ satisfying equations (2.77), (2.78). For $\alpha < 0.036$, the equilibrium $\mathcal{O}(\alpha)$ is stable. In Table 2.2, we localize Hopf bifurcation points along the horizontal direction, and specify isotypical components $V_{j,1}$ along the vertical direction. In each cell, we indicate the number of unstable roots of the corresponding characteristic polynomial $\mathcal{P}_{j,1}$ defined by (2.73). One can easily see a change of stability as α increases. An entry of the table is circled to indicate a “jump” in the number of unstable roots and hence a Hopf bifurcation point. In particular, Proposition 2.2.2 guarantees Hopf bifurcations of branches of relative equilibria as follows:

- (i) with symmetry (D_8) for $\alpha \approx 0.03606$;
- (ii) with symmetries $(\mathbb{Z}_8^{t_1}), (D_2^d)$ and (\tilde{D}_2^d) for $\alpha \approx 0.03607$;
- (iii) with symmetries $(\mathbb{Z}_8^{t_2}), (D_4^d)$ and (\tilde{D}_4^d) for $\alpha \approx 0.0361$;
- (iv) with symmetries $(\mathbb{Z}_8^{t_3}), (D_2^d)$ and (\tilde{D}_2^d) for $\alpha \approx 0.03613$;
- (v) with symmetry (D_8) for $\alpha \approx 0.03617$;
- (vi) with symmetries (D_8^d) and $(\mathbb{Z}_8^{t_1})$ for $\alpha \approx 0.0362$,

to mention a few (see Proposition 2.2.2 for the number of branches of each type).

Table 2.2: Number of unstable eigenvalues in each isotypical component for the equilibrium $\mathcal{O}(\alpha)$

Isotypical component	Intervals for values of parameter $\alpha \cdot 10^2$										
	[3.6, 3.606]	[3.6065, 3.607]	[3.6075, 3.6095]	[3.61, 3.613]	[3.6135, 3.617]	[3.618, 3.62]	[3.6205, 3.622]				
$V_{0,1}$	0	(2)	2	2	2	(4)	4				4
$V_{1,1}$	0	0	(4)	4	4	4	4				(8)
$V_{2,1}$	0	0	0	(4)	4	4	4				4
$V_{3,1}$	0	0	0	0	(4)	4	4				4
$V_{4,1}$	0	0	0	0	0	0	0				(2)
$\bigoplus_{j=0}^4 V_{j,1}$	0	2	6	10	14	16	22				

2.2.4 D_8 -configuration: bifurcation of relative periodic solutions

Application of Theorem 2.1.14 to the laser system

In this subsection, we show how Theorem 2.1.14 can be applied to classify symmetries of relative periodic solutions, which bifurcate from branches of relative equilibria of system (2.64) with $n = 8$. We restrict the presentation to bifurcations from relative equilibria that have 3 particular types of symmetry, (D_8) , $(\mathbb{Z}_8^{t_1})$, and (D_8^d) . These branches are listed under the items (i), (ii), and (vi), respectively, on page 53. Further, an infinite number of Hopf bifurcations of relative periodic solutions occurs along each branch of relative equilibria. To be specific, we consider a few successive Hopf bifurcations at the beginning of each branch of our choice. In contrast to the application of Proposition 2.1.8 to studying bifurcation of relative equilibria (in which case, all the necessary symbolic computations were explicitly presented), we have to resort to numerical computations for verifying conditions (A3), (A5) and (ii), (iii) of Theorem 2.1.14.

Based on the numerical evidence, Theorem 2.1.14 allows us to predict the following bifurcations of branches of relative periodic solutions.

Consider the (D_8) -symmetric branch of relative equilibria, which is denoted by (i) on page 53. The following branches of relative periodic solutions bifurcate from this branch (we refer to Appendix A for the notation):

- (i) with symmetries $(\mathbb{Z}_8^{t_1})$, (D_2^d) , (\tilde{D}_2^d) for $\alpha \approx 0.0386$;
- (ii) with symmetries $(\mathbb{Z}_8^{t_2})$, (D_4^d) , (\tilde{D}_4^d) for $\alpha \approx 0.0533$;
- (iii) with symmetry (D_8) for $\alpha \approx 0.0602$.

Consider the $(\mathbb{Z}_n^{t_1})$ -symmetric branch of relative equilibria, which is denoted by (ii) on page 53. The following branches of relative periodic solutions bifurcate from this branch:

- (i) with symmetries $(\mathbb{Z}_8^{t_1})$ and $(\mathbb{Z}_8^{t_2})$ for $\alpha \approx 0.0366$;

- (ii) with symmetry $(\mathbf{Z}_8^{t_3})$ for $\alpha \approx 0.0399$;
- (iii) with symmetries $(\mathbf{Z}_8^{t_1})$ and $(\mathbf{Z}_8^{t_3})$ for $\alpha \approx 0.0416$;
- (iv) with symmetry (\mathbf{Z}_8^c) for $\alpha \approx 0.064$;
- (v) with symmetry $(\mathbf{Z}_8^{t_2})$ for $\alpha \approx 0.0641$;
- (vi) with symmetry (\mathbf{Z}_8) for $\alpha \approx 0.0788$.

Consider the (D_8^d) -symmetric branch of relative equilibria, which is denoted by (vi) on page 53. The following branches of relative periodic solutions bifurcate from this branch:

- (i) with symmetries $(\mathbf{Z}_8^{t_2}), (D_4^d), (\tilde{D}_4^d)$ for $\alpha \approx 0.0384$;
- (ii) with symmetry (D_8) for $\alpha \approx 0.0405$;
- (iii) with symmetries $(\mathbf{Z}_8^{t_3}), (D_2^d), (\tilde{D}_2^d)$ for $\alpha \approx 0.0539$;
- (iv) with symmetry (D_8^d) for $\alpha \approx 0.066$;
- (v) with symmetry (D_8^d) for $\alpha \approx 0.0731$;
- (vi) with symmetries $(\mathbf{Z}_8^{t_1}), (D_2^d), (\tilde{D}_2^d)$ for $\alpha \approx 0.0757$.

Further bifurcations along these and other branches of relative equilibria can be classified in a similar manner. Note that branches of relative periodic solutions with symmetries $(\mathbf{Z}_8^{t_j}), (D_4^d), (\tilde{D}_4^d)$ come in pairs, while the branches with symmetries $(D_2^d), (\tilde{D}_2^d)$ appear in quadruples.

In the rest of this subsection, we show how the above bifurcations can be deduced from Theorem 2.1.14. Given a relative equilibrium with symmetry group \mathcal{H} , the verification of assumptions of Theorem 2.1.14 splits into the following steps: (a) finding the isotypical decomposition of $\mathcal{H} \times S^1$ -representation (2.31) and providing a list of maximal orbit types in each

component (see Subsections 2.2.4 and 2.2.4); (b) obtaining characteristic quasi-polynomials associated with each isotypical component (see Subsection 2.2.4); and, (c) analyzing roots of the quasi-polynomials and verifying conditions (A3), (A5), (i) and (ii) of Theorem 2.1.14 (see Subsections 2.2.4). The last step relies on numerical computations. Condition (A3) is reduced to an explicit inequality in Subsection 2.2.4.

Symmetries of relative equilibria

To begin with, below we will describe some of the relative equilibria identified in the previous subsection more explicitly.

Observe first that the group D_n described in Subsection 2.2.2 can be identified (for convenience) with $D_n = \{1, \xi, \dots, \xi^{n-1}, \kappa, \xi\kappa, \dots, \xi^{n-1}\kappa\}$, where

$$\xi := e^{\frac{2\pi i}{n}} = \begin{bmatrix} \cos(\frac{2\pi}{n}) & -\sin(\frac{2\pi}{n}) \\ \sin(\frac{2\pi}{n}) & \cos(\frac{2\pi}{n}) \end{bmatrix} \quad \text{and} \quad \kappa = \begin{bmatrix} 1 & 0 \\ 0 & -1 \end{bmatrix}. \quad (2.83)$$

Also, recall that the action of $\xi, \kappa \in D_n$ on $x = (g, q, a)^T \in \mathbb{R} \oplus \mathbb{R} \oplus \mathbb{C} \simeq \mathcal{V}$ is defined as:

$$\xi(g, q, a)^T = (g, q, \xi a)^T, \quad \kappa(g, q, a)^T = (g, q, \bar{a})^T.$$

Let $\mathbf{S}(\hat{x})$ be a relative equilibrium of system (2.64) (see Remark 2.2.1). Fix an integer l satisfying $0 \leq l < n$, put $\zeta := \xi^l$ and assume that

$$\hat{x} = (\hat{x}^o, \zeta \hat{x}^o, \zeta^2 \hat{x}^o, \dots, \zeta^{n-1} \hat{x}^o), \quad \hat{x}^o = (g, q, a) \in \mathcal{V}, \quad a \neq 0. \quad (2.84)$$

One can easily verify that in this case, under the $\mathcal{G} := D_n \times S^1$ -action, the isotropy of \hat{x} is completely determined by the relations

$$(\zeta^k, z) \in \mathcal{G}_{\hat{x}} \Leftrightarrow z\zeta^{-k} = 1 \Leftrightarrow z = \xi^{-lk},$$

where $0 \leq k \leq n-1$, and

$$(\kappa, z) \in \mathcal{G}_{\hat{x}} \Leftrightarrow l = 0 \text{ and } z = 1.$$

By direct verification, \hat{x} is of the form (2.84) if and only if

$$(\mathcal{G}_{\hat{x}}) = \begin{cases} (D_n \times \{1\}) \simeq (D_n) & \text{if } l = 0, \\ D_n^d & \text{if } l = \frac{n}{2}, \\ \mathbb{Z}_n^{t_l} := \left\{ (\xi^k, \xi^{kl}) \in D_n \times S^1 : k = 0, 1, \dots, n-1 \right\} & \text{otherwise.} \end{cases} \quad (2.85)$$

Remark 2.2.3. In what follows, as in Subsection 2.2.3, we will restrict ourselves to the case $n = 8$. As it was established in Table 2.1, twisted subgroups listed in (2.85) do not exhaust possible symmetries of relative equilibria of system (2.64). For example, one can easily check that if

$$\hat{x} = (\hat{x}^1, \hat{x}^2, \hat{x}^3, \hat{x}^4, \xi^{\frac{n}{2}} \hat{x}^1, \xi^{\frac{n}{2}} \hat{x}^2, \xi^{\frac{n}{2}} \hat{x}^3, \xi^{\frac{n}{2}} \hat{x}^4), \quad \hat{x}^i \in \mathcal{V},$$

then $(\mathcal{G}_{\hat{x}}) = (D_2^d)$, and if

$$\hat{x} = (\hat{x}^1, \xi^{\frac{n}{2}} \hat{x}^1, \hat{x}^2, \xi^{\frac{n}{2}} \hat{x}^2, \hat{x}^3, \xi^{\frac{n}{2}} \hat{x}^3, \hat{x}^4, \xi^{\frac{n}{2}} \hat{x}^4), \quad \hat{x}^i \in \mathcal{V},$$

then $(\mathcal{G}_{\hat{x}}) = (\tilde{D}_2^d)$. However, in order to keep this chapter reasonably simple and of appropriate size, we omit these cases.

$\mathcal{G}_{\hat{x}}$ -isotypical decomposition of V^c and maximal twisted orbit types

(a) Identification. In this subsection, we describe the \mathcal{H} -isotypical decomposition of the space V^c , where $\mathcal{H} = \mathcal{G}_{\hat{x}}$ for each isotropy group $\mathcal{G}_{\hat{x}}$ defined in (2.85). We will assume that $n > 2$ is an even integer and put $r := n/2$. Notice that $D_n \times \{1\}$ and D_n^d can be identified with D_n while $\mathbb{Z}_n^{t_l}$ can be identified with \mathbb{Z}_n .

Complex irreducible \mathbb{Z}_n -representations \mathcal{U}'_j can be easily described: (a) the trivial representation $\mathcal{U}'_0 = \mathbb{C}$, (b) $\mathcal{U}'_r = \mathbb{C}$ with the natural antipodal action of $\mathbb{Z}_2 := \mathbb{Z}_n/\mathbb{Z}_r$, and (c) $\mathcal{U}'_{\pm j} = \mathbb{C}$, where the \mathbb{Z}_n -action is given by

$$\xi z = \xi^{\pm j} \cdot z, \quad z \in \mathbb{C}.$$

In the case of the group D_n , we have the following irreducible D_n -representations: (a) the trivial representation $\mathcal{U}_0 = \mathbb{C}$, (b) the representation $\mathcal{U}_r = \mathbb{C}$ with the natural antipodal action of $\mathbb{Z}_2 := D_n/D_r$, and (c) the representations $\mathcal{U}_j = \mathbb{C} \oplus \mathbb{C}$ for $0 < j < r$ with the D_n -action given by

$$\xi(z_1, z_2) = (\xi^j \cdot z_1, \xi^{-j} \cdot z_2), \quad \kappa(z_1, z_2) = (z_2, z_1) \quad (z_1, z_2 \in \mathbb{C}).$$

Notice that $\mathbb{Z}_n \subset D_n$, therefore, for $0 < j < r$, we have the decomposition

$$\mathcal{U}_j = \mathcal{U}'_j \oplus \mathcal{U}'_{-j}.$$

We do not consider other (one-dimensional) irreducible D_n -representations since they are irrelevant for the decomposition of the substitutional D_n -representation we are dealing with in what follows.

If $\mathcal{H} \simeq \mathbb{Z}_n$, then the complex \mathcal{H} -representation V^c admits the following \mathbb{Z}_n -isotypical decomposition

$$V^c = U_0 \oplus U_1^+ \oplus U_1^- \oplus \cdots \oplus U_{r-1}^+ \oplus U_{r-1}^- \oplus U_r, \quad (2.86)$$

where the components U_j^\pm (resp. U_0 and U_r) are modeled on the complex irreducible \mathbb{Z}_n -representation $\mathcal{U}'_{\pm j}$ (resp. \mathcal{U}'_0 and \mathcal{U}'_r). Furthermore, if $\mathcal{H} \simeq D_n$, then

$$V^c = U_0 \oplus U_1 \oplus \cdots \oplus U_{r-1} \oplus U_r, \quad (2.87)$$

where $U_j = U_j^+ \oplus U_j^-$ for $0 < j < r$ and the isotypical component U_j is modeled on the irreducible D_n -representation \mathcal{U}_j . Also, U_0 and U_r are modeled on \mathcal{U}_0 and \mathcal{U}_r , respectively.

Remark 2.2.4. (i) The complexification \mathcal{V}^c of the space $\mathcal{V} := \mathbb{R}^2 \oplus \mathbb{C} = \mathbb{R}^2 \oplus (\mathbb{R} \oplus \mathbb{R})$ can be represented as

$$\mathcal{V}^c = \mathbb{C}^2 \oplus (\mathbb{C} \oplus \mathbb{C}) = \mathbb{C}^4, \quad (2.88)$$

thus $V^c = (\mathcal{V}^c)^n = (\mathbb{C}^4)^n$ for which decomposition (2.86) takes place.

(ii) Any complex \mathcal{H} -equivariant linear operator $A : V^c \rightarrow V^c$ is also \mathbb{Z}_n -equivariant, thus it preserves isotypical decomposition (2.86).

(iii) Clearly, the space V^c admits a natural S^1 -action induced by the complex multiplication. Put $\mathcal{K} := \mathcal{H} \times S^1$. Then (cf. (2.31)), the S^1 -action converts the (complex) \mathcal{H} -isotypical decomposition (2.87) into a (real) \mathcal{K} -isotypical decomposition

$$V^c = U_{0,1} \oplus U_{1,1} \oplus \cdots \oplus U_{r-1,1} \oplus U_{r,1}. \quad (2.89)$$

(iv) By inspection, for $n = 8$ (our case study), if (H) is a maximal twisted orbit type in an isotypical component of V^c , then (H) is a maximal twisted orbit type in V^c itself.

(b) $\mathcal{H} := D_n \times \{1\}$ -isotypical decomposition of V^c . One can explicitly describe the \mathcal{H} -isotypical components of (2.87) as follows:

$$\begin{aligned} U_0 &= \left\{ (z, z, \dots, z) : z \in \mathbb{C}^4 \right\}, \\ U_j &= U_j^+ \oplus U_j^-, \quad U_j^\pm := \left\{ (z, \xi^{\pm j} z, \dots, \xi^{\pm j(n-1)} z) : z \in \mathbb{C}^4 \right\} \quad (0 < j < r), \\ U_r &= \{(z, -z, z, -z, \dots, z, -z) : z \in \mathbb{C}^4\}. \end{aligned}$$

Further, one can easily verify that the coupling matrix $\mathcal{C} : V^c \rightarrow V^c$ given by (2.65) preserves the \mathcal{H} -isotypical components. Put

$$\mathcal{C}_j^\pm := \mathcal{C}|_{U_j^\pm}, \quad \mathcal{C}_0 := \mathcal{C}|_{U_0}, \quad \mathcal{C}_r := \mathcal{C}|_{U_r} \quad (0 < j < r). \quad (2.90)$$

Then,

$$\mathcal{C}_j^\pm = \begin{bmatrix} 0 & 0 \\ 0 & 2a_j \end{bmatrix} \otimes \Psi, \quad \mathcal{C}_0 = -\mathcal{C}_r = \begin{bmatrix} 0 & 0 \\ 0 & 2 \end{bmatrix} \otimes \Psi$$

where $a_j = \operatorname{Re}(\xi^j) = \cos(2\pi j/n)$ for $0 < j < r$, and

$$\Psi := \begin{bmatrix} \cos \psi & -\sin \psi \\ \sin \psi & \cos \psi \end{bmatrix}. \quad (2.91)$$

Finally, for $n = 8$, the list of maximal twisted types in each isotypical component of the $\mathcal{H} := D_8 \times \{1\}$ -representation V^c is given in Table 2.3 (see Appendix A.2 for the exact definition of the related twisted subgroups).

Table 2.3: Maximal twisted orbit types in the isotypical components of the $D_8 \times \{1\}$ -representation V^c .

Isotypical component	Maximal twisted orbit types
$U_{0,1}$	(D_8)
$U_{1,1}$	$(\mathbb{Z}_8^{t_1}), (D_2^d), (\tilde{D}_2^d)$
$U_{2,1}$	$(\mathbb{Z}_8^{t_2}), (D_4^d), (\tilde{D}_4^d)$
$U_{3,1}$	$(\mathbb{Z}_8^{t_3}), (D_2^d), (\tilde{D}_2^d)$
$U_{4,1}$	(D_8^d)

(c) $\mathcal{H} := \mathbb{Z}_n^{t_i}$ -isotypical decomposition of V^c . For this group \mathcal{H} , the \mathcal{H} -isotypical components of (2.87) can be described as follows (cf. (2.88)):

$$U_0 = \mathcal{U}_0 \oplus \mathcal{W}_0,$$

where

$$\mathcal{U}_0 := \{(z, z, \dots, z) : z \in \mathbb{C}^2\}$$

and

$$\mathcal{W}_0 := \left\{ \left(\left(\begin{bmatrix} z_1 \\ z_2 \end{bmatrix} \right)^T, \begin{bmatrix} \xi^l z_1 \\ \xi^{-l} z_2 \end{bmatrix}^T, \dots, \begin{bmatrix} \xi^{(n-1)l} z_1 \\ \xi^{-(n-1)l} z_2 \end{bmatrix} \right)^T : \begin{bmatrix} z_1 \\ z_2 \end{bmatrix} \in \mathbb{C} \oplus \mathbb{C} \right\};$$

$$U_j^\pm := \mathcal{U}_j^\pm \oplus \mathcal{W}_j^\pm \quad (0 < j < r),$$

where

$$\mathcal{U}_j^\pm = \{(z, \xi^{\pm j} z, \xi^{\pm 2j} z, \dots, \xi^{\pm(n-1)j} z) : z \in \mathbb{C}^2\}$$

and

$$\mathcal{W}_j^\pm := \left\{ \left(\begin{bmatrix} z_1 \\ z_2 \end{bmatrix}^T, \begin{bmatrix} \xi^{\mp j+l} z_1 \\ \xi^{\mp j-l} z_2 \end{bmatrix}^T, \dots, \begin{bmatrix} \xi^{(n-1)(\mp j+l)} z_1 \\ \xi^{(n-1)(\mp j-l)} z_2 \end{bmatrix}^T \right)^T : \begin{bmatrix} z_1 \\ z_2 \end{bmatrix} \in \mathbb{C} \oplus \mathbb{C} \right\};$$

$$U_r := \mathcal{U}_r \oplus \mathcal{W}_r,$$

where

$$\mathcal{U}_r := \{(z, -z, z, -z, \dots, z, -z) : z \in \mathbb{C}^2\}$$

and

$$\mathcal{W}_r := \left\{ \left(\begin{bmatrix} z_1 \\ z_2 \end{bmatrix}^T, \begin{bmatrix} -\xi^l z_1 \\ -\xi^{-l} z_2 \end{bmatrix}^T, \begin{bmatrix} \xi^{2l} z_1 \\ \xi^{2l} z_2 \end{bmatrix}^T, \dots, \begin{bmatrix} -\xi^{l(n-1)} z_1 \\ -\xi^{-l(n-1)} z_2 \end{bmatrix}^T \right)^T : \begin{bmatrix} z_1 \\ z_2 \end{bmatrix} \in \mathbb{C} \oplus \mathbb{C} \right\}.$$

Under the same notations as in (2.90), one has

$$\begin{aligned} \mathcal{C}_j^\pm &:= \begin{bmatrix} 0 & 0 \\ 0 & 2a_{\pm j} \end{bmatrix} \otimes \Psi, \quad a_{\pm j} = \cos \frac{2\pi(\pm j - 1)l}{n}, \quad 0 < j < r, \\ \mathcal{C}_0 &:= \begin{bmatrix} 0 & 0 \\ 0 & 2a_0 \end{bmatrix} \otimes \Psi, \quad \mathcal{C}_r := \begin{bmatrix} 0 & 0 \\ 0 & 2a_r \end{bmatrix} \otimes \Psi, \end{aligned}$$

where $a_0 := \cos \frac{2\pi l}{n}$ and $a_r := -\cos \frac{2\pi l}{n}$.

For $n = 8$, one obtains the list of maximal twisted types in the isotypical components of the $\mathcal{H} := \mathbb{Z}_8^{l_1} \times \{1\}$ -representation V^c , $l = 1, 2, 3$, given in Table 2.4 (see Appendix A.3 for the definition of the related twisted subgroups).

(d) $\mathcal{H} := D_n^d$ -isotypical decomposition of V^c . In this case, one can explicitly describe the \mathcal{H} -isotypical components of (2.87) as follows:

$$U_0 = \mathcal{U}_0 \oplus \mathcal{W}_0,$$

Table 2.4: Maximal twisted orbit types in the isotypical components of the $\mathbb{Z}_8^{t_i} \times \{1\}$ -representation V^c .

Isotypical component	Maximal twisted orbit types
$U_{0,1}$	(\mathbb{Z}_8)
$U_{1,1}$	$(\mathbb{Z}_8^{t_1})$
$U_{2,1}$	$(\mathbb{Z}_8^{t_2})$
$U_{3,1}$	$(\mathbb{Z}_8^{t_3})$
$U_{4,1}$	(\mathbb{Z}_8^c)

where

$$\mathcal{U}_0 := \{(z, z, \dots, z) : z \in \mathbb{C}^2\}$$

and

$$\mathcal{W}_0 := \left\{ \left(\begin{pmatrix} z_1 \\ z_2 \end{pmatrix}^T, \begin{pmatrix} -z_1 \\ -z_2 \end{pmatrix}^T, \begin{pmatrix} z_1 \\ z_2 \end{pmatrix}^T, \dots, \begin{pmatrix} -z_1 \\ -z_2 \end{pmatrix}^T \right)^T : \begin{pmatrix} z_1 \\ z_2 \end{pmatrix} \in \mathbb{C} \oplus \mathbb{C} \right\};$$

$$U_j^\pm := \mathcal{U}_j^\pm \oplus \mathcal{W}_j^\pm \quad (0 < j < r),$$

where

$$\mathcal{U}_j^\pm = \{(z, \xi^{\pm j} z, \xi^{\pm 2j} z, \dots, \xi^{\pm(n-1)j} z) : z \in \mathbb{C}^2\}$$

and

$$\mathcal{W}_j^\pm := \left\{ \left(\begin{pmatrix} z_1 \\ z_2 \end{pmatrix}^T, \begin{pmatrix} -\xi^{\mp j} z_1 \\ -\xi^{\mp j} z_2 \end{pmatrix}^T, \dots, \begin{pmatrix} (-\xi^{\mp j})^{n-1} z_1 \\ (-\xi^{\mp j})^{n-1} z_2 \end{pmatrix}^T \right)^T : \begin{pmatrix} z_1 \\ z_2 \end{pmatrix} \in \mathbb{C} \oplus \mathbb{C} \right\};$$

$$U_r := \mathcal{U}_r \oplus \mathcal{W}_r, \tag{2.92}$$

where

$$\mathcal{U}_r := \{(z, -z, z, -z, \dots, z, -z) : z \in \mathbb{C}^2\}$$

and

$$\mathscr{W}_r := \left\{ \left(\left(\begin{bmatrix} z_1 \\ z_2 \end{bmatrix}^T, \begin{bmatrix} z_1 \\ z_2 \end{bmatrix}^T, \dots, \begin{bmatrix} z_1 \\ z_2 \end{bmatrix}^T \right)^T : \begin{bmatrix} z_1 \\ z_2 \end{bmatrix} \in \mathbb{C} \oplus \mathbb{C} \right\}.$$

Also,

$$\mathcal{E}_j^\pm := \begin{bmatrix} 0 & 0 \\ 0 & 2a_{\pm j} \end{bmatrix} \otimes \Psi, \quad a_{\pm j} = -\cos \frac{2\pi j}{n} \quad (0 < j < r),$$

$$\mathcal{E}_r := -\mathcal{E}_0 := \begin{bmatrix} 0 & 0 \\ 0 & 2 \end{bmatrix} \otimes \Psi.$$

Hence, for $n = 8$, the list of maximal twisted types in the isotypical components of the $\mathcal{H} := D_n^d$ -representation V^c . is given in Table 2.5 (cf. Table 2.3). See Appendix A.4 for the definitions of the related twisted subgroups.

Table 2.5: Maximal twisted orbit types in the isotypical components of the D_8^d -representation V^c .

Isotypical component	Maximal twisted orbit types
$U_{0,1}$	(D_8)
$U_{1,1}$	$(\mathbf{Z}_8^{t_1}), (D_2^d), (\tilde{D}_2^d)$
$U_{2,1}$	$(\mathbf{Z}_8^{t_2}), (D_4^d), (\tilde{D}_4^d)$
$U_{3,1}$	$(\mathbf{Z}_8^{t_3}), (D_2^d), (\tilde{D}_2^d)$
$U_{4,1}$	(D_8^d)

Linearization on a relative equilibrium and characteristic quasi-polynomials

For any $\hat{x}^o = (g, q, a) \in \mathbb{R} \oplus \mathbb{R} \oplus \mathbb{C} \simeq \mathscr{V}$, one has (cf. (2.7)–(2.8) and (2.60)):

$$\tilde{\mathfrak{f}}(\alpha, i\omega, \hat{x}^o) = \begin{bmatrix} \alpha - \gamma_g g - \frac{1}{E_g} e^{-q} (e^g - 1) |a|^2 \\ q_0 - \gamma_q q - \frac{1}{E_q} (1 - e^{-q}) |a|^2 \\ -\gamma a + \gamma \sqrt{\kappa} \exp \left[\frac{(1-i\eta_g)g - (1-i\eta_q)q}{2} \right] a e^{-i\omega T} \end{bmatrix}. \quad (2.93)$$

Take $\lambda \in \mathbb{C}$. Combining (2.93) with (2.26), (2.27) and (2.29) allows us to define a “linearization operator” $\mathcal{R}_\alpha^\mathcal{Y}(\lambda) : \mathcal{Y}^c \rightarrow \mathcal{Y}^c$ by

$$\mathcal{R}_\alpha^\mathcal{Y}(\lambda) := \begin{bmatrix} -\gamma_g - \frac{1}{E_g} e^{-q} e^g |a|^2 & \frac{1}{E_g} e^{-q} (e^g - 1) |a|^2 & -\frac{2}{E_g} e^{-q} (e^g - 1) a \\ 0 & -\gamma_q - \frac{1}{E_q} e^{-q} |a|^2 & -\frac{2}{E_q} (1 - e^{-q}) a \\ B_{31}(\lambda) & B_{32}(\lambda) & B_{33}(\lambda) \end{bmatrix}, \quad (2.94)$$

where

$$\begin{aligned} B_{31}(\lambda) &= \frac{\gamma \sqrt{\kappa} (1 - i\eta_g)}{2} \exp \left[\frac{(1 - i\eta_g)g - (1 - i\eta_q)q}{2} \right] a e^{-i\omega T - \lambda T}; \\ B_{32}(\lambda) &= -\frac{\gamma \sqrt{\kappa} (1 - i\eta_q)}{2} \exp \left[\frac{(1 - i\eta_g)g - (1 - i\eta_q)q}{2} \right] a e^{-i\omega T - \lambda T}; \\ B_{33}(\lambda) &= -\gamma + \gamma \sqrt{\kappa} \exp \left[\frac{(1 - i\eta_g)g - (1 - i\eta_q)q}{2} \right] a e^{-i\omega T - \lambda T}. \end{aligned}$$

For any $\hat{x} = (\hat{x}^1, \dots, \hat{x}^n) \in V$, put

$$\tilde{f}_o(\alpha, i\omega, \hat{x}) := \left(\tilde{\mathbf{f}}(\alpha, i\omega, \hat{x}^1), \dots, \tilde{\mathbf{f}}(\alpha, i\omega, \hat{x}^n) \right). \quad (2.95)$$

For a given α , $\mathbf{S}(\hat{x}(\alpha))$ is a relative equilibrium for system (2.64) corresponding to the frequency $\omega(\alpha)$ if and only if

$$\Phi(\alpha, \omega(\alpha), \hat{x}(\alpha)) := \tilde{f}_o(\alpha, i\omega(\alpha), \hat{x}(\alpha)) + \eta \mathcal{E} \hat{x}(\alpha) - \omega(\alpha) J \hat{x}(\alpha) = 0 \quad (2.96)$$

Assume that $\mathbf{S}(\hat{x}(\alpha))$ is a relative equilibrium with $\mathcal{H} := \mathcal{G}_{\hat{x}(\alpha)}$ of the form (2.85). Take $\mathcal{R}_\alpha(\lambda)$ determined by (2.96) and (2.26)–(2.27) and consider decompositions (2.86)–(2.87).

Then, one has:

$$\mathcal{R}_\alpha(\lambda)|_{\mathfrak{U}} = \begin{cases} \mathcal{R}_\alpha^\mathcal{Y}(\lambda) + \eta \mathcal{C}_0 & \text{if } \mathfrak{U} = U_0; \\ \mathcal{R}_\alpha^\mathcal{Y}(\lambda) + \eta \mathcal{C}_j^\pm & \text{if } \mathfrak{U} = U_j^\pm, \quad 0 < j < r, \\ \mathcal{R}_\alpha^\mathcal{Y}(\lambda) + \eta \mathcal{C}_r & \text{if } \mathfrak{U} = U_r. \end{cases} \quad (2.97)$$

We refer to Subsection 2.2.4, where explicit formulas for \mathcal{C}_0 , \mathcal{C}_j^\pm and \mathcal{C}_r are given according to three possible values of \mathcal{H} . Combining (2.97) with (2.28) and (2.32), one can define the characteristic quasi-polynomials $\hat{\mathcal{P}}_j(\alpha, \lambda)$, $j = 0, \pm 1, \dots, \pm(r-1), r$ and study Hopf bifurcation of relative periodic solutions for different values of $\mathcal{H} = D_n \times \{1\}$, D_n^d , $\mathbb{Z}_n^{t_1}$.

Condition (A3)

Suppose that equation (2.64) with $n = 8$ has a relative equilibrium $\mathbf{S}(\hat{x})$, $\hat{x} = (g, q, a)$, for some $\hat{\alpha}$ and $\hat{\omega}$. Without loss of generality, assume that $a \in \mathbb{C}$ is *real*. Take decomposition (2.68) and let us describe the restriction of matrix (2.23) to $\mathbb{R} \times W_j$. For any $j = 0, \dots, 4$, define the operator $\mathcal{B}_j = \mathcal{B}_j(\hat{\alpha}, \hat{\omega}, \hat{x}) : \mathcal{V} \rightarrow \mathcal{V}$ by

$$\mathcal{B}_j := \mathcal{R}_{\hat{\alpha}}^{\mathcal{V}}(0) + \eta(\xi^j + \xi^{-j})C - \hat{\omega}J^{\mathcal{V}}. \quad (2.98)$$

Here $\mathcal{R}_{\hat{\alpha}}^{\mathcal{V}}(0)$ is considered as a *real* linear operator in $\mathcal{V} \simeq \mathbb{R}^2 \oplus \mathbb{C}$ (see (2.94)) and $J^{\mathcal{V}} : \mathcal{V} \rightarrow \mathcal{V}$ is given by $J^{\mathcal{V}}(\tilde{g}, \tilde{q}, \tilde{a})^T = (0, 0, i\tilde{a})^T$; see also (2.63) and (2.69). Define a vector $\mathcal{B} = \mathcal{B}(\hat{\alpha}, \hat{\omega}, \hat{x}) \in \mathcal{V} \simeq \mathbb{R}^2 \oplus \mathbb{C}$ by

$$\mathcal{B} := \left(0, 0, -iT\gamma\sqrt{\kappa} \exp\left[\frac{(1-i\eta_g)g - (1-i\eta_q)q}{2}\right] ae^{-i\omega T} - ia\right)^T. \quad (2.99)$$

Then (see (2.23), (2.93), (2.98) and (2.99)),

$$\left[D_{\omega}\Phi(\hat{\alpha}, \hat{\omega}, \hat{x}) \mid D_x\Phi(\hat{\alpha}, \hat{\omega}, \hat{x}) \right]_{\mathbb{R} \times W_j} = \begin{cases} [\mathcal{B} \mid \mathcal{B}_j] & \text{if } j = 0, 4 \\ \begin{bmatrix} [\mathcal{B} \mid \mathcal{B}_j] & 0 \\ 0 & [\mathcal{B} \mid \mathcal{B}_j] \end{bmatrix} & \text{if } j = 1, 2, 3. \end{cases} \quad (2.100)$$

Put $\mathfrak{B} := [\mathcal{B} \mid \mathcal{B}_j]$. It follows from (2.100) that condition (A3) is satisfied if $\text{rank}(\mathfrak{B}) = 4$. Note that $(0, 0, i)^T \in \mathbb{R}^2 \oplus \mathbb{C}$ is an eigenvector of \mathcal{B}_j corresponding to the zero eigenvalue. Denote by \mathcal{E} the direct sum of generalized eigenspaces corresponding to nonzero eigenvalues of \mathcal{B}_j . Clearly, $\text{rank}(\mathfrak{B}) = 4$ if

- (a) $\text{rank}(\mathcal{B}_j) = 3$ (i.e., zero is a simple eigenvalue of \mathcal{B}_j), and
- (b) $\mathfrak{B}e \notin \mathcal{E}$, where $e := (1, 0, 0, 0, 0) \in \mathbb{R}^5 \simeq \mathbb{R} \oplus \mathbb{R}^2 \oplus \mathbb{C} \simeq \mathbb{R} \oplus \mathcal{V}$.

Remark 2.2.5. Condition (a) can be effectively expressed in terms of the derivative of the characteristic polynomial associated with \mathcal{B}_j . Condition (b) is satisfied if

$$(b)' \quad \text{Im}\left(-iT\gamma\sqrt{\kappa} \exp\left[\frac{(1-i\eta_g)g - (1-i\eta_q)q}{2}\right] ae^{-i\omega T}\right) - a \neq 0, \quad \text{where } a \in \mathbb{R}.$$

Isotypical crossing

In order to apply Theorem 2.1.14 to classify symmetries of relative periodic solutions bifurcating from relative equilibria $\mathbf{S}(\hat{x})$ with $(\mathcal{G}_{\hat{x}})$ given by (2.85), it remains to analyze the isotypical crossing of the roots of characteristic quasi-polynomials $\hat{\mathcal{P}}_j(\alpha, \lambda)$, $j = 0, \pm 1, \dots, \pm 3, 4$ (cf. (2.97), (2.28) and (2.32)), as α crosses some critical value α_o . Numerical results illustrating isotypical crossing of characteristic roots through the imaginary axis are described in Table 2.6 for $(\mathcal{G}_{\hat{x}}) = D_n \times \{1\}$, in Tables 2.7, 2.8, 2.9 for $(\mathcal{G}_{\hat{x}}) = \mathbb{Z}_8^{t_1}, \mathbb{Z}_8^{t_2}, \mathbb{Z}_8^{t_3}$, respectively, and in Table 2.10 for $(\mathcal{G}_{\hat{x}}) = D_8^d$. All the parameters except α are the same as in Section 2.2.3. In these tables, we follow the same agreement as in Table 2.2 except that we use a circle to indicate a Hopf bifurcation point and a rectangle to indicate a steady-state bifurcation. In particular, an entry in a given cell indicates the number of unstable roots for the characteristic quasi-polynomial $\hat{\mathcal{P}}_j(\alpha, \lambda)$ associated with the isotypical component $U_{j,1}$ (shown in the left column) for the corresponding interval of α -values (shown in the upper row). The results presented in Subsection 2.2.4 follow from these tables.

2.2.5 S_n -configuration of identical semiconductor lasers

In this subsection, we apply Proposition 2.1.8 and Theorem 2.1.14 to a network of n all-to-all coupled identical laser devices (2.60). The adjacency matrix \mathcal{K} for this configuration is given by

$$\mathcal{K} := \begin{bmatrix} 0 & 1 & 1 & \dots & 1 & 1 \\ 1 & 0 & 1 & \dots & 1 & 1 \\ 1 & 1 & 0 & \dots & 1 & 1 \\ \vdots & \vdots & \vdots & \ddots & \vdots & \vdots \\ 1 & 1 & 1 & \dots & 0 & 1 \\ 1 & 1 & 1 & \dots & 1 & 0 \end{bmatrix}.$$

Table 2.6: Number of unstable eigenvalues for each isotypical component along the branch of the relative equilibrium with (D_8) symmetry (see item (i) on page 53)

Isotypical component	Intervals for values of parameter $\alpha \cdot 10^2$							
	[3.61, 3.69]	[3.70, 3.85]	[3.86, 4.01]	[4.02, 4.58]	[4.59, 5]	[5.01, 5.32]	[5.33, 6.01]	[6.02, 8.97]
$U_{0,1}$	0	0	0	0	0	0	0	②
$U_{1,1}$	0	②	⑥	6	6	6	6	6
$U_{2,1}$	0	0	0	②	2	2	⑥	6
$U_{3,1}$	0	0	0	0	②	2	2	2
$U_{4,1}$	0	0	0	0	0	①	1	1
$\bigoplus_{j=0}^4 U_{j,1}$	0	2	6	8	10	11	15	17

Table 2.7: Number of unstable eigenvalues for each isotypical component along the branch of the relative equilibrium with $(\mathbb{Z}_8^{t_1})$ symmetry (see item (ii) on page 53)

Isotypical component	Intervals for values of parameter $\alpha \cdot 10^2$							
	[3.61, 3.65]	[3.66, 3.98]	[3.99, 4.15]	[4.16, 4.2]	[4.21, 6.39]	6.40	[6.41, 7.87]	[7.88, 10.02]
$U_{0,1}$	0	0	0	0	0	0	0	②
$U_{1,1}$	2	④	4	⑥	6	6	6	6
$U_{2,1}$	0	②	2	2	2	2	④	4
$U_{3,1}$	0	0	②	④	4	4	4	4
$U_{4,1}$	0	0	0	0	①	③	3	3
$\bigoplus_{j=0}^4 U_{j,1}$	2	6	8	12	13	15	17	19

Table 2.8: Number of unstable eigenvalues for each isotypical component along the branch of the relative equilibrium with $(\mathbb{Z}_8^{t_2})$ symmetry (see item (iii) on page 53)

Isotypical component	Intervals for values of parameter $\alpha \cdot 10^2$					
	[3.61, 5.48]	[5.49, 6.6]	[6.61, 8.09]	[8.10, 8.47]	[8.48, 13.53]	
$U_{0,1}$	0	0	0	0	0	②
$U_{1,1}$	2	2	④	4	4	4
$U_{2,1}$	2	④	4	⑥	6	6
$U_{3,1}$	2	2	④	4	4	4
$U_{4,1}$	0	0	0	0	0	②
$\bigoplus_{j=0}^4 U_{j,1}$	6	8	12	14	18	18

Table 2.9: Number of unstable eigenvalues for each isotypical component along the branch of the relative equilibrium with $(\mathbb{Z}_8^{t_3})$ symmetry (see item (iv) on page 53)

Isotypical component	Intervals for values of parameter $\alpha \cdot 10^2$								
	[3.61, 3.68]	[3.69, 3.84]	3.85	[3.86, 5.24]	[5.25, 5.29]	[5.3, 5.52]	[5.53, 6.37]	[6.38, 8.65]	[8.66, 9.23]
$U_{0,1}$	0	0	0	0	0	0	0	0	②
$U_{1,1}$	2	2	④	4	4	⑥	6	6	6
$U_{2,1}$	2	④	4	⑥	6	6	6	6	6
$U_{3,1}$	4	4	⑥	6	6	6	6	⑧	8
$U_{4,1}$	2	2	2	2	④	4	4	4	4
$\bigoplus_{j=0}^4 U_{j,1}$	10	12	14	16	18	20	22	24	26

Table 2.10: Number of unstable eigenvalues for each isotypical component along the branch of the relative equilibrium with (D_8^d) symmetry (see item (vi) on page 53)

Isotypical component	Intervals for values of parameter $\alpha \cdot 10^2$							
	[3.62, 3.83]	[3.84, 4.04]	[4.05, 5.38]	[5.39, 6.59]	[6.6, 7.3]	[7.31, 7.56]	[7.57, 13.55]	
$U_{0,1}$	0	0	②	2	2	2	2	
$U_{1,1}$	4	4	4	4	4	4	⑧	
$U_{2,1}$	4	⑧	8	8	8	8	8	
$U_{3,1}$	4	4	4	⑧	8	8	8	
$U_{4,1}$	4	4	4	4	⑥	④	4	
$\bigoplus_{j=0}^4 U_{j,1}$	16	20	22	26	28	26	30	

Thus, we are interested in solutions to the equation

$$\dot{x} = f(\alpha, x, x_t) := f_o(\alpha, x_t) + \eta \mathcal{C}x, \quad x \in V, \quad (2.101)$$

where

$$\mathcal{C} = \mathcal{H} \otimes C = \begin{bmatrix} 0 & C & C & \dots & C & C \\ C & 0 & C & \dots & C & C \\ C & C & 0 & \dots & C & C \\ \vdots & \vdots & \vdots & \ddots & \vdots & \vdots \\ C & C & C & \dots & 0 & C \\ C & C & C & \dots & C & 0 \end{bmatrix} \quad \text{with} \quad C = \begin{bmatrix} 0 & 0 & 0 \\ 0 & 0 & 0 \\ 0 & 0 & e^{i\psi} \end{bmatrix}. \quad (2.102)$$

The space $\mathcal{V} = \mathbb{R} \oplus \mathbb{R} \oplus \mathbb{C} \simeq \mathbb{R}^4$ is equipped with the natural S^1 -representation (S^1 acts trivially on the first two components and by complex multiplication on the \mathbb{C} -component), and $V = \mathcal{V}^n$. The group S_n acts naturally on V by permutation of the coordinates of the vector $x \in V$. This action suggests the orthogonal $S_n \times S^1$ -representation on V given by

$$(h, e^{i\tau})x = (e^{i\tau}x^{h(1)}, e^{i\tau}x^{h(2)}, \dots, e^{i\tau}x^{h(n)}), \quad e^{i\tau} \in S^1, \quad h \in S_n, \quad (2.103)$$

where $x = (x^1, x^2, \dots, x^n) \in V$. Thus, system (2.101) satisfies condition (A0).

2.2.6 S_5 -configuration: bifurcation of symmetric relative equilibria

Hereafter, we assume that $n = 5$.

Isotypical decomposition and maximal twisted orbit types.

To apply Proposition 2.1.8 for studying relative equilibria bifurcating from the equilibrium $\mathcal{O}(\alpha)$, observe that V admits the isotypical S_5 -decomposition:

$$V = W_0 \oplus W_1, \quad (2.104)$$

where

$$W_0 = \{(x^1, \dots, x^5) \in V : x^1 = \dots = x^5\} \quad (2.105)$$

is modeled on the one-dimensional trivial S_5 -representation \mathcal{V}_0 , while

$$W_1 = \{(x^1, \dots, x^5) \in V : x^1 + \dots + x^5 = 0\} \quad (2.106)$$

is modeled on the standard four-dimensional irreducible representation \mathcal{V}_4 (sometimes called augmentation submodule [54]). Clearly, $\dim W_0 = 4$ and $\dim W_1 = 16$. Observe also that decomposition (2.104) can be refined to the $S_5 \times S^1$ -decomposition

$$W_j = V_{j,0} \oplus V_{j,1}, \quad j = 0, 1, \quad (2.107)$$

where $V_{j,0}$ (resp. $V_{j,1}$) corresponds to the trivial (resp. nontrivial) S^1 -action. Clearly, $\dim V_{0,0} = \dim V_{0,1} = 2$ while $\dim V_{1,0} = \dim V_{1,1} = 8$. Also, $V_{1,0}$ is reducible of multiplicity two (essentially modeled on the augmented module), while $V_{1,1}$ is irreducible.

In order to study relative equilibria in system (2.101), one needs to identify their twisted isotropy subgroups with respect to the $S_5 \times S^1$ -action, see Remark 2.2.1. The list of maximal twisted types in $V_{j,1}$, $j = 0, 1$, is in given in Table 2.11. The explicit description of all these subgroups can be found in A.5.

Table 2.11: Maximal twisted orbit types in each isotypical component of the S_5 -representation V .

Isotypical component	Maximal twisted orbit types
$V_{0,1}$	$(S_5 \times \{1\}) \simeq (S_5)$
$V_{1,1}$	$(D_6), (S_4), (D_6^d), (D_4^d), (\mathbb{Z}_4^t), (\mathbb{Z}_5^t), (\mathbb{Z}_6^c)$

Equivariant spectral reduction and condition (A1).

The linearization

$$D_{\mathbf{x}} f_o(\alpha, \mathbf{x}) : \mathbb{R} \times C_{-T}(V) \rightarrow V$$

of system (2.101) at $\mathcal{O}(\alpha)$ respects isotypical decomposition (2.107) (see also (2.104)). Then, setting

$$A := \left(\sqrt{\kappa} \exp \left[\frac{(1 - i\eta_g) \frac{\alpha}{\gamma_g} - (1 - i\eta_q) \frac{q_0}{\gamma_q}}{2} \right] - 1 \right) \gamma \quad (2.108)$$

(cf. (2.66)), and combining (2.105)–(2.106) with (2.61)–(2.101), one obtains the following formulas for the restrictions $A_{j,k} := D_{\mathbf{x}} f_o(\alpha, \mathbf{x})|_{V_{j,k}}$, $j, k = 0, 1$, to the isotypical components:

$$A_{j,k} = \begin{cases} \begin{bmatrix} -\gamma_g & 0 \\ 0 & -\gamma_q \end{bmatrix} & \text{if } j = 0, k = 0; \\ A + 4\eta e^{i\psi} & \text{if } j = 0, k = 1; \\ \begin{bmatrix} -\gamma_g \text{Id}_4 & 0 \\ 0 & -\gamma_q \text{Id}_4 \end{bmatrix} & \text{if } j = 1, k = 0; \\ (A - \eta e^{i\psi}) \otimes \text{Id}_4 & \text{if } j = 1, k = 1, \end{cases} \quad (2.109)$$

where $A + 4\eta e^{i\psi}$ and $A - \eta e^{i\psi}$ are considered as *real* 2×2 -matrices. Since the action of S^1 on (g, q) -components of (2.60) is trivial, it follows from (2.109) that $\det(D_{\mathbf{x}} f_o(\alpha, \mathcal{O}(\alpha))|_{V_{S^1}}) = (\gamma_g \gamma_q)^5 \neq 0$, hence (see (2.12)), $\mathcal{P}_0(\alpha, 0, \mathcal{O}(\alpha)) \neq 0$ so that system (2.101) satisfies condition (A1).

Characteristic quasi-polynomial and condition (A2)

Next, let us consider the characteristic quasi-polynomial $\mathcal{P}_*(\alpha, \lambda, \mathcal{O}(\alpha))$ (see (2.12)). Put

$$P := \lambda + \gamma - \gamma \sqrt{\kappa} \exp \left[\left(\frac{\alpha}{2\gamma_g} - \frac{q_0}{2\gamma_q} \right) + i \left(\frac{\eta_q q_0}{2\gamma_q} - \frac{\eta_g \alpha}{2\gamma_g} \right) \right] e^{-\lambda T}. \quad (2.110)$$

Then, the restriction of the characteristic quasi-polynomial to $V_{j,1}$ reads

$$\mathcal{P}_{j,1}(\alpha, \lambda, \mathcal{O}(\alpha)) = \begin{cases} P + 4\eta e^{i\psi} & \text{if } j = 0 \\ (P - \eta e^{i\psi})^4 & \text{if } j = 1 \end{cases} \quad (2.111)$$

so that

$$\mathcal{P}_*(\alpha, \lambda, \mathcal{O}(\alpha)) = \mathcal{P}_{0,1}(\alpha, \lambda, \mathcal{O}(\alpha)) \cdot \mathcal{P}_{1,1}(\alpha, \lambda, \mathcal{O}(\alpha)) \quad (2.112)$$

To study condition (A2), we need identify the values of α for which $\mathcal{O}(\alpha)$ is a center, i.e., we are looking for those values of α for which there exists $\omega > 0$ such that

$$\mathcal{P}_{j,1}(\alpha, i\omega, \mathcal{O}(\alpha)) = 0, \quad j = 0, 1. \quad (2.113)$$

Proposition 2.2.6. *Assume that $\alpha = \alpha_o^j$ is a root of (2.113) for $j = 0$ (resp. $j = 1$) with a corresponding $\omega = \omega(\alpha_o^j)$, and*

$$\gamma > 4\eta \cos(\psi) \quad \text{and} \quad \omega(\alpha_o^j) > 4\eta \sin(\psi) \quad (2.114)$$

$$\text{(resp. } \gamma > -\eta \cos(\psi) \quad \text{and} \quad \omega(\alpha_o^j) > -\eta \sin(\psi)), \quad (2.115)$$

then, the center $\mathcal{O}(\alpha_o^j)$ is isolated and condition (iii) from Proposition 2.1.8 is satisfied. Furthermore, the following continuous branches of relative equilibria bifurcate from the equilibrium $(\alpha_o^j, \mathcal{O}(\alpha_o^j))$ of equation (2.101):

- for $j = 0$, a branch with symmetry (S_5) ;
- for $j = 1$, ten branches with symmetry (D_6) , five branches with symmetry (S_4) , ten branches with symmetry (D_6^d) , fifteen branches with symmetry (D_4^d) , thirty branches with symmetry $(\mathbb{Z}_4^{t_1})$, twenty four branches with symmetry $(\mathbb{Z}_5^{t_1})$, and twenty branches with symmetry $(\mathbb{Z}_6^{t_2})$.

Recall that η stands for the coupling strength. Thus, conditions (2.114)–(2.115) are satisfied for any relatively weak coupling.

The proof of Proposition 2.2.6 follows the same argument as in the proof of Proposition 2.2.2.

Proposition 2.2.6 is illustrated in Table 2.12. We use the same set of parameters as in Subsection 2.2.2, i.e., $\eta = 2$, $\eta_g = 1$, $\eta_q = 1$, $\gamma_g = 10^{-2}$, $\gamma_q = 1$, $\gamma = 15$, $\kappa = \sqrt{0.2}$, $q_0 = 2$,

$E_g = 1$, $E_q = 0.1$, $T = 2.5$. Note that for these parameters, conditions (2.114) and (2.115) are fulfilled for all $(\alpha, \omega(\alpha))$ satisfying equation (2.113). The equilibrium $\mathcal{O}(\alpha)$ is stable for $\alpha < 0.036$. Table 2.12 uses the same agreement as in Table 2.2. Proposition 2.2.6 guarantees Hopf bifurcations of branches of relative equilibria

- (i) with symmetry (S_5) for $\alpha \approx 0.036018$, $\alpha \approx 0.0361215$, $\alpha \approx 0.0364415$;
- (ii) with symmetries (D_6) , (D_6^d) , (S_4) , (D_4^d) , $(\mathbb{Z}_5^{t_1})$, $(\mathbb{Z}_4^{t_1})$ and $(\mathbb{Z}_6^{t_2})$ for $\alpha \approx 0.0361515$, $\alpha \approx 0.0362365$, $\alpha \approx 0.0365865$,

to mention a few (see Proposition 2.2.6 for the number of branches of each type and Appendix A.5 for the explicit description of the subgroups).

2.2.7 S_5 -configuration: bifurcation of relative periodic solutions

Application of Theorem 2.1.14 to the laser system

In this subsection, we use Theorem 2.1.14 to classify symmetries of relative periodic solutions bifurcating from branches of relative equilibria of system (2.101). In order to avoid repetitions, we omit sections regarding finding linearization on a relative equilibrium and characteristic quasi-polynomials as well as checking condition (A3), because they are almost verbatim copies of the corresponding segments in Subsection 2.2.4.

$\mathcal{G}_{\hat{x}}$ -isotypical decomposition of V^c and maximal twisted orbit types

In order to use Theorem 2.1.14, first, we need to identify isotypical decompositions, maximal twisted orbit types and restrictions of the matrix \mathcal{C} to isotypical components relevant to the symmetry groups listed in Table 2.11.

Recall from Remark 2.2.4 that the complexification \mathcal{V}^c of the space $\mathcal{V} := \mathbb{R}^2 \oplus \mathbb{C} = \mathbb{R}^2 \oplus (\mathbb{R} \oplus \mathbb{R})$ can be represented as

$$\mathcal{V}^c = \mathbb{C}^2 \oplus (\mathbb{C} \oplus \mathbb{C}) = \mathbb{C}^4, \quad (2.116)$$

Table 2.12: Number of unstable eigenvalues in each isotypical component for the equilibrium $\mathcal{O}(\alpha)$

Isotypical component	Intervals for values of parameter $\alpha \cdot 10^2$									
	[3.6000, 3.6016]	[3.6020, 3.6119]	[3.6124, 3.6149]	[3.6154, 3.6234]	[3.6239, 3.6439]	[3.6444, 3.6584]	[3.6589, 3.6744]	[3.6749, 3.6829]	[3.6834, 3.6959]	
$V_{0,1}$	0	(2)	(4)	4	4	(6)	6	(8)	8	
$V_{1,1}$	0	0	0	(8)	(16)	16	(24)	24	(32)	8
$\bigoplus_{j=0}^4 V_{j,1}$	0	2	4	12	20	22	30	32	40	

therefore, $V^c = (\mathcal{V}^c)^5 = (\mathbb{C}^4)^5$.

(a) We consider the case $\mathcal{H} := S_5 \times \{1\}$. First, we consider the subgroup $\mathbb{Z}_5 \simeq \mathbb{Z}_5 \times \{1\}$ and describe the \mathbb{Z}_5 -isotypical decomposition of V^c . Namely, we have

$$V^c = U_0 \oplus U_1 \oplus U_2,$$

where

$$\begin{aligned} U_0 &= \{(z, z, z, z, z) : z \in \mathbb{C}^4\}, & U_j &= U_j^+ \oplus U_j^-, \quad j = 1, 2, \\ U_j^\pm &= \{(z, \xi^{\pm j} z, \xi^{\pm 2j} z, \xi^{\pm 3j} z, \xi^{\pm 4j} z) : z \in \mathbb{C}^4\} & j &= 1, 2, \quad \xi = e^{\frac{2\pi i}{5}}. \end{aligned}$$

Here, the action of any $\zeta \in \mathbf{S}$ on $(z_1, z_2, z_3, z_4)^T \in \mathbb{C}^4$ is given by

$$\zeta(z_1, z_2, z_3, z_4)^T = (z_1, z_2, \zeta z_3, \zeta z_4)^T.$$

One can easily notice that the coupling matrix $\mathcal{C} : V^c \rightarrow V^c$ given by (2.102) preserves the \mathbb{Z}_5 -isotypical components. Indeed, for any $z \in \mathbb{C}^4$

$$\mathcal{C}(z, z, z, z, z) = 4(Cz, Cz, Cz, Cz, Cz) \in U_0$$

$$\mathcal{C}(z, \xi^{\pm j} z, \xi^{\pm 2j} z, \xi^{\pm 3j} z, \xi^{\pm 4j} z) = -(Cz, \xi^{\pm j} Cz, \xi^{\pm 2j} Cz, \xi^{\pm 3j} Cz, \xi^{\pm 4j} Cz) \in U_j^\pm, \quad j = 1, 2.$$

Using the above \mathbb{Z}_5 -isotypical decomposition, we obtain for $\mathcal{H} := S_5 \times \{1\}$ the following S_5 -isotypical decomposition of V^c :

$$V^c = U_0 \oplus U_1 \tag{2.117}$$

where $U_1 = U_1^+ \oplus U_1^- \oplus U_2^+ \oplus U_2^-$. Moreover

$$\mathcal{C}|_{U_0} = \begin{bmatrix} 0 & 0 \\ 0 & 4 \end{bmatrix} \otimes \Psi, \quad \mathcal{C}|_{U_j^\pm} = \begin{bmatrix} 0 & 0 \\ 0 & -1 \end{bmatrix} \otimes \Psi, \quad j = 1, 2. \tag{2.118}$$

where

$$\Psi := \begin{bmatrix} \cos \psi & -\sin \psi \\ \sin \psi & \cos \psi \end{bmatrix}. \tag{2.119}$$

Hence, for the $\mathcal{H} := S_5$ -representation V^c , we have the list of maximal twisted types in the isotypical components given in Table 2.13 (see Appendix A.5 for the definitions of the subgroups).

Table 2.13: Maximal twisted orbit types in the isotypical components of the $S_5 \times \{1\}$ -representation V^c .

Isotypical component	Maximal twisted orbit types
$U_{0,1}$	(S_5)
$U_{1,1}$	$(D_6), (S_4), (D_6^d), (D_4^d), (\mathbb{Z}_4^{t_1}), (\mathbb{Z}_5^{t_1}), (\mathbb{Z}_6^{t_2})$

(b) We consider now the group $\mathcal{H} := \mathbb{Z}_5^{t_1} := \{(1, 1), (\xi, \xi), (\xi^2, \xi^2), (\xi^3, \xi^3), (\xi^4, \xi^4)\}$. Put

$$\mathcal{W} := \{(z_1, z_2, 0, 0)^T : z_1, z_2 \in \mathbb{C}\} \quad (2.120)$$

$$\mathcal{V} := \{(0, 0, z_1, z_2)^T : z_1, z_2 \in \mathbb{C}\}, \quad (2.121)$$

and define

$$W_0 := \{(z, z, z, z) : z \in \mathcal{W}\},$$

$$V_0 := \{(z, z, z, z) : z \in \mathcal{V}\},$$

$$W_j^\pm := \{(z, \xi^{\pm j} z, \xi^{\pm 2j} z, \xi^{\pm 3j} z, \xi^{\pm 4j} z) : z \in \mathcal{W}\},$$

$$V_j^\pm := \{(z, \xi^{\pm j} z, \xi^{\pm 2j} z, \xi^{\pm 3j} z, \xi^{\pm 4j} z) : z \in \mathcal{V}\}, \quad j = 1, 2, \quad \xi = e^{\frac{2\pi i}{5}}.$$

Then, one can easily verify that we have the following \mathcal{H} -isotypical decomposition of V^c :

$$V^c = U_0 \oplus U_1 \oplus U_2,$$

where $U_0 = W_0 \oplus V_1^-$, $U_1 = V_0 \oplus V_2^-$ and $U_2 = V_1^+ \oplus V_2^+$. Moreover, $\mathcal{C}|_{W_0} = \mathcal{C}|_{W_j^\pm} = 0$, $\mathcal{C}|_{V_0} = 4\Psi$, $\mathcal{C}|_{V_j^\pm} = -\Psi$.

Table 2.14 shows the list of maximal twisted types in the isotypical components for the $\mathcal{H} := \mathbb{Z}_5^{t_1}$ -representation V^c , (see Appendix A.6 for the definitions of the subgroups).

Table 2.14: Maximal twisted orbit types in the isotypical components of the $\mathbb{Z}_5^{t_1}$ -representation V^c .

Isotypical component	Maximal twisted orbit types
$U_{0,1}$	$(\mathbb{Z}_5^{t_1})$
$U_{1,1}$	$(\mathbb{Z}_5^{t_1, \mathbf{t}_1})$
$U_{2,1}$	$(\mathbb{Z}_5^{t_1, \mathbf{t}_1})$

(c) Next, we consider $\mathcal{H} := D_6^d$. Using (2.120) and (2.121), define

$$W_0 := \{(z^1, z^1, z^2, z^2, z^1) : z^1, z^2 \in \mathcal{W}\},$$

$$W_2 := W_2^+ \oplus W_2^-,$$

$$W_2^\pm := \{(z, \rho^{\pm 2}z, 0, 0, \rho^{\pm 4}z) : z \in \mathcal{W}\}, \quad \rho := e^{\frac{2\pi i}{6}},$$

$$W_3 := \{(0, 0, z, -z, 0) : z \in \mathcal{W}\},$$

$$V_0 := \{(z^1, z^1, z^2, z^2, z^1) : z_1, z^2 \in \mathcal{V}\},$$

$$V_2 := V_2^+ \oplus V_2^-,$$

$$V_2^\pm := \{(z, \rho^{\pm 2}z, 0, 0, \rho^{\pm 4}z) : z \in \mathcal{V}\}, \quad \rho := e^{\frac{2\pi i}{6}},$$

$$V_3 := \{(0, 0, z, -z, 0) : z \in \mathcal{V}\}.$$

Then by inspection, we have the following \mathcal{H} -isotypical decomposition of V^c :

$$V^c = U_0 \oplus U_1 \oplus U_2 \oplus U_3$$

where

$$U_0 = W_0 \oplus V_3, \quad U_1 = V_2, \quad U_2 = W_2, \quad U_3 = W_3 \oplus V_0.$$

The restrictions of \mathcal{C} to the subspaces U_j are given by

$$\mathcal{C}|_{U_j} = \begin{cases} \mathbf{0}_{6 \times 6} & \text{if } j = 0, \\ -\text{Id}_2 \otimes \Psi & \text{if } j = 1, \\ \mathbf{0}_{4 \times 4} & \text{if } j = 2, \\ \text{diag}(0, 4, -1) \otimes \Psi & \text{if } j = 3. \end{cases}$$

Table 2.15 shows the list of maximal twisted types in the isotypical components for the $\mathcal{H} := D_6^d$ -representation V^c , (see Appendix A.7 for the definitions of the subgroups).

Table 2.15: Maximal twisted orbit types in the isotypical components of the D_6^d -representation V^c .

Isotypical component	Maximal twisted orbit types
$U_{0,1}$	(D_6^d)
$U_{1,1}$	$(\mathbb{Z}_6^{t_3, t_1}), (D_2^{d, \hat{d}}), (D_2^{d, \hat{d}})$
$U_{2,1}$	$(\mathbb{Z}_6^{t_3, t_2}), (D_2^d), (D_2^{d, z})$
$U_{3,1}$	$(D_6^{d, \hat{d}})$

(d) Finally, we consider isotropy group $\mathcal{H} := S_4$. One can easily verify that the \mathcal{H} -isotypical decomposition of V^c is given by

$$V^c = U_0 \oplus U_4,$$

where the component U_4 is modeled on the irreducible S_4 -representation which is equivalent to the augmentation submodule of S_4 . These components are exactly:

$$U_0 = \{(z^1, z^2, z^2, z^2, z^2) : z^1, z^2 \in \mathbb{C}^4\}$$

$$U_4 = \{(0, z^1, z^2, z^3, z^4) : z^1 + z^2 + z^3 + z^4 = 0, z^i \in \mathbb{C}\}.$$

Put $U_0^1 := \{(z, z, z, z, z) : z \in \mathbb{C}^4\}$ and $U_0^2 := \{(-4z, z, z, z, z) : z \in \mathbb{C}^4\}$. Then, we can represent the restriction of \mathcal{C} to each component as follows:

$$\mathcal{C}|_{U_0^1} = \begin{bmatrix} 0 & 0 \\ 0 & 4 \end{bmatrix} \otimes \Psi, \quad \mathcal{C}|_{U_0^2} = \mathcal{C}|_{U_4} = \begin{bmatrix} 0 & 0 \\ 0 & -1 \end{bmatrix} \otimes \Psi.$$

Table 2.16 shows the list of maximal twisted types in the isotypical components for the $\mathcal{H} := S_4$ -representation V^c , (see Appendix A.8 for the definitions of the subgroups). Observe that, although the isotypical component $U_{4,1}$ contains a maximal twisted orbit type (D_3) , we cannot guarantee the existence of a branch with this symmetry since $U_{0,1}$ contains (S_4) as a maximal twisted orbit type.

Table 2.16: Maximal twisted orbit types in the isotypical components of the S_4 -representation V^c .

Isotypical component	Maximal twisted orbit types
$U_{0,1}$	(S_4)
$U_{4,1}$	$(\mathbb{Z}_4^{t_2}), (D_4^d), (D_2^d), (\mathbb{Z}_3^{t_1})$

Isotypical crossing

In order to apply Theorem 2.1.14 to classify symmetries of relative periodic solutions bifurcating from relative equilibria $\mathbf{S}(\hat{x})$ with $(\mathcal{G}_{\hat{x}})$ listed above, it remains to analyze the isotypical crossing of the roots of characteristic quasi-polynomials $\hat{\mathcal{P}}_{j,1}(\alpha, \lambda)$, as α crosses some critical value α_o . Numerical results illustrating isotypical crossing of characteristic roots through the imaginary axis are described in Table 2.17 for $(\mathcal{G}_{\hat{x}}) = (S_5)$, in Table 2.18 for $(\mathcal{G}_{\hat{x}}) = (\mathbb{Z}_5^{t_1})$, in Table 2.19 for $(\mathcal{G}_{\hat{x}}) = (D_6^d)$, and in Table 2.20 for $(\mathcal{G}_{\hat{x}}) = (S_4)$. All the parameters except α are the same as in Subsection 2.2.6. In these tables, we follow the same agreement as in Table 2.2.

Table 2.17: Number of unstable eigenvalues for each isotypical component along the branch of the relative equilibrium with (S_5) symmetry

Isotypical component	Intervals for values of parameter $\alpha \cdot 10^2$										
	[3.6020, 5.1788]	[5.6530, 7.1953]	[7.7030, 18.7684]	[19.2704, 22.2825]	[22.7846, 60.9689]	[61.4717, 91.6423]					
$U_{0,1}$	0	0	②	2	2	④					
$U_{1,1}$	0	④	4	⑫	⑳	20					
$\bigoplus_{j=0}^1 U_{j,1}$	0	4	6	14	22	24					

Table 2.18: Number of unstable eigenvalues for each isotypical component along the branch of the relative equilibrium with $(\mathbb{Z}_5^{t_1})$ symmetry

Isotypical component	Intervals for values of parameter $\alpha \cdot 10^2$															
	[3.6154, 3.6215]	[3.6240, 3.6349]	[3.6400, 3.6550]	[3.6600, 3.6650]	[3.6700, 3.6800]	[3.6850, 3.7100]	[3.7150, 3.7150]	[3.7200, 3.7450]	[3.7500, 3.7500]	[3.7550, 3.7600]	[3.7650, 3.7800]	[3.7850, 3.8450]				
$U_{0,1}$	0	0	0	0	0	0	0	0	0	0	0	0	0	0	0	0
$U_{1,1}$	4	⑧	8	⑫	12	⑩	16	16	⑳	20	20	20	20	20	⑳	17
$U_{2,1}$	5	5	⑦	7	⑨	9	⑪	⑬	13	⑮	⑰	17	17	17	17	17
$\bigoplus_{j=0}^2 U_{j,1}$	9	13	15	19	21	25	27	29	33	35	37	41	41	41	41	41

Table 2.19: Number of unstable eigenvalues for each isotypical component along the branch of the relative equilibrium with (D_6^d) symmetry

Isotypical component	Intervals for values of parameter $\alpha \cdot 10^2$															
	[3.6154, 3.6215]	[3.6240, 3.6349]	[3.6400, 3.6550]	[3.6600, 3.6650]	[3.6700, 3.6800]	[3.6850, 3.7100]	[3.7150, 3.7150]	[3.7200, 3.7450]	[3.7500, 3.7500]	[3.7550, 3.7600]	[3.7650, 3.7800]	[3.7850, 3.8150]				
$U_{0,1}$	0	0	0	0	0	0	0	0	0	0	0	0				
$U_{1,1}$	4	⑥	8	⑫	12	⑮	16	⑳	20	20	20	⑳				
$U_{3,1}$	5	5	⑦	7	⑨	9	⑪	⑬	⑮	⑮	⑰	17				
$\bigoplus_{j=0,1,3} U_{j,1}$	9	13	15	19	21	25	27	29	33	35	37	41				

Table 2.20: Number of unstable eigenvalues for each isotypical component along the branch of the relative equilibrium with (S_4) symmetry

Isotypical component	Intervals for values of parameter $\alpha \cdot 10^2$							
	[3.6154, 3.6242]	[3.6247, 3.6587]	[3.6592, 3.6627]	[3.6632, 3.6902]	[3.6907, 3.7058]	[3.7063, 3.7118]		
$U_{0,1}$	4	4	⑥	6	6	⑧		
$U_{1,1}$	6	⑫	12	⑮	⑳	24		
$\bigoplus_{j=0}^1 U_{j,1}$	10	16	18	24	30	32		

Based on the numerical evidence, Theorem 2.1.14 allows us to predict the following bifurcations of branches of relative periodic solutions.

(a) The following branches of relative periodic solutions bifurcate from (S_5) -symmetric branch of relative equilibria:

(i) with symmetry (S_5) for $\alpha \approx 0.0744915$, $\alpha \approx 0.612203$;

(ii) with symmetries (D_6) , (S_4) , $(D_6^{\mathbf{d}})$, $(D_4^{\mathbf{d}})$, $(\mathbb{Z}_4^{\mathbf{t}_1})$, $(\mathbb{Z}_5^{\mathbf{t}_1})$, $(\mathbb{Z}_6^{\mathbf{t}_2})$ for $\alpha \approx 0.054159$, $\alpha \approx 0.190194$, $\alpha \approx 0.2253355$.

(b) The following branches of relative periodic solutions bifurcate from $(\mathbb{Z}_5^{\mathbf{t}_1})$ -symmetric branch of relative equilibria:

(i) with symmetry $(\mathbb{Z}_5^{\mathbf{t}_1})$ for $\alpha \approx 0.072873$;

(ii) with symmetries $(\mathbb{Z}_5^{\mathbf{t}_1, \mathbf{t}_1})$ for $\alpha \approx 0.0367485$, $\alpha \approx 0.072873$.

(c) The following branches of relative periodic solutions bifurcate from $(D_6^{\mathbf{d}})$ -symmetric branch of relative equilibria:

(i) with symmetries $(\mathbb{Z}_6^{\mathbf{t}_3, \mathbf{t}_1})$, $(D_2^{\mathbf{d}, \mathbf{d}})$ and $(D_2^{\mathbf{d}, \hat{\mathbf{d}}})$ for $\alpha \approx 0.0362275$, $\alpha \approx 0.036575$, $\alpha \approx 0.036825$, $\alpha \approx 0.037475$, $\alpha \approx 0.037825$;

(ii) with symmetry $(D_6^{\mathbf{d}, \mathbf{d}})$ for $\alpha \approx 0.0363745$, $\alpha \approx 0.036675$, $\alpha \approx 0.037125$, $\alpha \approx 0.037175$, $\alpha \approx 0.037525$, $\alpha \approx 0.037625$.

Remark 2.2.7. Note that branches of relative periodic solutions with symmetries $(\mathbb{Z}_6^{\mathbf{t}_3, \mathbf{t}_2})$, $(D_2^{\mathbf{d}})$ and $(D_2^{\mathbf{d}, \mathbf{z}})$ do not bifurcate from $(D_6^{\mathbf{d}})$ symmetric relative equilibrium because S^1 acts trivially in isotypical component U_2 (see case (c) in Subsubsection 2.2.4).

(d) The following branches of relative periodic solutions bifurcate from (S_4) -symmetric branch of relative equilibria:

(i) with symmetry (S_4) for $\alpha \approx 0.0365895$;

(ii) with symmetries $(Z_4^{t_2})$, (D_4^d) , (D_2^d) and $(Z_3^{t_1})$ for $\alpha \approx 0.0362445$, $\alpha \approx 0.0366295$;

2.3 System with Hysteresis Operators

In this section, we consider an example of nonsmooth FDEs, in which nonsmoothness is introduced by a *hysteresis operator* [84]. To this end, we set up a model of an electric motor system with magnetic hysteresis losses in the inductor.

First, let us consider equations of an electric motor system without hysteresis, which is shown in Figure 2.1:

$$\begin{aligned}
 C\dot{v} + w + \beta v^3 - \alpha v &= j_0, \\
 L\dot{w} + \kappa\dot{\theta} &= v, \\
 m\rho^2\ddot{\theta} + 2m\rho\dot{\rho}\dot{\theta} &= \kappa w - \gamma\dot{\theta}, \\
 m\ddot{\rho} - m\rho\dot{\theta}^2 &= -\sigma(\rho - \rho_0) - \hat{\gamma}\dot{\rho}.
 \end{aligned}
 \tag{2.122}$$

Here v is the voltage across the capacitor with the capacitance C ; w denotes the current through the motor and the inductor with the inductance L ; the active circuit element composed of the battery and the tunnel diode has the cubic current-voltage characteristics $i = \beta v^3 - \alpha v$ with $\beta > 0$; j_0 is the constant current from the DC current source. The motor's rotor is modeled by a point mass m which has polar coordinates θ, ρ ; the term $-\sigma(\rho - \rho_0)$ is the elastic force; $\gamma\dot{\theta}$ and $\hat{\gamma}\dot{\rho}$ are the radial component and the torque of the friction force, respectively. Further, for simplicity, it is assumed that all losses are due to friction, while the losses associated with electrical resistance and conversion of the electrical energy into the mechanical energy are negligible. Hence, $v_m w = \tau\dot{\theta}$, where v_m is the voltage applied to the motor and τ is the torque which is proportional to the current, $\tau = \kappa w$, where κ is the motor torque constant.

We note that if the mechanical component is disconnected, i.e., $\kappa = 0$, then the electrical circuit is the Van der Pol oscillator which sustains self-oscillations for $\alpha > 0$. In other words,

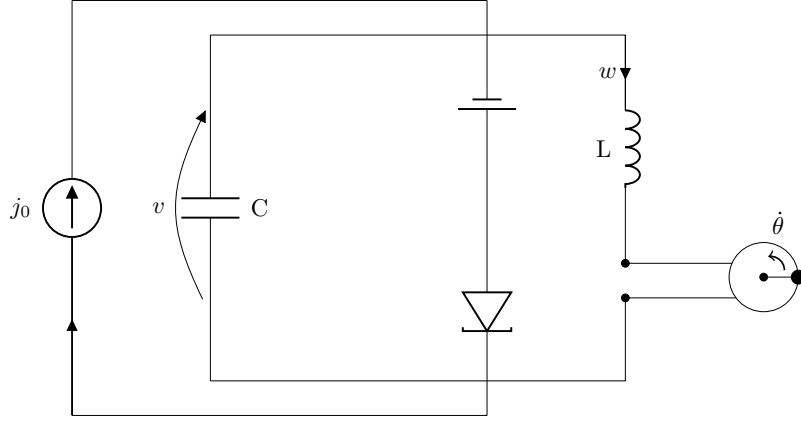


Figure 2.1: S^1 -equivariant electro-mechanical oscillator.

considering α as a bifurcation parameter with the other parameters fixed, the supercritical Hopf bifurcation occurs at $\alpha_0 = 0$. On the other hand, the electro-mechanical system (2.122) with $\kappa > 0$ admits the relative equilibrium solutions defined by the equations $\dot{\theta} = const$, $\rho = const$, $w = const$, $v = const$, which imply

$$m\rho\dot{\theta}^2 = \sigma(\rho - \rho_0), \quad v = \kappa\dot{\theta}, \quad \kappa w = \gamma\dot{\theta}, \quad w + \beta v^3 - \alpha v = j_0. \quad (2.123)$$

Oscillators (2.122) can be coupled into a symmetric configuration using mechanical or electrical coupling. For example, we consider the D_n -symmetric configuration with mechanical coupling as shown in Figure 2.2. of the rotors. Assuming that the connections of the rotors are elastic, this system is described by the equations

$$\begin{aligned} C\dot{v}_k + w_k + \beta v_k^3 - \alpha v_k &= j_0, \\ L\dot{w}_k + \kappa\dot{\theta}_k &= v_k, \\ m\rho_k^2\ddot{\theta}_k + 2m\rho_k\dot{\rho}_k\dot{\theta}_k &= \kappa w_k - \gamma\dot{\theta}_k + \delta(\theta_{k+1} - 2\theta_k + \theta_{k-1}), \\ m\dot{\rho}_k - m\rho_k\dot{\theta}_k^2 &= -\sigma(\rho_k - \rho_0) - \hat{\gamma}\dot{\rho}_k, \end{aligned} \quad (2.124)$$

where $k \in \mathbb{Z}_n$. If equation (2.122) admits a relative equilibrium $\dot{\theta} = \omega_*$, $\rho = \rho_*$, $w = w_*$, $v = v_*$, then system (2.124) has a fully synchronized (fully symmetric) relative equilibrium with

$$\dot{\theta}_1 = \cdots = \dot{\theta}_n = \omega_*, \quad \rho_1 = \cdots = \rho_n = \rho_*, \quad w_1 = \cdots = w_n = w_*, \quad v_1 = \cdots = v_n = v_*.$$

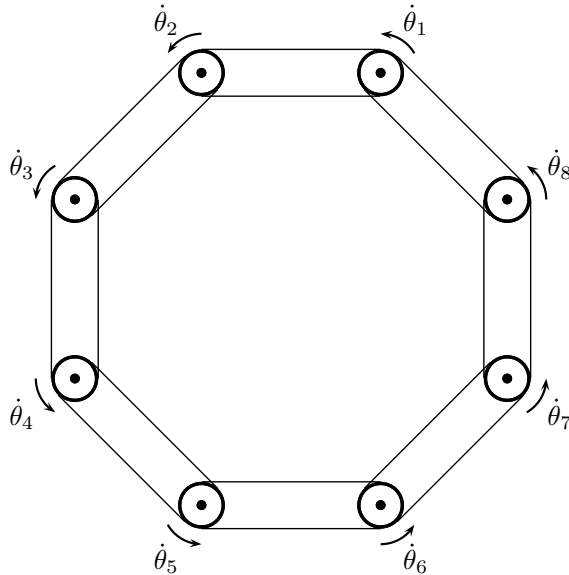


Figure 2.2: D_8 -symmetric mechanical coupling of 8 identical oscillators (2.122).

In addition to linear energy losses (which are present in (2.122) in the form of mechanical friction and could additionally include electrical energy losses due to resistance), further losses can be introduced by hysteresis nonlinearities. Possible sources of hysteresis in the mechanical components include dry friction and plasticity in the stress-strain relationship of the materials. The electrical component can be affected by the ferromagnetic hysteresis. Any form of hysteresis introduces nonsmoothness into the model.

As an example, let us consider the oscillator shown in Figure 2.1 in which the inductor has a ferromagnetic core exhibiting hysteresis. Due to hysteresis, an instantaneous value of the magnetization $m(t)$ of the ferromagnetic material depends not only on the value $h(t)$ of the magnetic field at the same moment, but also on previous values of h . Hence the constitutive relationship between m and h is an operator relationship. A widely used model for such an operator is the so-called Preisach operator [103],

$$m(t) = (P[\phi_0]h)(t), \tag{2.125}$$

which maps the variable magnetic field h to the variable magnetization m in the space $C(t_0, \infty)$ of continuous functions; here ϕ_0 is an infinite-dimensional parameter (called the initial state of the Preisach model) describing the physical state of the ferromagnetic material at the initial moment; see Section 1.2.4 for the definition of the Preisach operator; further details can be found in [26, 103].

Assuming the relationship (2.125) between h and m and taking into account that the magnetic field h is proportional to the current w , the second equation of system (2.122) transforms to

$$L \frac{d}{dt} \left(w + P[\phi_0]w + \kappa\theta \right) = v, \quad (2.126)$$

where the parameters of the Preisach operator are properly rescaled when passing from (2.125) to (2.126). Coupled system (2.124) changes accordingly to

$$\begin{aligned} C\dot{v}_k + w_k + \beta v_k^3 - \alpha v_k &= j_0, \\ L \frac{d}{dt} \left(w_k + P[\phi_0]w_k + \kappa\theta_k \right) &= v_k, \\ m\rho_k^2 \ddot{\theta}_k + 2m\rho_k \dot{\rho}_k \dot{\theta}_k &= \kappa w_k - \gamma \dot{\theta}_k + \delta(\theta_{k+1} - 2\theta_k + \theta_{k-1}), \\ m\ddot{\rho}_k - m\rho_k \dot{\theta}_k^2 &= -\sigma(\rho_k - \rho_0) - \hat{\gamma} \dot{\rho}_k, \quad k \in \mathbb{Z}_n. \end{aligned} \quad (2.127)$$

This system possesses the same relative equilibria as system (2.124) because $w = \text{const}$ implies $P[\phi_0]w = \text{const}$.

The Preisach operator is not differentiable on a dense subset of its domain (this is a common feature of hysteresis operators [153, 26]). In particular, the operator-differential systems such as (2.127) do not possess smooth integral manifolds. However, as it was shown in [13, 2], the Preisach operator $P[\phi_0]$ is differentiable and has zero derivative at any point $w = \text{const}$ (for admissible values of the initial state parameter ϕ_0). As a consequence, the operator equation of the periodic problem for system (2.127) (which can be constructed in the same way as in Section 2.1, see [13] for details) is differentiable at the relative equilibrium. Hence the theorems of Section 2.1 apply. Moreover, the linearization of the operator equation at

the relative equilibrium point is the same for system (2.124) without hysteresis and system (2.127) with hysteresis because the Preisach operator is asymptotically small compared to the linear terms near this point [13]. This simplifies the application of Theorem 2.1.14³.

Table 2.21 illustrates the application of Theorem 2.1.14 to the fully symmetric relative equilibrium state of system (2.127) with $n = 8$. We use α as a bifurcation parameter. All other parameters are unit except for the motor torque constant κ which is set to 0.3. When α varies from 0.02 to 0.1705 Hopf bifurcations occur in different isotypical components giving rise to relative periodic solutions with corresponding symmetries. In particular, the following branches are born:

- (i) with symmetry (D_8) at $\alpha \approx 0.06325$;
- (ii) with symmetries $(Z_8^{t_1}), (D_2^d), (\tilde{D}_2^d)$ at $\alpha \approx 0.07925$;
- (iii) with symmetries $(Z_8^{t_2}), (D_4^d), (\tilde{D}_4^d)$ at $\alpha \approx 0.06925$;
- (iv) with symmetries $(Z_8^{t_3}), (D_2^d), (\tilde{D}_2^d)$ at $\alpha \approx 0.04175$;
- (v) with symmetry (D_8^d) at $\alpha \approx 0.03675$.

Plasticity effects in the rotor can also produce hysteresis with the associated energy losses. These can be taken into account, for example, by introducing the Prandtl-Ishlinskii operator into the last equation of system (2.127) as a model of the stress-strain relation of an elastoplastic material. This operator is a particular case of the Preisach operator [26]. Systems involving both hysteresis nonlinearities and delays can be analyzed in a similar fashion. As an example, one can consider a counterpart of system (2.127) with a delay in the coupling.

³However, one can show that hysteresis affects the asymptotics and stability properties of cycles born via the Hopf bifurcation.

Table 2.21: Number of unstable eigenvalues in each isotypical component along the branch of the relative equilibrium with (D_8) symmetry.

Isotypical component	Intervals for values of parameter $\alpha \cdot 10^2$							
	[2.00, 3.65]	[3.70, 4.15]	[4.20, 6.30]	[6.35, 6.90]	[6.95, 7.90]	[7.95, 17.05]		
$U_{0,1}$	0	0	0	②	2	2	2	2
$U_{1,1}$	0	0	0	0	0	0	④	4
$U_{2,1}$	0	0	0	0	0	④	4	4
$U_{3,1}$	0	0	④	4	4	4	4	4
$U_{4,1}$	0	②	2	2	2	2	2	2
$\bigoplus_{j=0}^4 U_{j,1}$	0	2	6	8	12	16	16	16

CHAPTER 3

PERIODIC PULSATING DYNAMICS OF SLOW-FAST DELAYED SYSTEMS WITH A PERIOD CLOSE TO THE DELAY¹

The main goal of this chapter is to study a class of singularly perturbed delayed models of population dynamics, which exhibit periodic pulsating solutions with a period close to the delay. Such models show an apparent resemblance to the model of mode-locked semiconductor laser (1.1) both in the mechanism of the formation of the pulses and in their properties. We employ asymptotic techniques to establish the behavior of pulsating solutions and the form of spectra of the equilibria they bifurcate from.

In Section 3.2, we introduce a population model, perform a linear stability analysis of both the zero and positive steady states near the threshold, and discuss the bifurcations that initiate the pulsating dynamics. Further, the role of the competition for the realization of the bifurcation scenario is highlighted. In Section 3.3, we derive asymptotic approximations for the pulsating periodic solutions. The last section contains further discussion and conclusions.

3.1 Main prototype model

We consider the system

$$\gamma^{-1}A' = -A + \kappa G(t - T)A(t - T) - \mu QA, \quad (3.1)$$

$$\gamma_q^{-1}Q' = q_0 - \beta Q - sAQ, \quad (3.2)$$

$$G' = g_0 - \alpha G - kAG, \quad (3.3)$$

¹The material of this chapter was published in *European Journal of Applied Mathematics*. Copyright: ©Cambridge University Press 2017. Reprinted with permission.

where the real variables A, Q, G are population densities of three species; T is the maturity delay of the species A , see [133]; and, all the parameters are positive². The species A is a predator for the prey G ; the species Q competes with A .

The rate of population processes for the three species is assumed to be different with A being the fastest species (with faster metabolism, higher reproductive rate etc.), G being the slowest species, and Q changing at an intermediate rate, that is $1 \leq \gamma_q \leq \gamma$. Further, the species A is assumed to be much faster than the species G , thus $\gamma \gg 1$. The species G and Q can have comparable rates ($\gamma_q \approx 1$) or Q can be much faster than G ($1 \ll \gamma_q$). However, it is important to stress that the parameters γ and γ_q play different roles in the following asymptotic analysis. Namely, our asymptotic formulas are obtained in the limit of $\gamma \rightarrow \infty$ while we keep γ_q fixed. In numerical simulations, we use γ_q ranging from 1 to γ .

The species Q plays an important role which will be clarified in further sections. In particular, we will see that the system of the two equations (3.1) (with zero Q) and (3.3) does not demonstrate pulsating dynamics near the threshold.

The species Q and G are assumed to be recruited through constant immigration in (3.1)–(3.3). In further sections, we will show that similar systems with different recruitment terms, including recruitment with constant birth rate, show similar pulsating dynamics near the threshold. Also, delaying different terms has little effect on solutions in our examples; for instance, replacing the delayed term $G(t - T)$ by $G(t)$ in (3.1)–(3.3) preserves the periodic pulsating dynamics.

We will discuss nonnegative solutions only. Note that system (3.1)–(3.3) is positively invariant.

We associate the pulsating regime of system (3.1)–(3.3) near the point of the transcritical bifurcation of equilibria with the Hopf bifurcations from the positive equilibrium. The recruitment rate g_0 of the prey G will be used as the bifurcation parameter.

²The death rate of the species A is scaled to 1. The number of parameters can be further reduced in a standard way by rescaling the phase variables and time.

3.2 Bifurcation analysis

3.2.1 Bifurcations at the equilibrium with $A = 0$

System (3.1)–(3.3) has an equilibrium with zero A ,

$$A_o = 0, \quad Q_o = \frac{q_0}{\beta}, \quad G_o = \frac{g_0}{\alpha}, \quad (3.4)$$

for all positive g_0 , and a positive equilibrium either for $g_0 > g_0^*$ or for $g_0 < g_0^*$, where the threshold value g_0^* is defined by

$$\frac{\kappa g_0^*}{\alpha} - \frac{\mu q_0}{\beta} = 1. \quad (3.5)$$

These two equilibria collide in a transcritical bifurcation for $g_0 = g_0^*$. The positive equilibrium near the threshold is defined by the asymptotic formulas

$$A_* = \tilde{a}\delta + O(\delta^2), \quad Q_* = \frac{q_0}{\beta} + \tilde{q}\delta + O(\delta^2), \quad G_* = \frac{g_0^*}{\alpha} + \tilde{g}\delta + O(\delta^2) \quad (3.6)$$

where $\delta = g_0 - g_0^*$ and the coefficients of the first order correction are given by

$$\tilde{a} = \frac{1}{\frac{\kappa g_0^*}{\alpha} - \frac{\alpha \mu s q_0}{\kappa \beta^2}}, \quad \tilde{q} = \frac{1}{\frac{\alpha \mu}{\kappa} - \frac{\kappa g_0^* \beta^2}{\alpha s q_0}}, \quad \tilde{g} = \frac{\mu}{\kappa} \tilde{q}.$$

We will assume that

$$\frac{\kappa g_0^*}{\alpha^2} > \frac{\mu s q_0}{\kappa \beta^2}. \quad (3.7)$$

In this case, the positive equilibrium exists for $g_0 > g_0^*$ and is stable near the threshold. (If the opposite inequality holds, then the positive equilibrium exists for $g_0 < g_0^*$ and is unstable near the threshold.)

The eigenvalues of the linearization of system (3.1)–(3.3) at the equilibrium (3.4) with zero A are defined by the relations $\lambda = -\gamma\beta < 0$, $\lambda = -\alpha < 0$ and

$$1 + \frac{\lambda}{\gamma} = \frac{\kappa g_0}{\alpha} e^{-\lambda\Gamma} - \frac{\mu q_0}{\beta}. \quad (3.8)$$

The solutions of (3.8) satisfy $\text{Re } \lambda < 0$ in a left neighbourhood of the threshold, more precisely, for $g_0 < g_0^* = \alpha(1 + \mu q_0/\beta)/\kappa$. Hence, the equilibrium (3.4) is stable below the

threshold, i.e., for $g_0 < g_0^*$. Consequently, the positive equilibrium (3.6) is stable in a small right neighborhood of the threshold, i.e., for small $\delta = g_0 - g_0^* > 0$.

The equilibrium (3.4) undergoes a sequence of Hopf bifurcations in a small right neighborhood of the threshold $g_0 = g_0^*$ for large γ . To see this, first note that in the limit $\gamma = \infty$ the solutions of the characteristic equation (3.8) have the form

$$\lambda = i\omega_n, \quad \omega_n = \frac{2\pi n}{T}, \quad n = 1, 2, \dots,$$

i.e., the equilibrium satisfies the necessary condition for infinitely many simultaneous Hopf bifurcations at the threshold point $g_0 = g_0^*$. Moreover, these bifurcations are in resonance with each other as the frequencies ω_n are all multiples of $2\pi/T$. For finite γ , setting $\lambda = i\omega$ in (3.8) in order to satisfy the Hopf bifurcation condition, and rearranging, we obtain the equations

$$\frac{\omega}{\gamma} = -\frac{\kappa g_0^*}{\alpha} \tan \omega T, \quad (3.9)$$

$$\delta = g_0^* \left(\frac{1}{\cos \omega T} - 1 \right) > 0, \quad (3.10)$$

which define the frequency of the cycle and the bifurcation value of the parameter $g_0 = g_0^* + \delta$ for each Hopf bifurcation from the equilibrium (3.4). Figure 3.1 illustrates solutions of the transcendental equation (3.9). For $\gamma \gg 1$, the solutions of (3.9), (3.10) are approximated by the asymptotic formulas

$$\omega_n = \frac{2\pi n}{T} \left(1 - \frac{\alpha}{\kappa g_0^* \gamma T} + \frac{\alpha^2}{(\kappa g_0^* \gamma T)^2} \right) + O(\gamma^{-3}), \quad (3.11)$$

$$\delta_n = \frac{\alpha^2}{2\kappa^2 g_0^*} \left(\frac{2\pi n}{\gamma T} \right)^2 + O(\gamma^{-3}) \quad (3.12)$$

with $n = 1, 2, \dots$. Hence, the n -th Hopf bifurcation after the threshold has a frequency close to $2\pi n/T$ and $O(\sqrt{\gamma})$ Hopf bifurcations occur within the distance of order $1/\gamma$ from the threshold on the parameter g_0 axis.

Following [95, 168], the spectrum of the zero equilibrium defined by (3.8) can be called *weak* or *pseudocontinuous* spectrum. It is characterized by a specific scaling of the real and imaginary parts of the eigenvalues $\lambda = x + i\gamma\omega$ with $\gamma \gg 1$, where x and ω are of order 1. Using this scaling, we obtain from (3.8) an approximate relationship between the real and imaginary parts of the eigenvalues:

$$x(\omega) = \frac{1}{2T} \left(2 \ln \left(\frac{g_0}{g_0^*} \right) - \ln \left(1 + \left(\frac{\alpha\omega}{g_0^* \kappa} \right)^2 \right) \right) + O(\gamma^{-1}), \quad (3.13)$$

which is dual to formulas (3.11), (3.12). The curve (3.13) carrying the eigenvalues simply moves to the right with increasing g_0 , see Figure 3.2a.

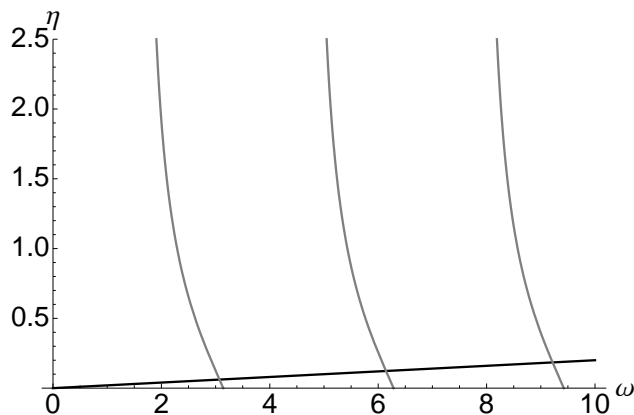


Figure 3.1: Solution of (3.9). The horizontal axis is ω . Every second intersection of the straight line $\eta = \omega/\gamma$ and the function $\eta = -\kappa g_0^* \tan(\omega T)/\alpha$ satisfies the condition (3.10). Here $\gamma = 100$, $T = 1$.

3.2.2 Bifurcations at the positive equilibrium

As the bifurcation parameter g_0 increases across the threshold, the positive equilibrium (3.6) also undergoes a sequence of Hopf bifurcations, which we deem responsible for the creation and formation of the periodic pulsating solution. The first Hopf bifurcation with the frequency close to $2\pi/T$ destabilizes the positive equilibrium and creates a stable cycle (see branch H_1 in Figure 3.3). As the parameter g_0 increases further, this cycle changes its shape

continuously into a pulsating periodic solution, see Figure 3.4. The amplitudes of harmonics of the A -component $A(t/\tau) = \sum_{n=1}^{\infty} A_n \cos(2\pi n t/\tau + \phi_n)$ of the periodic solution, where τ is the period of A , grow with g_0 , while the phase differences $\phi_k - \phi_1$ almost vanish, see Figure 3.5. At the same time the positive equilibrium undergoes a cascade of secondary Hopf bifurcations with the frequencies of the higher harmonics. The whole cascade of the Hopf bifurcations and the transformation of the cycle to a pulsating solution happen in a small right neighbourhood of the threshold $g_0 = g_0^*$, see Figure 3.5.

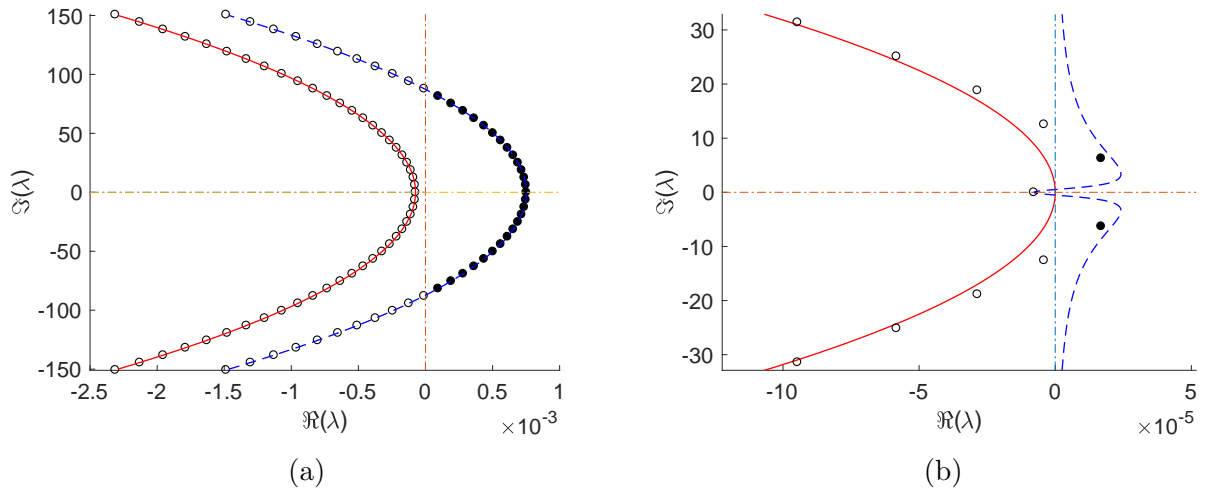


Figure 3.2: Panel (a): Spectra of the zero equilibrium for $g_0 = 3.7497$ and $g_0 = 3.7528$. Numerical values of the eigenvalues are shown by circles; lines are obtained from (3.13). Filled circles correspond to unstable eigenvalues. Panel (b): Spectrum of the positive equilibrium of system (3.1)–(3.3) after the first Hopf bifurcation ($g_0 = 3.75003$), i.e., exactly one pair of complex conjugate eigenvalues cross the imaginary axis from left to right. Solid line defined by (3.19) carries the weak spectrum; dashed line (3.18) carries the strong spectrum. Parameters are as follows: $\gamma = 1000$, $\gamma_q = 10$, $\kappa = 0.6$, $\mu = 0.5$, $\alpha = 1$, $q_0 = 2.5$, $\beta = 1$, $s = 1$, $k = 0.7$, $T = 1$.

The characteristic equation for the positive equilibrium is

$$e^{T\lambda} = \frac{G_*\kappa(\alpha + \lambda)(A_*s\gamma_q + \beta\gamma_q + \lambda)}{(A_*k + \alpha + \lambda)\left(A_*s\gamma_q\left(1 + \frac{\lambda}{\gamma}\right) + (\beta\gamma_q + \lambda)\left(1 + \frac{\lambda}{\gamma} + Q_*\mu\right)\right)}. \quad (3.14)$$

Using asymptotic formulas (3.6) and the ansatz $\lambda = i\omega$ for the eigenvalues of the linearization, we obtain the following asymptotic formulas for the frequency and the bifurcation value of

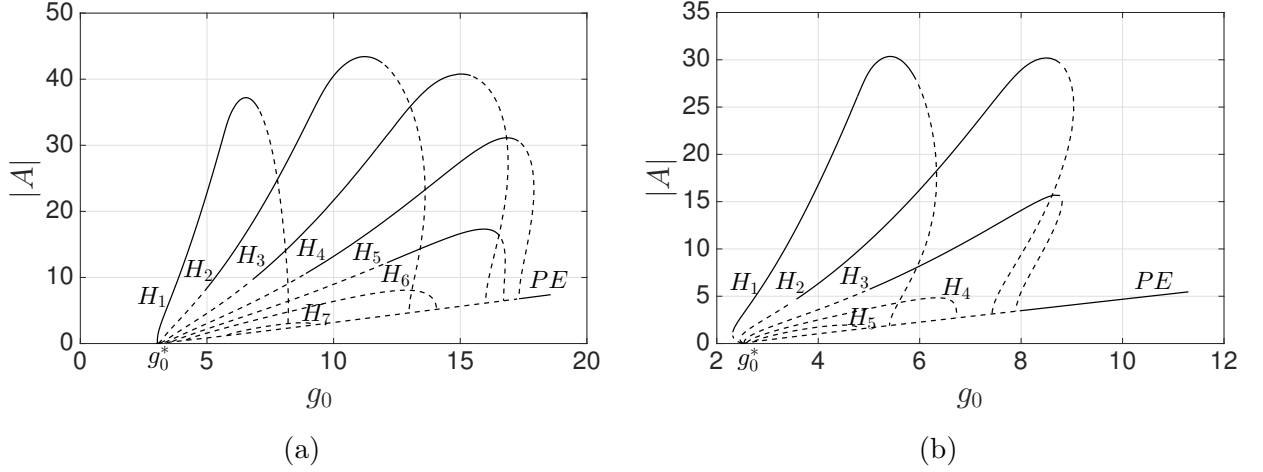


Figure 3.3: Bifurcation diagrams obtained with numerical package DDE-BIFTOOL for system (3.1)–(3.3) for two parameter sets. The vertical axis shows the maximum of the A -component of a periodic solution. The PE line corresponds to the positive equilibrium. Branches H_1 – H_7 (H_1 – H_5 on panel (b)) correspond to the periodic solutions born via Hopf bifurcations on the positive equilibrium. Stable branches are shown by solid lines and unstable branches are shown by dashed lines. The branch H_1 on panel (b) exhibits slight hysteresis near the threshold g_0^* . All the branches connect to the branch of the positive equilibrium at Hopf bifurcation points at both ends.

the parameter at each Hopf bifurcation point³:

$$\omega_n = \frac{2\pi n}{T} \left(1 - \frac{\alpha}{\kappa g_0^* \gamma T} \right) + O(\gamma^{-2}), \quad (3.15)$$

$$\delta_n = \left(\frac{2\pi n}{\gamma T} \right)^2 \frac{(\beta^2 g_0^* \kappa k - \alpha^2 \mu q_0 s) \left(\beta^2 + \left(\frac{2\pi n}{T \gamma_q} \right)^2 \right)}{2\kappa^2 g_0^* \beta^2 \left(\mu q_0 s - g_0^* \kappa k \left(\frac{\beta^2 + \left(\frac{2\pi n}{T \gamma_q} \right)^2}{\alpha^2 + \left(\frac{2\pi n}{T} \right)^2} \right) \right)} + O(\gamma^{-3}). \quad (3.16)$$

We assume that, along with the relation (3.7), the conditions

$$\mu q_0 s > g_0^* \kappa k \left(\frac{\beta^2 + \left(\frac{2\pi}{T \gamma_q} \right)^2}{\alpha^2 + \left(\frac{2\pi}{T} \right)^2} \right) \quad \text{and} \quad \gamma_q > \frac{\alpha}{\beta} \quad (3.17)$$

are satisfied. Under these conditions, relation (3.16) implies $\delta = g_0 - g_0^* > 0$ for $n = 1, 2, \dots$

That is, according to (3.7), (3.16), conditions (3.17) ensure that the positive equilibrium

³The term of order γ^{-2} in the expansion (3.15) is different from the corresponding term in the expansion (3.11).

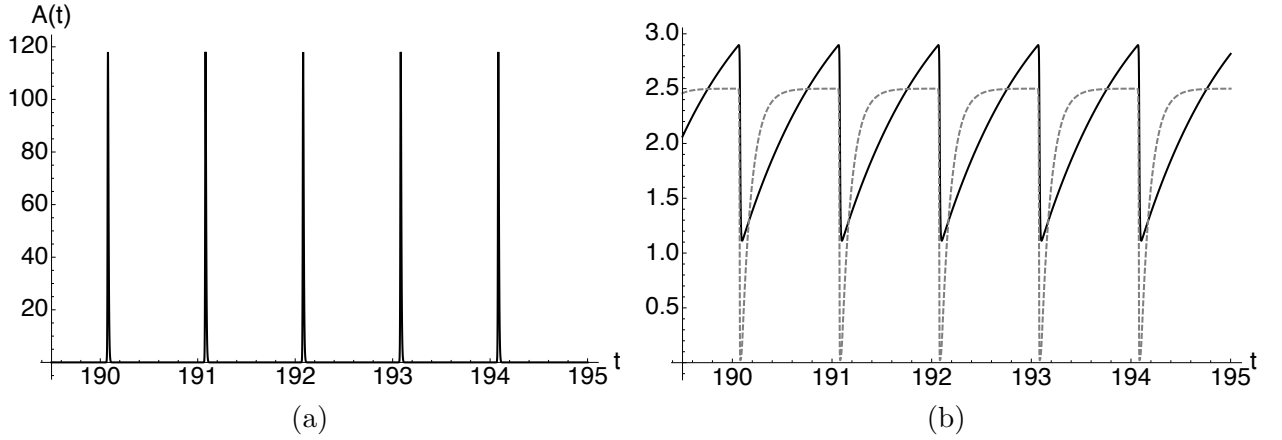


Figure 3.4: Time trace of the periodic solution of system (3.1)–(3.3). Panel (a): the A -component; Panel (b): the G -component (solid) and the Q -component (dashed). The A -component is almost zero between the pulses. The Q -component almost reaches the equilibrium value $g_0/\beta = 2.5$ between the pulses of the A -component and drops almost to zero during the pulse because $\gamma_q = 10$ is relatively large. The G -component drops fast during the pulse and then recovers slowly between the pulses. The period of the solution is close to the delay $T = 1$. The following parameters were used: $\gamma = 400$, $\gamma_q = 10$, $\kappa = 0.6$, $g_0 = 4$, $q_0 = 2.5$, $\alpha = 1$, $\beta = 1$, $s = 1$, $k = 0.7$, $T = 1$. The threshold value is $g_0^* = 3.75$.

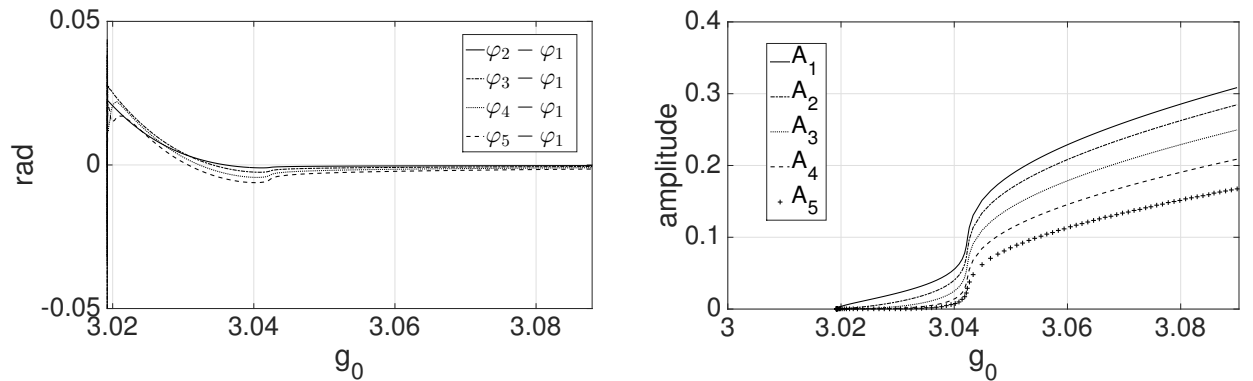


Figure 3.5: The phase and amplitude of the Fourier coefficients for the A -component $A(t/\tau) = \sum_{n=1}^{\infty} A_n \cos(2\pi n t/\tau + \phi_n)$ of the periodic solution along the branch H_1 shown in Figure 3.3a where τ is the period of solution.

undergoes the Hopf bifurcations with the frequencies close to the multiples $2\pi n/T$ of $2\pi/T$

for $n = 1, 2, \dots$ as g_0 increases across the threshold.

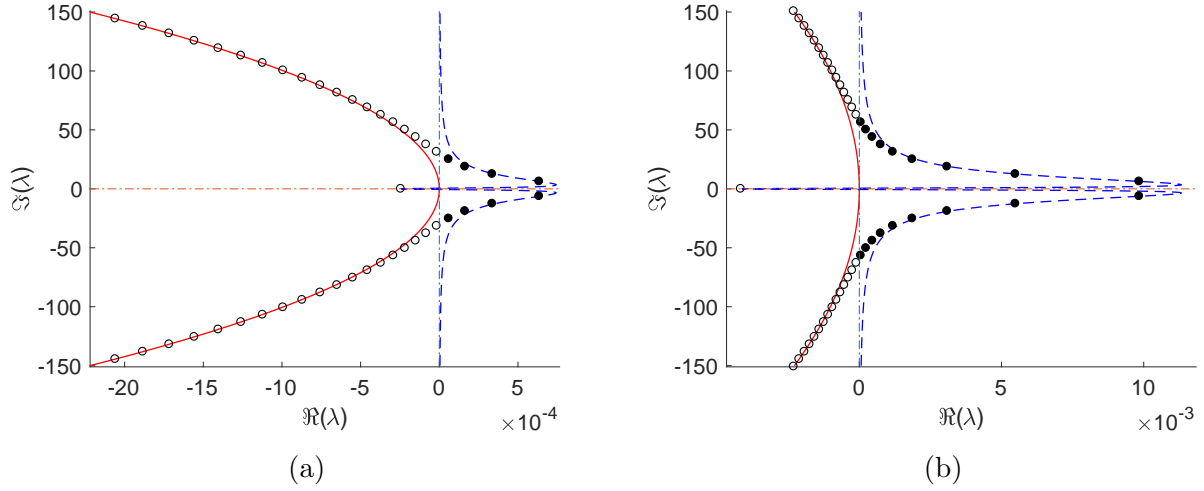


Figure 3.6: Spectrum of the positive equilibrium and curves (3.19), (3.18) for $g_0 = 3.7509$ (panel (a)) and $g_0 = 3.7648$ (panel(b)). Notation and other parameters are the same as in Figure 3.2b.

The spectrum of the positive equilibrium can be divided into two parts, which have different asymptotic properties with respect to the large parameter γ , cf. [95]. The *strong* spectrum consists of the eigenvalues $\lambda = x + i\omega + O(\gamma^{-1})$, which originate from the limit $\gamma = \infty$. Equation (3.14) implies the following approximate implicit relationship between the real and imaginary parts for these eigenvalues:

$$\frac{G_*^2 \kappa^2 ((\alpha + x)^2 + \omega^2) ((\gamma_q (A_* s + \beta) + x)^2 + \omega^2)}{((\alpha + A_* k + x)^2 + \omega^2) ((\gamma_q (A_* s + \beta + \beta \mu Q_*) + \mu Q_* x + x)^2 + (\mu Q_* \omega + \omega)^2)} = e^{2Tx}. \quad (3.18)$$

The *weak* spectrum is characterized by the asymptotic relationship $\lambda = x + i\gamma\omega$ and satisfies the approximate relationship

$$x(\omega) = \frac{1}{2T} \ln \left(\frac{G_*^2 \kappa^2}{G_*^2 \kappa^2 + \omega^2} \right). \quad (3.19)$$

With increasing g_0 , branches of the curve (3.19) “open”. Simultaneously, weak eigenvalues with smaller imaginary part leave this curve, cross imaginary axis producing the Hopf

Table 3.1: Comparison of the asymptotic and numerical values of δ_n, ω_n for the following set of parameters: $\gamma = 600, \gamma_q = 40, \kappa = 0.6, \mu = 0.5, \alpha = 1, q_0 = 2.5, \beta = 1, s = 1, k = 0.7, T = 1$

n	$\delta_n = g_0 - g_0^*$			ω_n		
	Asymptotic	Numerical	Error (%)	Asymptotic	Numerical	Error (%)
1	$1.1177 \cdot 10^{-5}$	$1.1170 \cdot 10^{-5}$	0.06	6.2785	6.2785	$< 10^{-4}$
2	$4.6817 \cdot 10^{-5}$	$4.6896 \cdot 10^{-5}$	0.17	12.5571	12.5571	$< 10^{-4}$
3	$1.1665 \cdot 10^{-4}$	$1.1731 \cdot 10^{-4}$	0.56	18.8356	18.8356	$1.60 \cdot 10^{-4}$
4	$2.3632 \cdot 10^{-4}$	$2.3903 \cdot 10^{-4}$	1.13	25.1141	25.1140	$3.57 \cdot 10^{-4}$
5	$4.2773 \cdot 10^{-4}$	$4.3593 \cdot 10^{-4}$	1.88	31.3927	31.3925	$6.18 \cdot 10^{-4}$
6	$7.1905 \cdot 10^{-4}$	$7.3993 \cdot 10^{-4}$	2.82	37.6712	37.6708	$9.45 \cdot 10^{-4}$

bifurcations described by (3.15), (3.16), and become a part of the strong spectrum (3.18), see Figures 3.2b and 3.6.

In Table 3.1, the asymptotic values of ω_n and δ_n given by formulas (3.15) and (3.16) are compared with the numerical values obtained for $\gamma = 600, \gamma_q = 40, \kappa = 0.6, \mu = 0.5, \alpha = 1, q_0 = 2.5, \beta = 1, s = 1, k = 0.7, T = 1$. Using these parameters for numerical continuation we observe 24 branches of periodic solutions. Table 3.1 features the first six branches. The accuracy of the asymptotic formulas decreases with increasing n .

We have conducted a number of further numerical simulations with different parameter sets satisfying conditions (3.7) and (3.17) and observed bifurcation diagrams and oscillating periodic solutions similar to those presented in Figures 3.3 and 3.4.

3.2.3 The role of competition

Here we briefly discuss the critical role of the species Q , which competes with the fast species A , in creating the pulsating periodic dynamics via the bifurcation scenario described above.

In order to highlight the role of the Q -species, we compare the dynamics of system (3.1)–(3.3) with that of the dynamics of the system

$$\gamma^{-1}A' = -A + \kappa G(t - T)A(t - T), \quad (3.20)$$

$$G' = g_0 - \alpha G - kAG, \quad (3.21)$$

which is obtained by setting $Q = 0$ in (3.1) and dropping (3.2). Dynamics of system (3.20), (3.21) is essentially the same as dynamics of system (3.1)–(3.3) with zero immigration rate $q_0 = 0$ of the Q -species.

System (3.20), (3.21) has two equilibrium points

$$A = 0, \quad G = \frac{g_0}{\alpha}; \quad A = \frac{\kappa(g_0 - g_0^*)}{k} = \frac{\kappa\delta}{k}, \quad G = \frac{1}{\kappa},$$

which collide in the transcritical bifurcation at the threshold value

$$g_0^* = \frac{\alpha}{\kappa} \quad (3.22)$$

of the bifurcation parameter g_0 . Like in the case of the three-dimensional systems (3.1)–(3.3), the equilibrium with zero A is stable below the threshold and unstable above the threshold, while the equilibrium with nonzero A is positive and stable above the threshold, i.e., for $g_0 > g_0^*$ (without any additional assumptions about the parameters of (3.20), (3.21)). The unstable equilibrium undergoes the cascade of Hopf bifurcations at the bifurcation points, and with the frequencies, defined by relations (3.9), (3.10) and satisfying the asymptotic formulas (3.11), (3.12). However, the positive equilibrium remains stable for all $g_0 > g_0^*$ and the system exhibits the equilibrium dynamics rather than a periodic dynamics above the threshold. The reason is that the equilibrium with nonzero A undergoes the cascade of Hopf bifurcations below the threshold, that is in the parameter domain $g_0 < g_0^*$ where this equilibrium has a negative A -component and is unstable, rather than above the threshold

where the equilibrium is positive and stable. Indeed, substituting the ansatz $\lambda = i\omega$ in the characteristic equation

$$\gamma^{-1}(\lambda + \kappa g_0)\lambda + (1 - e^{-\lambda T})\lambda + \kappa g_0 - \alpha e^{-\lambda T} = 0 \quad (3.23)$$

of the linearization of the system at the equilibrium with nonzero A , we obtain the asymptotic formula

$$\delta = -\frac{\alpha}{2\kappa} \left(\frac{2\pi n}{\gamma T} \right)^2 \left(1 + \left(\frac{2\pi n}{\alpha T} \right)^2 \right) + O(\gamma^{-3}),$$

where the negative sign of $\delta = g_0 - g_0^*$ indicates that the Hopf bifurcation occurs below the threshold. Equation (3.23) implies

$$(\omega^2 + \kappa^2 g_0^2)(1 + \omega^2 \gamma^{-2}) = \omega^2 + \alpha^2$$

for $\lambda = i\omega$, which is only possible for $g_0 \leq g_0^* = \alpha/\kappa$, that is below the threshold, thus proving stability of the positive equilibrium. Clearly (3.23) cannot have real positive eigenvalues for $g_0 > g_0^*$ either.

3.3 Scaling with γ . Approximate solution

3.3.1 Separation of slow and fast stages

In order to analyze and approximate the asymptotic behavior of the pulsating periodic solution for large γ , we adapt the approach proposed by New and Haus for modeling optical systems in [111, 59] by partial differential equations and an extension of this approach to delay differential models of mode-locked semiconductor lasers developed in [156].

Consider a pulsating periodic solution of (3.1)–(3.3). We divide the period into two stages, the short fast stage $t_b \leq t \leq t_e$ containing the pulse and the slow stage $t_e \leq t \leq t_b + \tau$, during which A is close to zero. Here $\tau \approx T$ is the period of the solution, t_b is the moment when a pulse begins, t_e is the moment when the pulse ends, $t_e - t_b \ll 1$. We then further introduce

a partition $t_b < t'_b < t'_e < t_e$ of the fast stage into three subintervals. During the interval $[t_b, t'_b]$ the variable A grows from a small value ε to a large value ε^{-1} , it stays larger than ε^{-1} over the interval $[t'_b, t'_e]$, and decreases back to the small value ε over the interval $[t'_e, t_e]$ (to be specific, $\varepsilon = \varepsilon(\gamma)$ scales with γ in such a way that $\varepsilon(\gamma) \rightarrow 0$ and $-\gamma^{-1} \ln \varepsilon(\gamma) \rightarrow 0$ as $\gamma \rightarrow \infty$). We assume that A grows exponentially on $[t_b, t'_b]$ as $e^{\gamma\lambda_1 t}$ and exponentially decreases as $e^{\gamma\lambda_2 t}$ on $[t'_e, t_e]$ with $\lambda_1 > 0 > \lambda_2$. These assumptions will be shown to lead to a self-consistent answer for the pulse (in particular the values of λ_1 and λ_2 are evaluated below). Further, they imply that

$$G(t_b) \approx G(t'_b), \quad Q(t_b) \approx Q(t'_b), \quad \int_{t_b}^{t_e} A(\theta) d\theta \approx \int_{t'_b}^{t'_e} A(\theta) d\theta \quad (3.24)$$

for large γ (that is, the left and right sides of each relation in (3.24) have the same limit as $\gamma \rightarrow \infty$). This allows us to identify t_b with t'_b and t_e with t'_e in the asymptotic approximations below.

Finally, we assume that the period of the periodic solution scales with γ as

$$\tau = T \left(1 + \frac{c}{\gamma T} \right) + O(\gamma^{-2}), \quad (3.25)$$

which again proves to lead to consistent asymptotic approximations.

3.3.2 Area of the pulse

During the phase $[t'_b, t'_e]$ of the pulse of A , the terms AQ and AG in the Q and G equations are large compared to the other terms, which therefore can be neglected. Hence, during this phase (3.2), (3.3) can be approximated by the equations

$$\begin{aligned} \gamma_q^{-1} Q' &= -sAQ, \\ G' &= -kAG. \end{aligned}$$

Integrating these equations and using the approximations (3.24), we obtain for the full fast stage $[t_b, t_e]$:

$$Q(t) = Q(t'_b) e^{-\gamma q s \int_{t'_b}^t A(\theta) d\theta} \approx Q_b e^{-\gamma q s P(t)}, \quad G(t) = e^{-k \int_{t'_b}^t A(\theta) d\theta} \approx G_b e^{-k P(t)}, \quad (3.26)$$

where $Q_b = Q(t_b)$, $G_b = G(t_b)$ and

$$P(t) = \int_{t_b}^t A(\theta) d\theta. \quad (3.27)$$

In particular, for the values $G(t_e) = G_e$, $Q_e = Q(t_e)$ at the moment $t = t_e$, we have

$$G_e = G_b e^{-k p}, \quad Q_e = Q_b e^{-\gamma q s p}, \quad (3.28)$$

where

$$p = \int_{t_b}^{t_e} A(\theta) d\theta.$$

On the other hand, integrating (3.1) over the fast stage and using the fact that A is close to zero at the moments t_b and t_e , we obtain the approximate equation

$$p = \kappa \int_{t_b - T}^{t_e - T} G(\theta) A(\theta) d\theta - \mu \int_{t_b}^{t_e} Q(\theta) A(\theta) d\theta. \quad (3.29)$$

The exponential form of the pulse that we assumed on the subintervals $[t_b, t'_b]$ and $[t'_e, t_e]$ of the fast stage and the estimate $\tau - T = O(\gamma^{-1})$ for the small difference between the period and the delay, which follows from (3.25), imply that $\int_{t_b - T}^{t_e - T} G(\theta) A(\theta) d\theta \approx \int_{t_b - \tau}^{t_e - \tau} G(\theta) A(\theta) d\theta$. Hence, the integrals in the right hand side of (3.29) are essentially integrals over the fast stage for two successive pulses. Therefore, using the periodicity of the solution and relations (3.26), we can rewrite (3.29) approximately as

$$\begin{aligned} p = \kappa \int_{t_b - \tau}^{t_e - \tau} G(\theta) A(\theta) d\theta - \mu \int_{t_b}^{t_e} Q(\theta) A(\theta) d\theta = \\ \int_{t_e}^{t_b} (\kappa G_b e^{-k P(\theta)} - \mu Q_b e^{-\gamma q s P(\theta)}) A(\theta) d\theta. \end{aligned}$$

Further, using (3.27), $A(\theta) d\theta = dP(\theta)$, hence

$$p = \frac{\kappa G_b}{k}(1 - e^{-kp}) - \frac{\mu Q_b}{\gamma_q s}(1 - e^{-\gamma_q s p}). \quad (3.30)$$

During the slow stage, the terms AQ and AG are small compared to the other terms in the Q and G equations. Neglecting these terms results in the linear equations

$$\begin{aligned} \gamma_q^{-1} Q' &= q_0 - \beta Q, \\ G' &= g_0 - \alpha G. \end{aligned}$$

Integrating these equations over the slow stage $[t_e, t_b + \tau]$ and combining the integrals

$$\begin{aligned} g_0 - \alpha G_b &= (g_0 - \alpha G_e) e^{-\alpha(t_b + \tau - t_e)} \approx (g_0 - \alpha G_e) e^{-\alpha T}, \\ q_0 - \beta Q_b &= (q_0 - \beta Q_e) e^{-\gamma_q \beta(t_b + \tau - t_e)} \approx (q_0 - \beta Q_e) e^{-\gamma_q \beta T} \end{aligned}$$

with (3.28), we obtain

$$G_b = \frac{g_0(1 - e^{-\alpha T})}{\alpha(1 - e^{-\alpha T - kp})}, \quad Q_b = \frac{q_0(1 - e^{-\gamma_q \beta T})}{\beta(1 - e^{-\gamma_q \beta T - \gamma_q s p})}. \quad (3.31)$$

Hence, (3.30) implies the fixed-point condition

$$p = \frac{\kappa g_0(1 - e^{-\alpha T})(1 - e^{-kp})}{k\alpha(1 - e^{-\alpha T - kp})} - \frac{\mu q_0(1 - e^{-\gamma_q \beta T})(1 - e^{-\gamma_q s p})}{\gamma_q s \beta(1 - e^{-\gamma_q \beta T - \gamma_q s p})} =: \eta(p). \quad (3.32)$$

The right hand side $\eta(p)$ is zero at zero, has the derivative $\kappa g_0/\alpha - \mu q_0/\beta > 1$ at zero, and converges to a constant as $p \rightarrow \infty$, see Figure 3.7a. Therefore, (3.32) has a positive root. Under further assumptions, the positive root is unique. For instance, the uniqueness is guaranteed whenever we increase the parameter γ_q keeping all the other parameters in (3.32) fixed. In particular, the positive root is unique in all the examples below. The conclusion is that the integral of the A -component over a period converges to a positive root p_* of (3.32) as $\gamma \rightarrow \infty$ (with other parameters fixed).

Figure 3.7b compares the value $p(\gamma)$ of this integral with its limit value p_* . The integral has been evaluated numerically for 40 values of γ from the interval $100 \leq \gamma \leq 4000$ by direct simulation of equations (3.1)–(3.3). The power law fit

$$\phi(\gamma) = \hat{p}_* + b\gamma^{-\nu},$$

was used to obtain the estimate \hat{p}_* of the limit value p_* of the integral. For the parameter set in Figure 3.7b, the error between the numerical estimate \hat{p}_* and the analytic value of $p_* = 0.492$ obtained from (3.32) satisfies $|p_* - \hat{p}_*| < 10^{-3}$.

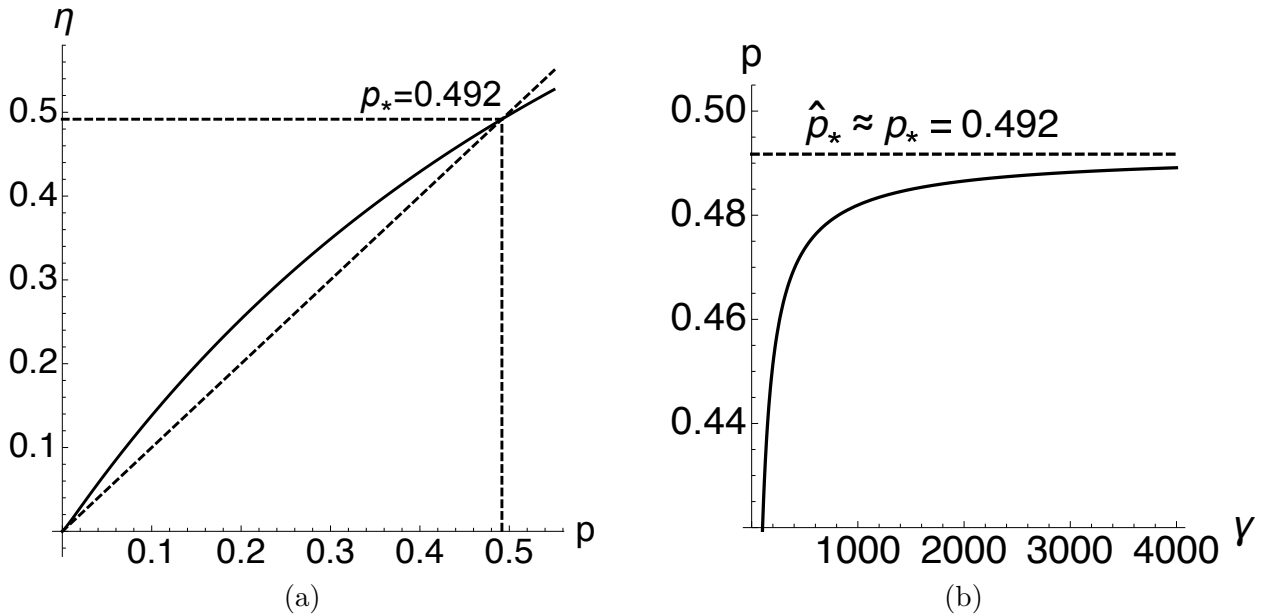


Figure 3.7: Panel (a) shows the solution of (3.32). Panel (b) shows the dependence of the integral of A -component of system (3.1)–(3.3) over one period on γ . The power law fit is shown by the solid line. The horizontal asymptote $p = \hat{p}_*$ coincides with analytic value p_* shown on panel (a). Here $\kappa = 0.6$, $\mu = 0.5$, $\alpha = 1$, $q_0 = 1$, $\beta = 1$, $s = 2$, $k = 1$, $T = 1$, $\gamma_q = 100$, $g_0 = 2.6$.

We conclude that in the limit of γ tending to infinity, the component A of the periodic solution converges to the periodic sequence of delta functions (Dirac comb),

$$A \rightarrow p_* \sum_{n=-\infty}^{\infty} \delta(t - nT), \quad (3.33)$$

which has the period T equal to the delay. The components G grows according to the equation $G' = g_0 - \alpha G$ from the value $G_e = G_b e^{-kp^*}$ to the value G_b defined by (3.31), i.e.,

$$G(t) = \frac{g_0}{\alpha} - \left(\frac{g_0}{\alpha} - G_e \right) e^{-\alpha(t-nT)}, \quad nT < t < (n+1)T,$$

between the pulses of A , and drops back to the value G_e during the pulse. Similarly, the component Q is as approximated between the pulses as

$$Q(t) = \frac{q_0}{\beta} - \left(\frac{q_0}{\beta} - Q_e \right) e^{-\gamma_q \beta(t-nT)}, \quad nT < t < (n+1)T.$$

The interval $g_0^* < g_0 < g_0^* + \varepsilon$ of the parameter values, over which the cycle born via Hopf bifurcation on the positive equilibrium transforms to the pulsating solution, collapses to the threshold, that is $\varepsilon \rightarrow 0$, as γ grows to infinity. In other words, the pulsating solution described by (3.33) can be found “immediately” beyond the threshold for large γ .

3.3.3 Pulse shape

The above approximation does not provide information about the fast stage of the solution such as the profile of the pulse or the deviation of the period from the delay T . In order to obtain such information, one can adapt the approach of Haus and its modifications, see [59, 156]. We briefly outline a possible approach without going into much detail. This approach gives us the law of scaling of the pulse shape and the period with γ .

Using the periodicity of the solution and the asymptotic formula (3.25) for the period, we can rewrite (3.1) as

$$\gamma^{-1} A'(t) + A(t) + \mu Q(t) A(t) = \kappa G(t + c\gamma^{-1}) A(t + c\gamma^{-1}).$$

Integrating this equation from t_b over a part of the fast stage $t_b \leq t \leq t_e$, using the approximations (3.24) and $P(t_b + c\gamma^{-1}) \approx 0$, and taking into account that $A(t_b) \approx 0$, we obtain an approximate equation

$$\gamma^{-1} A(t) + \int_{t_b}^t A(\theta) d\theta + \mu Q_b \int_{t_b}^t e^{-\gamma_q s P(\theta)} A(\theta) d\theta = \kappa G_b \int_{t_b + c\gamma^{-1}}^{t + c\gamma^{-1}} e^{-kP(\theta)} A(\theta) d\theta.$$

As $A = P'$, we obtain, similarly to (3.30),

$$\gamma^{-1}P'(t) + P(t) + \frac{\mu Q_b}{\gamma_q s}(1 - e^{-\gamma_q s P(t)}) = \frac{\kappa G_b}{k}(1 - e^{-kP(t+c\gamma^{-1})}), \quad (3.34)$$

where G_b, Q_b are defined by (3.31) with $p = p_*$ being a positive root of (3.32). Introducing the fast and reversed time scale $\theta = -\gamma t$, and changing the variable $\bar{P}(\theta) = P(t - c\gamma^{-1})$ we rewrite (3.34) as

$$-\bar{P}'(\theta) + \bar{P}(\theta) + \frac{\mu Q_b}{\gamma_q s}(1 - e^{-\gamma_q s \bar{P}(\theta)}) = \frac{\kappa G_b}{k}(1 - e^{-k\bar{P}(\theta-c)}), \quad (3.35)$$

where G_b, Q_b are defined from (3.30), (3.31). A single pulse of the pulsating periodic solution is, therefore, described by a solution of (3.35) satisfying the boundary conditions

$$\bar{P}(-\infty) = p_*, \quad \bar{P}(\infty) = 0. \quad (3.36)$$

Note that both 0 and p_* are equilibrium points of (3.35). Therefore conditions (3.36) define a heteroclinic orbit of this equation. More precisely, if \tilde{P} denotes the heteroclinic solution of (3.35) satisfying (3.36), and $\tilde{A} = \tilde{P}'$, then a pulse of the periodic solution of system (3.1)–(3.3) is approximated by the formula

$$A(t) = \gamma \tilde{A}(-\gamma t) = \gamma \tilde{P}'(-\gamma t) \quad (3.37)$$

for large γ . Hence, according to this approximation, the amplitude of the pulse scales linearly with γ , the width of the pulse is inverse proportional to γ , and the period is approximated by (3.25).

Linearizing system (3.35) at 0 and p_* , we obtain

$$-P'(\theta) + (1 + \mu Q_b)P(\theta) = \kappa G_b P(\theta - c) \quad (3.38)$$

and

$$-P'(\theta) + (1 + \mu Q_e)P(\theta) = \kappa G_e P(\theta - c), \quad (3.39)$$

respectively, where Q_e, G_e are defined by (3.28) with $p = p_*$. The characteristic equation of linearization (3.38) is

$$-\lambda + 1 + \mu Q_b = \kappa G_b e^{-\lambda c}. \quad (3.40)$$

The characteristic equation of (3.39) has a similar form

$$-\lambda + 1 + \mu Q_e = \kappa G_e e^{-\lambda c}. \quad (3.41)$$

We will assume that

$$\kappa G_b - \mu Q_b - 1 < 0, \quad \kappa G_e - \mu Q_e - 1 < 0. \quad (3.42)$$

These conditions can be associated with New's stability criterion [111], which ensures stability of the background of the pulses, that is, in our context, stability with respect to small perturbations of the A -component at the beginning and at the end of the slow stage when A is close to zero. Relations (3.42) imply that each of (3.40), (3.41) has two real roots of different signs. A typical spectrum of these equations is shown in Figure 3.8. Here, all the

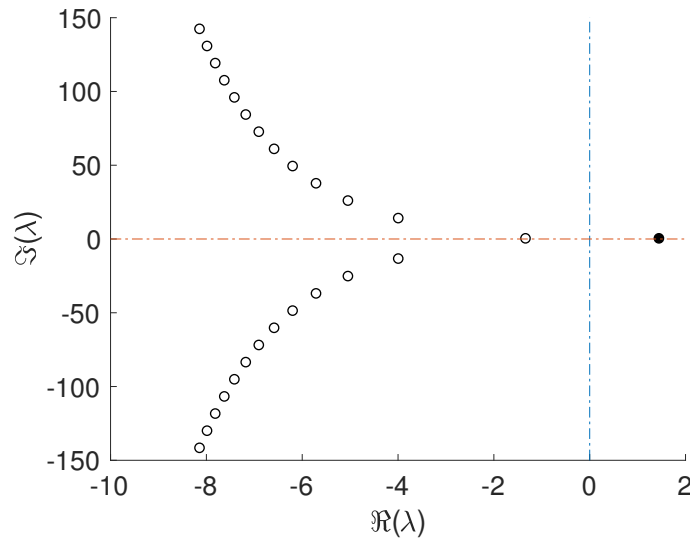


Figure 3.8: A typical spectrum of equations (3.40) and (3.41) when condition (3.42) is satisfied. The notation is the same as in Figure 3.2.

complex eigenvalues have a negative real part, which is less than the real negative eigenvalue. In such a case, both equilibrium points $\bar{P} = 0$ and $\bar{P} = p_*$ of (3.35) are saddles with a one-dimensional unstable manifold and a codimension 1 stable manifold. Therefore, for a specific value of the parameter c , which can be considered as a bifurcation parameter in (3.35), the unstable manifold of the equilibrium point p_* can connect to the stable manifold of the zero equilibrium forming a heteroclinic orbit. The value of c , for which the heteroclinic orbit is formed, defines the period of the solution of system (3.1)–(3.3) according to the asymptotic formula (3.25), and the heteroclinic orbit \tilde{P} defines the profile of the pulse according to (3.37). Figure 3.9 illustrates how the heteroclinic orbit and the corresponding c can be found by the shooting method. Further, the heteroclinic solution $\tilde{P}(\theta)$ converges to the equilibrium p_* exponentially as $e^{\lambda_+^e \theta}$ in the limit $\theta \rightarrow -\infty$, where λ_+^e is the positive real root of (3.41); and, to the zero equilibrium as $e^{\lambda_-^b \theta}$ in the limit $\theta \rightarrow \infty$, where λ_-^b is the negative real root of (3.40). Hence, (3.37) implies that the pulse of A has similar exponential tails. Specifically, A grows exponentially as $e^{-\gamma \lambda_-^b t}$ at the beginning of the fast stage and decays as $e^{-\gamma \lambda_+^e t}$ at the end of the fast stage. This result is consistent with the exponential growth assumptions that we made earlier about the pulse. In particular the assumed exponential asymptotics of the pulse tails hold with $\lambda_1 \approx -\lambda_-^b$ and $\lambda_2 \approx -\lambda_+^e$ (cf. page 103).

The above exponential asymptotics of the pulse tails have been derived for the phase when G and Q change fast. The same asymptotics can be obtained directly from (3.1) for the beginning and the end of the slow stage when G and Q change slowly. Indeed, replacing $A(t - T)$ with $A(t + c\gamma^{-1})$ according to (3.25), setting $G = G_e, Q = Q_e$ for the beginning of the slow stage and $G = G_b, Q = Q_b$ for the end of the slow stage, and using the exponential ansatz $A = A_0 e^{-\gamma \lambda t}$ corresponding to the fast evolution of A results in the same characteristic equations (3.40), (3.41). Thus, the exponential asymptotics at the slow and fast stages match.

Figure 3.10 compares a pulse of the periodic solution of system (3.1)–(3.3) with the approximation obtained from the heteroclinic orbit of (3.35).

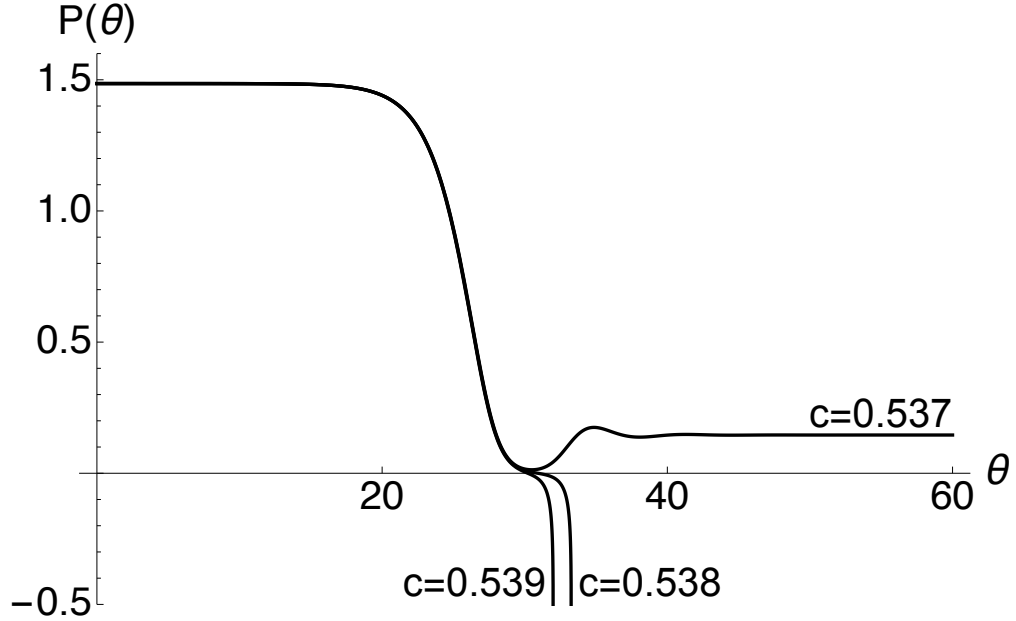


Figure 3.9: We adopt the shooting method in order to find parameter c in equation (3.35). The three curves correspond to three trajectories starting near the equilibrium $p_* = 1.486$ with different values of c . Other parameters are $G_b = 2.906$, $Q_b = 2.5$, $k = 0.7$, $\gamma_q = 10$, $s = 1$, $\mu = 0.5$, $\kappa = 0.6$. Note that with this set of parameters equation (3.35) has an additional positive equilibrium $p_† = 0.146$ which is an asymptotically stable focus. For one exact value $c = c_*$ ($0.537 < c_* < 0.538$) there exists a heteroclinic orbit of (3.35) connecting the equilibria p_* and 0. This orbit describes the shape of the pulse, and the value c_* defines the period of the pulsating solution. For $c < c_*$, trajectories starting near p_* belong to the basin of attraction of the positive equilibrium $p_†$; for $c > c_*$, such trajectories become negative and go to negative infinity.

3.3.4 Approximation for $\gamma_q \gg 1$

The parameter γ_q controls the rate of the population processes for the species Q . Denote by \tilde{p} the unique positive root of the equation

$$p = \frac{\kappa g_0 (1 - e^{-\alpha T})(1 - e^{-kp})}{k\alpha(1 - e^{-\alpha T - kp})}$$

(cf. (3.32)). If we increase the value of γ_q keeping the parameters in the right hand side of (3.1)–(3.3) fixed, then p_* , $G_{b,e}$, $Q_{b,e}$ approach the following values:

$$p_* \approx \tilde{p}, \quad G_b \approx \frac{g_0(1 - e^{-\alpha T})}{\alpha(1 - e^{-\alpha T - k\tilde{p}})}, \quad G_e \approx G_b e^{-k\tilde{p}}, \quad Q_b \approx q_0/\beta, \quad Q_e \approx 0.$$

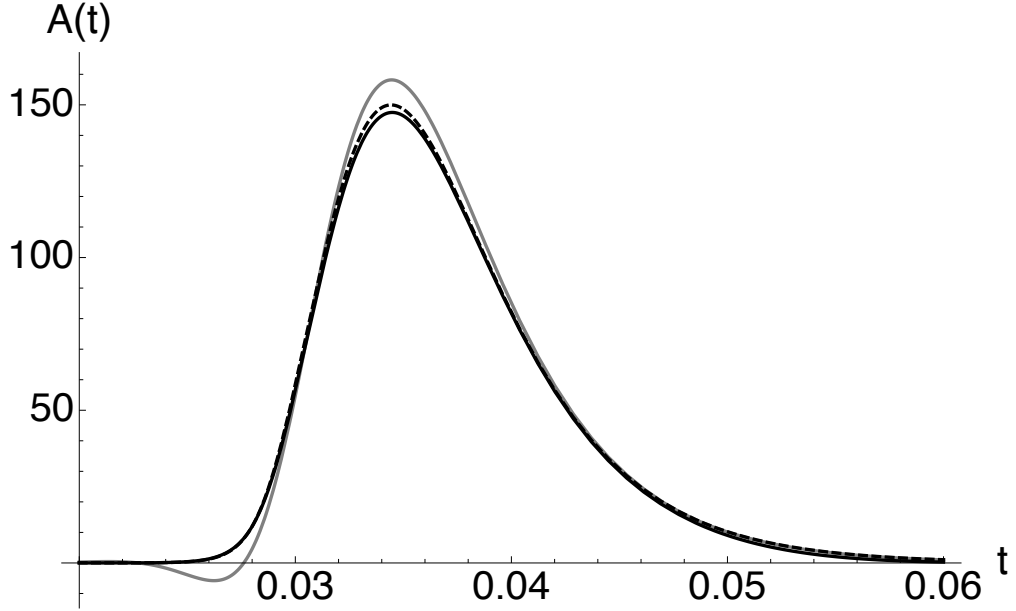


Figure 3.10: Black solid curve represents a single pulse of the A -component of the periodic pulsating solution of system (3.1)–(3.3) with the following parameters: $g_0 = 4$, $k = 0.7$, $q_0 = 2.5$, $s = 1$, $T = 1$, $\alpha = 1$, $\beta = 1$, $\gamma = 400$, $\kappa = 0.6$, $\mu = 0.5$, $\gamma_q = 100$. Dashed curve is the derivative of the heteroclinic solution of (3.35) satisfying the boundary conditions (3.36). This solution exists for $c = 0.3736$ which was found using the shooting method, see Figure 3.9. gray solid curve is the derivative of the heteroclinic solution of the approximating (3.43) connecting the saddle equilibrium point $\tilde{p} = 1.6968$ and the stable focus at zero. This curve oscillates near the focus and fails to approximate the leading edge of the pulse (left tail).

Further, (3.35) for the pulse profile can be approximated by the equation

$$-\bar{P}'(\theta) + \bar{P}(\theta) = \frac{\kappa G_b}{k}(1 - e^{-k\bar{P}(\theta-c)}), \quad (3.43)$$

which has the equilibrium points $\bar{P} = 0$ and $\bar{P} = \tilde{p}$. Since $Q_e \approx 0$, the characteristic equation of the linearization of (3.43) at the equilibrium $\bar{P} = \tilde{p}$ approximates (3.41). However, the characteristic equation $-\lambda + 1 = \kappa G_b e^{-\lambda c}$ of the linearization at zero is different from (3.40). For example, one can show that if $\kappa G_b c < 1$, then the zero equilibrium of (3.43) is stable; at the same time, the first relation in (3.42) ensures that zero is a saddle for (3.35). This situation is illustrated in Figure 3.10. The heteroclinic orbit, which connects the saddle point \tilde{p} with the stable zero equilibrium of (3.43) approximates the pulse well for the main part of

the fast stage, but fails to approximate the pulse tails. The heteroclinic orbit of (3.35) gives a better approximation.

3.3.5 Pulses with unstable background

Pulsating periodic solutions with a period close to T can be obtained also when one of the conditions (3.42), or both of them, are violated. According to the classification of New [111], such pulses have unstable background. For example, consider the case when

$$\kappa G_b - \mu Q_b - 1 > 0, \quad \kappa G_e - \mu Q_e - 1 < 0. \quad (3.44)$$

Here, the main role is played by the characteristic equation

$$-\lambda + 1 + \mu \hat{Q}(\hat{t}) = \kappa \hat{G}(\hat{t}) e^{-\lambda c}, \quad 0 \leq \hat{t} \leq T \quad (3.45)$$

with $t = t_b - \hat{t}$ varying over the slow stage, where

$$\hat{G}(\hat{t}) = \frac{g_0}{\alpha} + e^{\alpha \hat{t}} \left(G_b - \frac{g_0}{\alpha} \right), \quad \hat{Q}(\hat{t}) = \frac{q_0}{\beta} + e^{\gamma_q \beta \hat{t}} \left(Q_b - \frac{q_0}{\beta} \right)$$

and c is considered as a parameter again. To be definite, assume that for each \hat{t} , equation (3.44) has two real roots $\lambda_-(\hat{t}) < \lambda_+(\hat{t})$ that depend continuously on \hat{t} and satisfy the relations

$$\lambda_-(\hat{t}) < \lambda_+(\hat{t}) < 0 \quad \text{for} \quad 0 \leq \hat{t} < t_o; \quad \lambda_-(\hat{t}) < 0 < \lambda_+(\hat{t}) \quad \text{for} \quad t_o < \hat{t} \leq T, \quad (3.46)$$

which are compatible with (3.44). Further, suppose that $\text{Re } \lambda < \lambda_-(\hat{t})$ for all the complex roots. Then the zero equilibrium $\bar{P} = 0$ of (3.35) is stable, while the equilibrium $\bar{P} = p_*$ has a one-dimensional unstable manifold. Assuming that this unstable manifold belongs to the basin of attraction of zero, it contains a heteroclinic orbit that defines the pulse profile during the fast stage. This orbit is robust with respect to variations of the parameter c . Therefore, c (and the period (3.25)) cannot be identified as an isolated value for which the heteroclinic

solution is formed (as it was the case for pulses with stable background satisfying (3.42) where the heteroclinic orbit connected saddle equilibria). Instead, c is determined by the evolution of A during the slow stage, when A is small, and the periodic solution satisfies the approximate equation

$$-\gamma^{-1} \frac{A}{d\hat{t}} = -A + \kappa \hat{G}(\hat{t}) A(\hat{t} - \gamma^{-1}c) - \mu \hat{Q}(\hat{t}) A.$$

The zero equilibrium of this equation exhibits the delayed loss of stability so that $A \approx A(0)e^{\gamma\lambda_+(\hat{t})}$ approaches zero very closely over an interval of time $[0, t_o]$ when $\lambda_+(\hat{t}) < 0$ (see (3.46)) and then returns to its initial value $A(T) = A(0)$ over the interval $[t_o, T]$. This allows us to predict that for the pulsating periodic solution of (3.1)–(3.3), in the limit $\gamma \rightarrow \infty$, one has

$$\int_0^T \lambda_+(\hat{t}) d\hat{t} = 0. \quad (3.47)$$

Since $\lambda_+ = \lambda_+(t; c)$ depends on c , condition (3.47) selects c and defines the period (3.25).

It should be noted that condition (3.47) was not satisfied in the numerical simulations that we performed. The reason is that A gets extremely close to zero and becomes affected by numerical noise between the pulses. The effect can be understood if we replace (3.1) with the equation

$$\gamma^{-1} A' = -A + \kappa G(t - T) A(t - T) - \mu Q A + \eta$$

containing a small immigration term $\eta > 0$. This modification makes sense from the modeling perspective too because it precludes A from becoming as small as $e^{-\gamma}$ between the pulses. For this equation (coupled with (3.2), (3.3)), the period depends on both γ and η as we confirmed numerically. However, one can predict that the pulsating periodic solution with a period $\tau \approx T$ should disappear in the limit $\gamma \rightarrow \infty$ with a fixed η . On the other hand, if η decreases with γ as fast as $e^{-\gamma}$, pulses with the period defined by (3.25), (3.47) can exist.

3.4 Conclusion

We have explored a class of pulsating periodic regimes, which can evolve due to the delay, the nonlinearity, and the slow-fast structure in delay differential systems. These solutions have a period close to the delay and are characterized by a specific scaling of the pulse width and height with the parameter $\gamma \gg 1$ measuring the ratio of the fast and slow time scales. Further, the periodic pulses are formed close to some threshold value of the bifurcation parameter, at which a zero equilibrium undergoes the transcritical bifurcation and a positive equilibrium appears. Through a case study of a population model, which involves a fast predator and a slow prey, we have shown that the formation of periodic pulses is simultaneous with a cascade of multiple, almost simultaneous resonant Hopf bifurcations that occur in the immediate vicinity of the threshold on the positive equilibrium. Using the asymptotic analysis at zero, we have obtained explicit relationships between the parameters, which ensure this scenario (such as (3.7) and (3.17)). In particular, we have highlighted the role of competition and shown that the pulses with the associated Hopf bifurcations appear when the fast species competes with another species; in the absence of competition, pulses do not form near the threshold⁴.

The same analysis can be applied to a wider class of population models. In particular, we obtained counterparts of relationships (3.7), (3.16) and (3.17) for several variants of model (3.1)–(3.3) with different growth terms. We then confirmed numerically the same bifurcation scenario leading to the formation of pulses near the threshold. In one variation of the model, the constant immigration and linear death terms $q_0 - \beta Q$ and $g_0 - \alpha G$ in equations (3.2), (3.3) have been replaced with the logistic terms, $Q(q_0 - \beta Q)$ and $G(g_0 - \alpha G)$,

⁴It is worth noting that the model in [119] also has a predator-prey structure. The pulses in this model, or in the models considered in this work, are not related to switching between stable branches of a critical manifold of a singularly perturbed system.

respectively. In another variant of the model,

$$\begin{aligned}\gamma^{-1}A' &= \kappa G(t-T)A(t-T) - \tau A - \mu QA - fA^2, \\ \gamma_q^{-1}Q' &= \nu GQ - \beta Q - sAQ - rQ^2, \\ G' &= g_0 - \alpha G - kAG - mQG,\end{aligned}$$

the A and Q species both predate on G , and the intraspecific competition is included. Interestingly, the counterpart of condition (3.7) for this system requires $\mu s > fr$ in order to guarantee that the positive equilibrium undergoes the cascade of Hopf bifurcations in a small neighborhood of the threshold. The relation $\mu s > fr$ means that interspecific competition between the species A and Q is stronger than intraspecific competition. In the classical competing species model, this condition ensures the competitive exclusion scenario; the opposite inequality $\mu s < fr$ implies the coexistence scenario.

Using the method of matched asymptotic expansions at the slow and fast stages of the dynamics, we have obtained an approximation to the pulsating solution, which provides an accurate prediction of the area of the pulse. Furthermore, a modification of the method of Haus has allowed us to obtain asymptotics of the period and the pulse shape as $\gamma \rightarrow \infty$. This shape is described by a heteroclinic solution of a scalar delay equation that depends only on three parameters. The heteroclinic orbit connects two saddle equilibrium points, each having a one-dimensional unstable manifold.

Similar periodic pulsating solutions have been previously found in the laser model (1.1) and its variations [156, 155]. The main advance of this work is a detailed asymptotic analysis of the pulses and linear stability analysis near the bifurcation point. This analyses can be extended to lasers. Some differences between population and laser models arise from the fact that population systems are positively invariant, and the pulsating regime in this setting is positive. On the other hand, the pulsating variable A in the laser model (1.1) is

complex-valued. Also, different types of nonlinearities in population and laser models result in different power laws for the scaling of pulses with γ .

Due to positive invariance, the transcritical bifurcation with the associated zero eigenvalue is an important ingredient of the bifurcation scenario described in this work. It is interesting to compare this scenario with the Eckhaus and modulational instabilities, which are well known in the context of spatially distributed systems and have been recently studied for systems containing large delays [167, 126]. The evolution of the pseudocontinuous spectrum of the zero equilibrium shown in Figure 3.2a is similar to the picture associated with the Eckhaus instability. The “parabola” carrying the pseudocontinuous spectrum moves as a whole to the unstable half-plane as the bifurcation parameter increases. Furthermore, as in the Eckhaus scenario [149], we observe the appearance of multiple unstable periodic solutions, which then stabilize via secondary bifurcations leading to co-existence of multiple periodic attractors, see Figure 3.3. On the other hand, the evolution of the spectrum of the positive equilibrium that intersects the zero equilibrium in the transcritical bifurcation reminds the modulation instability scenario, in which the “parabola” carrying the pseudocontinuous spectrum develops two humps that cross the imaginary axis, while the vertex of the parabola at zero is not moving [126]. Interestingly, although similar humps are observed in Figure 3.6, they are formed through a different mechanism. Namely, eigenvalues with smaller imaginary part that belong to the pseudocontinuous spectrum get absorbed by the strongly stable spectrum as the bifurcation parameter increases. This interaction of the pseudocontinuous and strongly stable spectra results in the formation of humps and, further, in stabilization of the positive equilibrium for higher values of the bifurcation parameter. However, a common feature of all the above scenarios is that eigenvalues with smaller imaginary part cross the imaginary axis from the stable to the unstable domain before eigenvalues with larger imaginary part do. Hence, all these scenarios can be viewed as long-wavelength instabilities.

CHAPTER 4

SELECTIVE PYRAGAS CONTROL OF HAMILTONIAN SYSTEMS¹

In this chapter we consider a Newtonian equation in the form

$$\ddot{x} + \nabla V(x) = 0,$$

which has a surface of neutrally stable periodic solutions. The goal is to select a particular orbit from this surface and to transform it to the exponentially stable orbit using Pyragas delay-feedback control in the form $K((x-T)-x(t))$ where T is the period of the targeted orbit to be stabilized and K is an arbitrarily small gain matrix. We discuss sufficient conditions from two perspectives.

In Section 4.1 we treat the case of small amplitude solutions where sufficient conditions for exponential stability are framed in terms of the asymptotic expansion of $\nabla V(x)$ at the equilibrium $x = 0$ up to the third order. The importance of the third order expansion is motivated by the Lyapunov Center Theorem and the normal form for the Hopf bifurcation.

Section 4.2 deals with arbitrary periodic solutions, but instead of being framed in terms of the asymptotic expansion of the field $\nabla V(x)$, we use conditions on the Floquet modes of the targeted orbit as a solution of the uncontrolled system.

Each section is supplemented with examples.

In a brief Section 4.3 we show how the conditions in Section 4.2 agree with those from Section 4.1 in the case of small amplitude cycles. Finally we present conclusions. An Appendix B containing the derivation of the normal form for the Hopf bifurcation in a delayed system is included at the end of the dissertation for convenience of the reader.

¹The material of this chapter was published in *Discrete & Continuous Dynamical Systems – S*. Reprinted with permission.

4.1 Stabilization of small periodic orbits

4.1.1 Main statement

Consider the system

$$\ddot{x} + \nabla V(x) = K(x_\tau - x), \quad x \in \mathbb{R}^N. \quad (4.1)$$

with a sufficiently smooth potential V , where $x_\tau = x(t - \tau)$. Let x^* be an equilibrium of the uncontrolled system

$$\ddot{x} + \nabla V(x) = 0. \quad (4.2)$$

Without loss of generality, assume that $x^* = 0$, i.e., $\nabla V(0) = 0$. Denote by $H = D^2V$ the Hessian of V and by H_0 the value of the Hessian at zero, $H_0 = D^2V(0)$. We will use the third order expansion of ∇V at zero:

$$\nabla V(x) = H_0x + \frac{1}{2}L(x, x) + \frac{1}{6}Q(x, x, x) + o(\|x\|^3) \quad \text{as } x \rightarrow 0 \quad (4.3)$$

with a bilinear map $L : \mathbb{R}^N \times \mathbb{R}^N \rightarrow \mathbb{R}^N$ and a trilinear map $Q : \mathbb{R}^N \times \mathbb{R}^N \times \mathbb{R}^N \rightarrow \mathbb{R}^N$. Here and henceforth, $\langle \cdot, \cdot \rangle$ is the usual scalar product and $\| \cdot \|$ is the corresponding Euclidean norm in \mathbb{R}^N .

Denote by $\text{Sp}(H_0)$ the spectrum of the symmetric matrix H_0 . We make the following assumptions about the uncontrolled system (4.2).

- **Stability of the zero equilibrium:** The Hessian H_0 is positive definite.

Hence, the spectrum of H_0 is positive:

$$\text{Sp}(H_0) = \{\omega_1^2, \dots, \omega_N^2\}.$$

with $\omega_n > 0$.

- **Nonresonance condition:** For some k and all $n \neq k$, $1 \leq n \leq N$, the ratio ω_n/ω_k is not an integer number. Further $\omega_n \neq \omega_m$ for $n \neq m$.

Denote by e_n a unit eigenvector of the Hessian H_0 corresponding to the eigenvalue ω_n^2 and set

$$a_k = \frac{1}{2} (4\omega_k^2 \text{Id} - H_0)^{-1} L(e_k, e_k), \quad b_k = -H_0^{-1} L(e_k, e_k), \quad (4.4)$$

where Id denotes the identity matrix.

• **Nonzero Lyapunov quantity:**

$$\xi_k := \left\langle e_k, L(e_k, a_k + b_k) + \frac{1}{2} Q(e_k, e_k, e_k) \right\rangle \neq 0. \quad (4.5)$$

By the Lyapunov Center Theorem, the nonresonance condition ensures that the uncontrolled system (4.2) has a continuous branch (one-parameter family) Γ_k of small periodic orbits with the (minimal) periods satisfying $T \rightarrow 2\pi/\omega_k$ as $\|x\|_\infty \rightarrow 0$ (e.g. [97]). We note that if the nonresonance condition is satisfied for several ω_k , then there are several branches of small periodic orbits near zero. In particular, if no frequency is a multiple of any other frequency, then there are n branches of small periodic orbits with pairwise different asymptotic periods.

Theorem 4.1.1. *Let a matrix D satisfy*

$$\sin(2\pi\omega_n/\omega_k) \langle e_n, De_n \rangle > 0, \quad 1 \leq n \leq N, \quad n \neq k, \quad (4.6)$$

and

$$\xi_k \langle e_k, De_k \rangle > 0. \quad (4.7)$$

Then, for every sufficiently small $\varepsilon > 0$ there is a $\delta_0 = \delta_0(\varepsilon) > 0$ such that if $K = \varepsilon D$ and $\tau = 2\pi/\omega_k - \xi_k \delta$ with $\delta \in (0, \delta_0)$, then the small τ -periodic orbit of the uncontrolled system (4.2) is orbitally asymptotically stable for the controlled system (4.1).

The proof of the theorem uses the following simple statement.

Lemma 4.1.2. *Let A and B be two $N \times N$ matrices and $0 < \varepsilon \ll 1$. Assume that A is diagonal. Then,*

$$\det(A + \varepsilon B) = \det A + \varepsilon \sum_{i=1}^N \left(\prod_{\substack{k=1 \\ k \neq i}}^N A_{kk} \right) B_{ii} + O(\varepsilon^2). \quad (4.8)$$

Proof. Consider the function $g(\varepsilon) = \det(A + \varepsilon B)$. By Taylor's formula,

$$g(\varepsilon) = \det A + \varepsilon g'(0) + O(\varepsilon^2), \quad (4.9)$$

where by the chain rule

$$g'(0) = \sum_{i=1}^N \sum_{j=1}^N \frac{\partial(\det C)}{\partial C_{ij}} \Big|_{C=A} \cdot \frac{dC_{ij}}{d\varepsilon} \Big|_{\varepsilon=0} \quad (4.10)$$

with $C(\varepsilon) := A + \varepsilon B$. Here

$$\frac{\partial(\det C)}{\partial C_{ij}} \Big|_{C=A} = \frac{d \det(A + h E^{ij})}{dh} \Big|_{h=0},$$

where E^{ij} is the $N \times N$ matrix with 1 at the i -th row and the j -th column, and zero everywhere else. Recall that A is diagonal, therefore

$$\det(A + h E^{ij}) = \begin{cases} \det A, & i \neq j, \\ \det A + h \prod_{\substack{k=1 \\ k \neq i}}^N A_{kk}, & i = j. \end{cases}$$

Hence,

$$\frac{\partial \det(C)}{\partial C_{ij}} \Big|_{C=A} = \begin{cases} 0, & i \neq j, \\ \prod_{\substack{k=1 \\ k \neq i}}^N A_{kk}, & i = j. \end{cases}$$

Combining this with (4.9) and (4.10) gives (4.8). \square

Proof of Theorem 4.1.1. Denote by S an orthogonal matrix that diagonalizes H_0 :

$$\Omega := \text{diag} \{ \omega_1^2, \dots, \omega_N^2 \} = S^T H_0 S.$$

The characteristic equation of the linearization of the controlled system (4.1) with $K = \varepsilon D$ at zero can be written as

$$\det(\lambda^2 \text{Id} + \Omega + \varepsilon(1 - e^{-\lambda\tau})\tilde{D}) = 0, \quad (4.11)$$

where $\tilde{D} = S^T D S$. For $\varepsilon = 0$, the roots of this equation are $\pm i\omega_n$, $n = 1, \dots, N$. Let us set $\tau = 2\pi/\omega_k$, take $n \neq k$, and consider a small perturbation $\lambda = i\omega_n + \rho_n$ of the root $i\omega_n$ for $0 < \varepsilon \ll 1$. Substituting the expression $\lambda_n = i\omega_n + \rho_n$ in (4.11) and using Lemma 4.1.2, we see that the zero order terms vanish, and keeping the first correction terms, we obtain

$$2i\omega_n\rho_n + \varepsilon(1 - e^{-2\pi i\omega_n/\omega_k})\tilde{D}_{nn} + o(\varepsilon + |\rho_n|) = 0,$$

where $\tilde{D}_{nn} = \langle e_n, \tilde{D}e_n \rangle$ is the corresponding diagonal entry of the matrix \tilde{D} . This implies

$$\text{Re } \lambda_n = \text{Re } \rho_n = \frac{-\sin(2\pi\omega_n/\omega_k) \langle e_n, D e_n \rangle}{2\omega_n} \varepsilon + o(\varepsilon), \quad n \neq k. \quad (4.12)$$

Now, we fix an $\varepsilon > 0$ and note that the characteristic equation (4.11) has the roots $\pm i\omega_k$ for $\tau = 2\pi/\omega_k$. Considering a small perturbation $\tau = 2\pi/\omega_k - \xi_k\delta$ of the delay, for the perturbed root $\lambda_k = i\omega_k + \rho_k$ of (4.11) we obtain

$$2i\omega_k\rho_k + \varepsilon(-i\omega_k\xi_k\delta + 2\pi\rho_k/\omega_k)\tilde{D}_{kk} + o(|\delta| + |\rho_k|) = 0,$$

where δ is considered as a small parameter and ε is fixed. Hence,

$$\text{Re } \lambda_k = \text{Re } \rho_k = \frac{\xi_k\omega_k^2 \langle e_k, D e_k \rangle}{2\omega_k^2 + 2(\pi\tilde{D}_{kk}\varepsilon/\omega_k)^2} \varepsilon\delta + o(\delta). \quad (4.13)$$

Relations (4.6), (4.7) combined with (4.12), (4.13) ensure that the controlled system (4.1) with the delay τ considered as the bifurcation parameter and $K = \varepsilon D$ satisfies the conditions of the Hopf Bifurcation Theorem (e.g. [58]) for any sufficiently small fixed $\varepsilon > 0$. Indeed, relations (4.7) and (4.13) imply that the complex conjugate eigenvalues $\lambda_k(\tau), \bar{\lambda}_k(\tau)$ cross the imaginary axis transversally at the points $\pm i\omega_k$ for $\tau_* = 2\pi/\omega_k$. At the same time,

relations (4.6) and (4.12) imply that all the eigenvalues $\lambda_n(\tau), \bar{\lambda}_n(\tau)$ with $n \neq k, 1 \leq n \leq N$ have negative real parts for any τ close to τ_* , while the smallness of ε ensures the same property for all the other eigenvalues. Hence, equation (4.1) has a continuous branch (one-parameter family) $\hat{\Gamma}$ of small periodic orbits with (minimal) periods satisfying $T \rightarrow 2\pi/\omega_k$ and $\tau \rightarrow 2\pi/\omega_k$ as $\|x\|_\infty \rightarrow 0$. Further, stability of these small periodic orbits is determined by the Lyapunov quantity [42]. A computation of this quantity is included in the Appendix for convenience of the reader. In particular, it is shown that condition (4.7) ensures that the Hopf bifurcation is supercritical, i.e., all the small orbits of the branch $\hat{\Gamma}$ are asymptotically stable. Finally, the Hopf Bifurcation Theorem implies that all the small periodic orbits of (4.1) that exist for τ close to τ_* and have periods close to τ_* belong to $\hat{\Gamma}$ (e.g. [58]), in particular the branch Γ_k of small periodic orbits of the uncontrolled system (4.2) is included in $\hat{\Gamma}$.² This completes the proof. \square

Remark 4.1.3. An asymptotic analysis presented in Appendix B shows that the period of a small periodic orbit of the uncontrolled system (4.2) scales with the amplitude of the orbit as

$$T = \tau_* - \frac{\xi_k \pi}{4\omega_k^3} \|x\|_\infty^2 + o(\|x\|_\infty^2). \quad (4.14)$$

Combining this with (4.7) and assuming that (4.6) holds, we see that if $|T - \tau_*|$ scales quadratically with the amplitude of the orbit and T decreases with $\|x\|_\infty$, then the stabilization of small periodic orbits is achieved when $\langle e_k, Ke_k \rangle > 0$. On the other hand, if T increases with $\|x\|_\infty$, then the stabilization is achieved when $\langle e_k, Ke_k \rangle < 0$.

4.1.2 Example: Duffing oscillator

Consider the scalar equation

$$\ddot{x} + x + x^3 = \kappa(x_\tau - x).$$

²As a matter of fact, $\hat{\Gamma} = \Gamma_k$ because system (4.1) has at most one small periodic orbit for every τ close to τ_* .

Without the control ($\kappa = 0$), the scaling of the period of the periodic orbit near the origin can be found, for example, by the Poincaré–Lindstedt method [80]:

$$\omega^2 x'' + x + x^3 = 0,$$

where prime denotes the derivative with respect to the rescaled time $\tilde{t} = \omega t$ and

$$x = r \cos \tilde{t} + r^3 \tilde{x}, \quad \omega = 1 + Ar^2,$$

where r measures the amplitude of the small periodic solution. The first correction of order r^3 has no secular terms for $A = 3/8$. Hence, the frequency increases and the period T decreases with the amplitude r of the periodic orbit:

$$T = 2\pi \left(1 - \frac{3}{8}r^2 \right) + o(r^2).$$

According to Remark 4.1.3, the condition

$$\kappa > 0$$

ensures the noninvasive stabilization of small periodic orbits provided that κ is sufficiently small and $\tau < 2\pi$ is close to 2π . Similarly, a sufficiently small control with $\kappa < 0$ and $\tau > 2\pi$, $\tau \approx 2\pi$ stabilizes a small periodic orbit of the equation

$$\ddot{x} + x - x^3 = \kappa(x_\tau - x).$$

4.1.3 Example: Two coupled Duffing oscillators

Now, let us consider two coupled Duffing oscillators:

$$\ddot{x} + \nabla V(x) = K(x_\tau - x), \quad x = (x_1, x_2)^T \in \mathbb{R}^2$$

with the potential

$$V(x) = \frac{1}{2} \left(x_1^2 + \frac{x_2^2}{2} + \frac{3}{5}(x_1 - x_2)^2 + \frac{x_1^4}{2} + \frac{x_2^4}{2} \right). \quad (4.15)$$

Here the eigenvalues and eigenvectors of the Hessian H_0 are

$$\omega_1^2 = 2, \quad \omega_2^2 = 0.7, \quad e_1 = \frac{1}{\sqrt{13}}(3, -2)^\top, \quad e_2 = \frac{1}{\sqrt{13}}(2, 3)^\top. \quad (4.16)$$

Using the diagonalizing coordinate transformation

$$x = Sy, \quad S = \frac{1}{\sqrt{13}} \begin{bmatrix} 3 & 2 \\ -2 & 3 \end{bmatrix},$$

we obtain

$$\ddot{y}_1 + 2y_1 + \frac{3}{169}(3y_1 + 2y_2)^3 - \frac{2}{169}(-2y_1 + 3y_2)^3 = 0,$$

$$\ddot{y}_2 + 0.7y_2 + \frac{2}{169}(3y_1 + 2y_2)^3 + \frac{3}{169}(-2y_1 + 3y_2)^3 = 0.$$

Two branches of periodic orbits can be obtained by the Poincaré–Lindstedt method using the following expansions:

$$\tilde{t} = \omega t, \quad \omega = \sqrt{2} + \gamma_1 r^2, \quad y_1 = r \cos \tilde{t} + r^3 \tilde{y}_1, \quad y_2 = r^3 \tilde{y}_2$$

and

$$\tilde{t} = \omega t, \quad \omega = \sqrt{0.7} + \gamma_2 r^2, \quad y_1 = r^3 \tilde{y}_1, \quad y_2 = r \cos \tilde{t} + r^3 \tilde{y}_2$$

with $r \ll 1$. Elimination of the secular terms in the first correction is achieved for

$$\gamma_1 = \frac{3 \cdot 97}{8 \cdot 169 \sqrt{2}}$$

for the first branch with $\omega \approx \sqrt{2}$ and

$$\gamma_2 = \frac{3 \cdot 97}{8 \cdot 169 \sqrt{0.7}}$$

for the second branch with $\omega \approx \sqrt{0.7}$. Since $\gamma_{1,2} > 0$, the frequency increases and the period of the periodic orbit decreases on each branch with the amplitude r of the orbit. According to (4.14), it means that the Lyapunov quantity (4.5) for each branch satisfies $\xi_{1,2} > 0$.

Let us assume a diagonal control matrix

$$K = \begin{bmatrix} \kappa_1 & 0 \\ 0 & \kappa_2 \end{bmatrix}.$$

Using (4.16) and $\xi_1 > 0$, the conditions (4.6), (4.7) for the branch of small periodic orbits with $\omega \approx \sqrt{2}$ have the form

$$\begin{aligned} 0.9\kappa_1 + 0.4\kappa_2 &> 0, \\ 0.4\kappa_1 + 0.9\kappa_2 &< 0. \end{aligned} \tag{4.17}$$

According to Theorem 4.1.1, these conditions ensure that the branch with $\omega \approx \sqrt{2}$ stabilizes provided that κ_1, κ_2 are sufficiently small in absolute value.

Similarly, the branch of small periodic orbits with $\omega \approx \sqrt{0.7}$ stabilizes if the opposite inequalities hold:

$$\begin{aligned} 0.9\kappa_1 + 0.4\kappa_2 &< 0, \\ 0.4\kappa_1 + 0.9\kappa_2 &> 0. \end{aligned} \tag{4.18}$$

On the other hand, if

$$V(x) = \frac{1}{2} \left(x_1^2 + \frac{x_2^2}{2} + \frac{3}{5}(x_1 - x_2)^2 - \frac{x_1^4}{2} - \frac{x_2^4}{2} \right),$$

then each of the branches will be stabilized if

$$\begin{aligned} 0.9\kappa_1 + 0.4\kappa_2 &< 0, \\ 0.4\kappa_1 + 0.9\kappa_2 &< 0. \end{aligned}$$

4.2 Stabilization of large periodic orbits

4.2.1 Main statement

We consider now a branch of periodic orbits of the uncontrolled system (4.2) further away from zero. Consider a particular periodic orbit $x_* = x_*(t)$ of period T_* . Since the orbit is included in the branch, it has a characteristic multiplier $\mu = 1$ of algebraic multiplicity greater than 1. We make the following assumption.

- **Genericity assumption:** The characteristic multiplier $\mu = 1$ of the periodic orbit x_* has geometric multiplicity 1 and algebraic multiplicity 2.

This is the generic situation for a periodic orbit embedded into a surface of such orbits. More precisely, we write the uncontrolled system in the phase space:

$$\dot{x} = -p, \quad \dot{p} = \nabla V(x), \quad x, p \in \mathbb{R}^N, \quad (4.19)$$

consider the periodic solution $(x_*(t), p_*(t)) = (x_*(t), -\dot{x}_*(t))$, and consider the linearization of system (4.19) on the periodic solution:

$$\dot{y} = B(t)y, \quad y \in \mathbb{R}^{2N}, \quad (4.20)$$

with $y = (x, p)$ and

$$B(t) = \begin{bmatrix} 0 & -\text{Id} \\ H(x_*(t)) & 0 \end{bmatrix}, \quad (4.21)$$

where $H(x_*(t)) = H(x_*(t))^T$. Hence, $B(t) \equiv B(t+T_*)$. Floquet modes are solutions of (4.20) of the form

$$y_n(t) = (u_n(t), -\dot{u}_n(t)) = \mu_n^{t/T_*} q_n(t), \quad q_n(t) \equiv q_n(t + T_*), \quad (4.22)$$

where μ_n is a (complex) characteristic multiplier. In particular, denote $u_0(t) = \dot{x}_*(t)$, then $y_0(t) = (u_0(t), -\dot{u}_0(t))$ is the periodic Floquet mode, which satisfies

$$u_0(t) \equiv u_0(t + T_*)$$

and has the characteristic multiplier $\mu_0 = 1$. Also, according to the genericity assumption above, equation (4.20) has a solution $(v_0(t), -\dot{v}_0(t))$ satisfying

$$v_0(t + T_*) \equiv v_0(t) + u_0(t),$$

which can be called the generalized Floquet mode.

Further, assume that

- **Stability assumption:** All the characteristic multipliers $\mu_n \neq 1$ of (4.20) are simple and satisfy $|\mu_n| = 1$.

In other words, the periodic solution $x_*(t)$ of the uncontrolled system is stable.

Theorem 4.2.1. *Suppose that a matrix D satisfies*

$$\left(\langle u_0(t), \dot{v}_0(t) \rangle - \langle \dot{u}_0(t), v_0(t) \rangle \right) \int_0^{T_*} \langle u_0(s), Du_0(s) \rangle ds > 0, \quad (4.23)$$

where $(u_0(t), -\dot{u}_0(t))$ and $(v_0(t), -\dot{v}_0(t))$ are a Floquet mode and the generalized Floquet mode of (4.20) corresponding to the characteristic multiplier $\mu_0 = 1$. Suppose that

$$\operatorname{Im} \left(\langle \dot{u}_n(t), u_n(t) \rangle \right) \operatorname{Im} \left((\bar{\mu}_n - 1) \int_0^{T_*} \langle u_n(s), Du_n(s) \rangle ds \right) > 0 \quad (4.24)$$

for all the Floquet modes (4.22) corresponding to the characteristic multipliers $\mu_n \neq 1$. Then, for every sufficiently small $\varepsilon > 0$, the periodic solution $x_*(t)$ of the controlled system (4.1) with $\tau = T_*$ and $K = \varepsilon D$ is orbitally asymptotically stable.

Note that in (4.23), (4.24),

$$\langle u_0(t), \dot{v}_0(t) \rangle - \langle \dot{u}_0(t), v_0(t) \rangle \equiv \text{const}, \quad \langle \dot{u}_n(t), u_n(t) \rangle \equiv \text{const}$$

(see the proof below).

Proof. Let

$$\dot{y} = B(t)y + \varepsilon G(y(t - T_*) - y), \quad y \in \mathbb{R}^{2N}, \quad (4.25)$$

be the linearization of the controlled system (4.1) with the delay $\tau = T_*$ and the gain matrix εG near x_* . Suppose that μ is a characteristic Floquet multiplier of system (4.25), hence this system has a solution (Floquet mode)

$$y_\mu(t) = \mu^{t/T_*} q(t) \quad (4.26)$$

with a periodic $q(t) \equiv q(t + T_*)$. Since the delay in (4.25) equals the period of q , we see that y_μ satisfies the ordinary differential system

$$\dot{y} = (B(t) + \varepsilon(\mu^{-1} - 1)G) y. \quad (4.27)$$

Denoting by $\Psi_{\varepsilon,\mu}(t)$ the fundamental matrix of (4.27), we conclude that the monodromy matrix $\Psi_{\varepsilon,\mu}(T_*)$ of (4.27) also has the characteristic multiplier μ . Hence, this multiplier μ is a root of the characteristic equation

$$\det(\Psi_{\varepsilon,\mu}(T_*) - \mu \text{Id}) = 0. \quad (4.28)$$

Denote by $\Phi(t)$ the fundamental matrix of system (4.20). Clearly, $\Phi(t) = \Psi_{0,\mu}(t)$. Suppose that the monodromy matrix $\Phi(T_*)$ of system (4.20) has a simple eigenvalue $\mu_* \neq 1$ on the unit circle, hence μ_* is a root of (4.28) for $\varepsilon = 0$. Let us consider the perturbation $\mu = \mu_* + \rho$ of this root for small ε . Note that the fundamental matrices $\Phi(t)$ and $\Psi_{\varepsilon,\mu}(t)$ are related by the identity

$$\Psi_{\varepsilon,\mu}(t) = \Phi(t) \left(\text{Id} + \varepsilon(\mu^{-1} - 1) \int_0^t \Phi^{-1}(s)G\Psi_{\varepsilon,\mu}(s) ds \right),$$

which implies

$$\Psi_{\varepsilon,\mu}(T_*) \approx \Phi(T_*) \left(\text{Id} + \varepsilon(\mu^{-1} - 1) \int_0^{T_*} \Phi^{-1}(t)G\Phi(t) dt \right), \quad (4.29)$$

where we omit the terms of order $o(\varepsilon)$. In the following, the approximate equality also means that $o(\varepsilon)$ terms are omitted. Let us denote by S the transition matrix to a basis in which the matrix $\Phi(T_*)$ assumes the Jordan form Λ ; for convenience, we also agree that S^{-1} maps the eigenvector e_* corresponding to the simple eigenvalue μ_* to the vector $S^{-1}e_* = e_1 := (1, 0, \dots, 0)^T \in \mathbb{R}^{2N}$. In this new basis, using (4.29), we can rewrite (4.28) as

$$\det \left(\Lambda - \mu \text{Id} + \varepsilon(\mu^{-1} - 1) \Lambda \int_0^{T_*} S^{-1} \Phi^{-1}(t)G\Phi(t)S dt \right) \approx 0 \quad (4.30)$$

with $\mu = \mu_* + \rho$. Since $\Lambda_{11} = \mu_*$, this implies

$$\rho \approx \varepsilon(1 - \mu_*)M_{11} \quad \text{with} \quad M := \int_0^{T_*} S^{-1}\Phi^{-1}(t)G\Phi(t)S dt.$$

Taking into account that $y_*(t) = \Phi(t)e_* = \Phi(t)Se_1$ is the Floquet mode of (4.20) corresponding to the characteristic multiplier μ_* and $\varphi_*^\dagger(t) = [\Phi^{-1}(t)]^T e_*^\dagger = [\overline{S}^{-1}\Phi^{-1}(t)]^T e_1$ is the adjoint Floquet mode corresponding to the multiplier $1/\overline{\mu}_* = \mu_*$ and normalized by the condition $\langle \varphi_*^\dagger(t), y_*(t) \rangle \equiv 1$, we see that

$$M_{11} = e_1^T M e_1 = \int_0^{T_*} e_1^T S^{-1} \Phi^{-1}(t) G \Phi(t) S e_1 dt = \int_0^{T_*} \langle \varphi_*^\dagger(t), G y_*(t) \rangle dt,$$

hence

$$\rho \approx \varepsilon(1 - \mu_*) \int_0^{T_*} \langle \varphi_*^\dagger(t), G y_*(t) \rangle dt.$$

Therefore, the stabilization condition $|\mu_* + \rho| < 1$, which is equivalent to $\text{Re}(\rho \overline{\mu}_*) < 0$ for small ρ , is

$$\text{Re} \left((\overline{\mu}_* - 1) \int_0^{T_*} \langle \varphi_*^\dagger(t), G y_*(t) \rangle dt \right) < 0. \quad (4.31)$$

Now we consider the perturbation $\mu = 1 + \rho$ of the eigenvalue 1. By assumption, the Jordan form Λ of the matrix $\Phi(T_*)$ has the Jordan block

$$\begin{bmatrix} 1 & 1 \\ 0 & 1 \end{bmatrix};$$

again, without loss of generality, we can assume that this block is in the first and second rows and columns of Λ . Then, (4.30) implies

$$\det \begin{bmatrix} -\rho & 1 \\ -\varepsilon \rho M_{21} & -\rho \end{bmatrix} \approx 0,$$

hence

$$\rho \approx -\varepsilon M_{21},$$

which gives the stabilization condition

$$\operatorname{Re} M_{21} > 0.$$

Here

$$M_{21} = e_2^T M e_1 = \int_0^{T_*} e_2^T S^{-1} \Phi^{-1}(t) G \Phi(t) S e_1 dt$$

with $e_1 = (1, 0, \dots, 0)^T$, $e_2 = (0, 1, \dots, 0)^T$, and we can think that the transition matrix S is real. This matrix maps the vector e_1 to the eigenvector e_* of $\Phi(T_*)$ corresponding to the eigenvalue 1 and the vector e_2 to a generalized eigenvector g_* corresponding to the same eigenvalue, i.e.,

$$\Phi(T_*)e_* = e_*, \quad \Phi(T_*)g_* = g_* + e_*, \quad S^{-1}e_* = e_1, \quad S^{-1}g_* = e_2, \quad (4.32)$$

which implies

$$[\Phi^{-1}(T_*)]^T e_*^\dagger = e_*^\dagger, \quad [\Phi^{-1}(T_*)]^T g_*^\dagger = g_*^\dagger - e_*^\dagger \quad \text{for} \quad S^T e_*^\dagger = e_2, \quad S^T g_*^\dagger = e_1. \quad (4.33)$$

Further, $y_*(t) = \Phi(t)e_* = \Phi(t)S e_1$ is the Floquet mode of (4.20) corresponding to the multiplier 1 and $\varphi_*^\dagger(t) = [\Phi^{-1}(t)]^T e_*^\dagger = [S^{-1}\Phi^{-1}(t)]^T e_2$ is the adjoint Floquet mode. Therefore

$$M_{21} = \int_0^{T_*} \langle \varphi_*^\dagger(t), G y_*(t) \rangle dt$$

and the stabilization condition reads

$$\operatorname{Re} \int_0^{T_*} \langle \varphi_*^\dagger(t), G y_*(t) \rangle dt > 0. \quad (4.34)$$

Notice that $\langle \varphi_*^\dagger(t), y_*(t) \rangle \equiv 0$ automatically, and relations (4.32), (4.33) imply the following normalization condition in terms of $z_* = \Phi(t)g_*$:

$$\langle \varphi_*^\dagger(t), z_*(t) \rangle = \langle [\Phi^{-1}(t)]^T e_*^\dagger, \Phi(t)g_* \rangle \equiv e_2^T S^{-1} S e_2 = 1. \quad (4.35)$$

Thus, conditions (4.31) and (4.34) ensure the stabilization.

Finally, let us rewrite this conditions using the specific structure of our system and the specific structure of the control matrix G . First, note that due to the block structure of the matrix (4.21), each eigenfunction has the form $y_*(t) = (u_*(t), -\dot{u}_*(t))$ where u_* has values in \mathbb{R}^N . Further, we see that if an eigenfunction $y_*(t) = (u_*(t), -\dot{u}_*(t))$ corresponds to an eigenvalue μ , then $\varphi_*^\dagger(t) = \alpha(\dot{u}_*(t), u_*(t))$ is an adjoint eigenfunction corresponding to the same eigenvalue for any $\alpha \neq 0$. For $\mu = \mu_* \neq 1$, these eigenfunctions should satisfy the normalizing condition $\langle \varphi_*^\dagger(t), y_*(t) \rangle \equiv 1$, i.e.,

$$\bar{\alpha}(\dot{\bar{u}}_*^\top(t)u_*(t) - \bar{u}_*^\top(t)\dot{u}_*(t)) = 1,$$

which gives

$$\bar{\alpha} = \frac{-i}{2 \operatorname{Im} \left(\dot{\bar{u}}_*^\top(t)u_*(t) \right)} = \frac{-i}{2 \operatorname{Im} (\langle \dot{u}_*(t), u_*(t) \rangle)}.$$

On the other hand,

$$G = \begin{bmatrix} 0 & 0 \\ -D & 0 \end{bmatrix},$$

hence (4.31) is equivalent to

$$\operatorname{Im} \left(\langle \dot{u}_*(t), u_*(t) \rangle \right) \operatorname{Im} \left((\bar{\mu}_* - 1) \int_0^{T_*} \langle u_*(s), Du_*(s) \rangle ds \right) > 0 \quad (4.36)$$

(cf. (4.24)).

Now, consider $\mu_* = 1$. Using the formulas $y_*(t) = (u_*(t), -\dot{u}_*(t))$, $\varphi_*^\dagger(t) = \alpha(\dot{u}_*(t), u_*(t))$, and $z_*(t) = (v_*(t), -\dot{v}_*(t))$, where all the functions are real-valued, and the block structure of G , we can rewrite conditions (4.34) and (4.35) as

$$\alpha \int_0^{T_*} \langle u_*(t), Du_*(t) \rangle dt < 0, \quad \alpha \left(\langle \dot{u}_*(t), v_*(t) \rangle - \langle u_*(t), \dot{v}_*(t) \rangle \right) \equiv 1.$$

Combining these two relations, we obtain

$$\left(\langle u_*(t), \dot{v}_*(t) \rangle - \langle \dot{u}_*(t), v_*(t) \rangle \right) \int_0^{T_*} \langle u_*(s), Du_*(s) \rangle ds > 0$$

(cf. (4.23)). This completes the proof. \square

4.2.2 Example

Again, we consider two coupled Duffing oscillators with the potential (4.15). We have already established that there are two branches of periodic solutions emanating from the origin. Close to the origin the frequencies of these branches are $\omega \approx \sqrt{2}$ and $\omega \approx \sqrt{0.7}$. Moreover we have shown that small periodic orbits can be stabilized by the diagonal control matrix $K = \text{diag}(\kappa_1, \kappa_2)$ satisfying conditions (4.17) and (4.18) for $\omega = \sqrt{2}$ and $\omega = \sqrt{0.7}$, respectively. Using numerical continuation with the delay τ as a continuation parameter we can “travel” along the branch of interest and study the stability of the periodic solutions away from the origin. The period of the orbit equals the delay, $T = \tau$.

Figure 4.1 presents the branch of periodic orbits starting from the zero equilibrium at $\tau = 2\pi/\sqrt{0.7}$. The period decreases and the amplitude increases along the branch. Depending on the value of $\kappa = (\kappa_1, \kappa_2)$, different parts of the branch are stable/unstable. Panels (A) and (B) present the stability of the solutions along the branch for $\tilde{\kappa} = (-0.02, 0.012)$ and $\hat{\kappa} = (-0.02, 0.02)$, respectively. Both $\tilde{\kappa}$ and $\hat{\kappa}$ satisfy conditions (4.18), therefore the small-amplitude solutions are asymptotically stable. For $\kappa = \tilde{\kappa}$ the orbit destabilizes at the point B (see Figure 4.1(A)), while for $\kappa = \hat{\kappa}$ all the orbits remain stable for all the values of τ considered (see Figure 4.1(B)). Continuation of the branch was performed using DDE-BIFTOOL package for MATLAB[®] [37, 38].

Conditions (4.23), (4.24) were evaluated numerically for three points A , B and C of the branch, see Figure 4.1. For each point, these conditions define a sector with the vertex at the origin in the plane of control parameters (κ_1, κ_2) . The three corresponding sectors, A_1OA_2 , B_1OB_2 , C_1OC_2 , are shown in Figure 4.2. In particular, if κ belongs to the interior of the sector A_1OA_2 and $\|\kappa\|$ is sufficiently small, then Theorem 4.2.1 ensures that the periodic orbit corresponding to the point A is asymptotically stable for the controlled system when the delay is set to $\tau = \tau_A$. Figure 4.2 suggests that the sector becomes more narrow with the decreasing τ . Correspondingly, since $\hat{\kappa}$ belongs to C_1OC_2 , the stable part of the branch

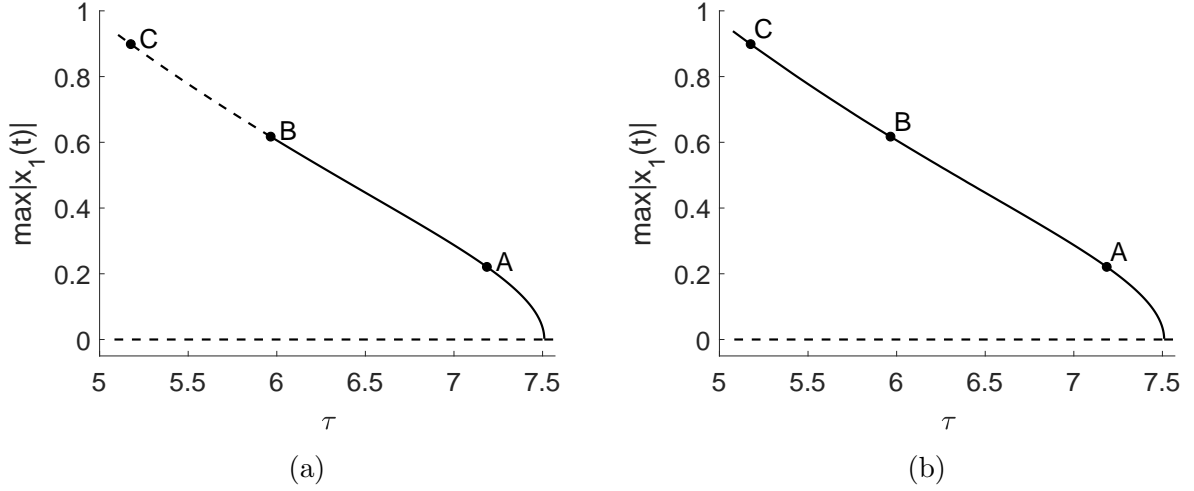


Figure 4.1: Panel (A): Bifurcation diagram of the controlled system for $\tilde{\kappa} = (-0.02, 0.012)$. Points A , B and C on the branch correspond to the delays $\tau_A = 7.1857$, $\tau_B = 5.9655$ and $\tau_C = 5.1761$, respectively. Panel (B): The same branch of periodic solutions has different stability properties for $\hat{\kappa} = (-0.02, 0.02)$. Stable and unstable solutions are shown by solid and dashed lines, respectively.

extends from its origin at least to the point C for the controlled system with $K = \text{diag}(\hat{\kappa}_1, \hat{\kappa}_2)$. On the other hand, for $K = \text{diag}(\tilde{\kappa}_1, \tilde{\kappa}_2)$, the stable part of the branch extends only to the point B because $\tilde{\kappa}$ lies on the boundary of the sector B_1OB_2 . This agrees with Figure 4.1.

4.3 How do stability conditions for small and large cycles agree?

For a small cycle, the Hessian is close to its constant value at zero. Therefore the Floquet modes are close to the eigenfunctions at zero. In particular, for $n \neq k$, we have $u_*(t) \approx e^{i\omega_n t} e_n$. Using this approximation,

$$\langle \dot{u}_*(t), u_*(t) \rangle \approx -i\omega_n \|e_n\|^2, \quad \mu_n \approx e^{2\pi i \omega_n / \omega_k}, \quad \langle u_*(t), Du_*(t) \rangle \approx \langle e_n, De_n \rangle,$$

and we see that (4.24) is equivalent to (4.6).

On the other hand, the solution is approximately $x_*(t) \approx r e_k \cos(\omega_k t)$ and for $n = k$, we have $u_*(t) = \dot{x}_*(t) \approx -r \omega_k e_k \sin(\omega_k t)$. If we assume in addition to (4.5) that the period T is

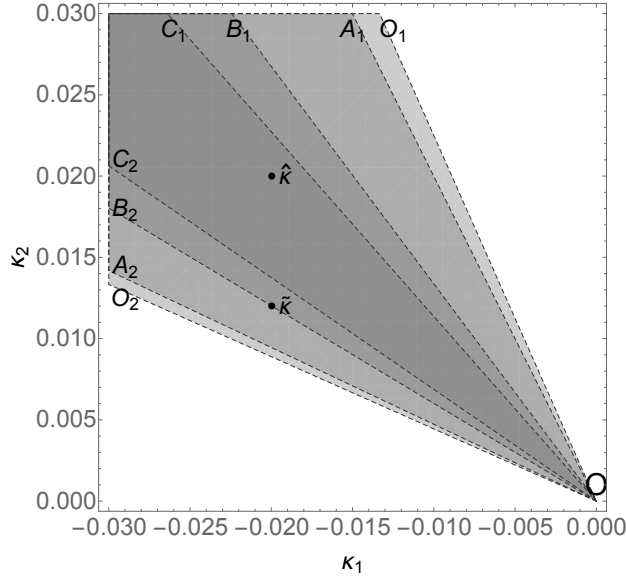


Figure 4.2: Control parameters plane. Conditions (4.18) of Theorem 4.1.1 are satisfied within the sector O_1OO_2 . Sectors A_1OA_2 , B_1OB_2 , C_1OC_2 are defined by conditions (4.23) and (4.24) for the periodic solutions indicated by points A , B and C , respectively, on Figure 4.1. Point $\tilde{\kappa} = (-0.02, 0.012)$ corresponds to control parameters used in Figure 4.1(A); parameters $\hat{\kappa} = (-0.02, 0.02)$ are used in Figure 4.1(B).

a strictly monotone function of the amplitude $\|x\|_\infty$ of the periodic orbit along the branch (for small cycles), and the derivative $\partial T / \partial \|x\|_\infty$ is well-defined and is nonzero, then the sign of this derivative is opposite to the sign of ξ_k (cf. (4.14)). To be definite, assume that $\xi_k > 0$, hence T decreases with $\|x\|_\infty$ along the branch. Then, $v_*(t) \approx \hat{r}e_k \cos(\omega_k t)$ where $\hat{r} > 0$. Therefore,

$$\langle u_*(t), \dot{v}_*(t) \rangle - \langle \dot{u}_*(t), v_*(t) \rangle \approx \omega_k^2 \hat{r} \|e_k\|^2, \quad \langle u_*(t), Du_*(t) \rangle \approx \omega_k^2 \hat{r}^2 \sin^2(\omega_k t) \langle e_k, De_k \rangle,$$

and we see that (4.23) implies $\langle e_k, De_k \rangle > 0$, which agrees with (4.7). In the case $\xi_k < 0$, we have $v_*(t) \approx \hat{r}e_k \cos(\omega_k t)$ with $\hat{r} < 0$, which leads to (4.7) again.

4.4 Conclusions

We considered an extension of the Pyragas delayed control method from general differential equations to Newtonian systems that possess a branch of neutrally stable periodic orbits.

We proposed sufficient conditions which allow arbitrarily small Pyragas control to transform the stability of one selected periodic solution from neutrally stable to exponentially stable. In the case of small amplitude periodic solutions our conditions were given in terms of the asymptotic expansion of the vector field, while in the case of general periodic orbits we expressed the conditions in terms of the Floquet modes of the target orbit as a solution of the uncontrolled system. The theorem were illustrated by analytical and numerical examples. The results can be naturally extended to Newtonian systems with controls $K(\dot{x}_\tau - \dot{x})$ and to Hamiltonian systems $\dot{x} = J\nabla H(x)$ with controls $K(x_\tau - x)$.

APPENDIX A

TWISTED SUBGROUPS

A.1 Notations used for the twisted subgroups of $\mathcal{K} := D_8 \times S^1$

The following symbols are used for the twisted subgroups of \mathcal{K} :

$$D_8 := \{(\xi^k, 1) : k = 0, 1, \dots, 7\} \cup \{(\xi^k \kappa, 1) : k = 0, 1, \dots, 7\},$$

$$D_8^d := \{(\xi^k, (-1)^k) : k = 0, 1, \dots, 7\} \cup \{(\xi^k \kappa, (-1)^k) : k = 0, 1, \dots, 7\},$$

$$\tilde{D}_4^d := \{(1, 1), (i, -1), (-1, 1), (-i, -1), (\xi \kappa, 1), (\xi i \kappa, -1), (-\xi \kappa, 1), (-\xi i \kappa, -1)\},$$

$$D_4^d := \{(1, 1), (i, -1), (-1, 1), (-i, -1), (\kappa, 1), (i \kappa, -1), (-\kappa, 1), (-i \kappa, -1)\},$$

$$D_2^d := \{(1, 1), (-1, -1), (\kappa, 1), (-\kappa, -1)\},$$

$$\tilde{D}_2^d := \{(1, 1), (-1, -1), (\xi \kappa, 1), (-\xi \kappa, -1)\},$$

$$\mathbb{Z}_8^{t_1} := \{(\xi^k, \xi^k) : k = 0, 1, \dots, 7\},$$

$$\mathbb{Z}_8^{t_2} := \{(\xi^k, \xi^{2k}) : k = 0, 1, \dots, 7\},$$

$$\mathbb{Z}_8^{t_3} := \{(\xi^k, \xi^{3k}) : k = 0, 1, \dots, 7\}.$$

Here

$$\xi := e^{\frac{\pi i}{4}} \quad \text{and} \quad \kappa := \begin{bmatrix} 1 & 0 \\ 0 & -1 \end{bmatrix}.$$

A.2 Notations used for the twisted subgroups of $\mathcal{K} := D_8 \times \{1\} \times S^1$

The following symbols are used for the twisted subgroups of \mathcal{K} :

$$\begin{aligned}
D_8 &:= D_8 \times \{1\} \times \{1\}, \\
\mathbf{Z}_8^{t_1} &:= \{(\xi^k, 1, \xi^k) \in \mathcal{K} : k = 0, 1, \dots, 7\}, \quad \xi := e^{\frac{\pi i}{4}}, \\
D_2^d &:= \{(1, 1, 1), (-1, 1, -1), (\kappa, 1, 1), (-\kappa, 1, -1)\}, \\
\tilde{D}_2^d &:= \{(1, 1, 1), (-1, 1, -1), (\xi\kappa, 1, 1), (-\xi\kappa, 1, -1)\}, \\
\mathbf{Z}_8^{t_2} &:= \{(\xi^k, 1, \xi^{2k}) \in \mathcal{K} : k = 0, 1, \dots, 7\}, \\
D_4^d &:= \{(1, 1, 1), (i, 1, -1)(-1, 1, 1), (-i, 1, -1), (\kappa, 1, 1), (i\kappa, 1, -1), \\
&\quad (-\kappa, 1, 1), (-i\kappa, 1, -1)\}, \\
\tilde{D}_4^d &:= \{(1, 1, 1), (i, 1, -1)(-1, 1, 1), (-i, 1, -1), (\xi\kappa, 1, 1), (i\xi\kappa, 1, -1), \\
&\quad (-\xi\kappa, 1, 1), (-i\xi\kappa, 1, -1)\}, \\
\mathbf{Z}_8^{t_3} &:= \{(\xi^k, 1, \xi^{3k}) \in \mathcal{K} : k = 0, 1, \dots, 7\}, \\
D_8^d &:= \{(\xi^k, 1, (-1)^k), (\xi^k \kappa, 1, (-1)^k) \in \mathcal{H} : k = 0, 1, \dots, 7\}.
\end{aligned}$$

A.3 Notations used for the twisted subgroups of $\mathcal{K} := \mathbb{Z}_8^{t_l} \times S^1$, $l = 1, 2, 3$

In this case, the following symbols are used for the twisted subgroups of \mathcal{K} :

$$\begin{aligned}
\mathbf{Z}_8 &:= \mathbb{Z}_8^{t_l} \times \{1\}, \\
\mathbf{Z}_8^{t_1} &:= \{(\xi^k, \xi^{lk}, \xi^k) \in \mathcal{K} : k = 0, 1, \dots, 7\}, \quad \xi := e^{\frac{\pi i}{4}}, \\
\mathbf{Z}_8^{t_2} &:= \{(\xi^k, \xi^{lk}, \xi^{2k}) \in \mathcal{K} : k = 0, 1, \dots, 7\}, \\
\mathbf{Z}_8^{t_3} &:= \{(\xi^k, \xi^{lk}, \xi^{3k}) \in \mathcal{K} : k = 0, 1, \dots, 7\}, \\
\mathbf{Z}_8^c &:= \{(\xi^k, \xi^{lk}, (-1)^k) \in \mathcal{K} : k = 0, 1, \dots, 7\}.
\end{aligned}$$

A.4 Notations used for the twisted subgroups of $\mathcal{K} := D_8^d \times S^1$

For this group, the following symbols are used for the twisted subgroups of \mathcal{K} :

$$D_8 := D_8^d \times \{1\},$$

$$\mathbf{Z}_8^{t_1} := \{(\xi^k, (-1)^k, \xi^k) \in \mathcal{K} : k = 0, 1, \dots, 7\}, \quad \xi := e^{\frac{\pi i}{4}},$$

$$D_2^d := \{(1, 1, 1), (-1, 1, -1), (\kappa, 1, 1), (-\kappa, 1, -1)\},$$

$$\tilde{D}_2^d := \{(1, 1, 1), (-1, 1, -1), (\xi\kappa, -1, 1), (-\xi\kappa, -1, -1)\},$$

$$\mathbf{Z}_8^{t_2} := \{(\xi^k, (-1)^k, \xi^{2k}) \in \mathcal{K} : k = 0, 1, \dots, 7\},$$

$$D_4^d := \{(1, 1, 1), (i, 1, -1)(-1, 1, 1), (-i, 1, -1), (\kappa, 1, 1), (i\kappa, 1, -1), \\ (-\kappa, 1, 1), (-i\kappa, 1, -1)\},$$

$$\tilde{D}_4^d := \{(1, 1, 1), (i, 1, -1)(-1, 1, 1), (-i, 1, -1), (\xi\kappa, -1, 1), (i\xi\kappa, -1, -1), \\ (-\xi\kappa, -1, 1), (-i\xi\kappa, -1, -1)\},$$

$$\mathbf{Z}_8^{t_3} := \{(\xi^k, (-1)^k, \xi^{3k}) \in \mathcal{K} : k = 0, 1, \dots, 7\},$$

$$D_8^d := \{(\xi^k, (-1)^k, (-1)^k), \{(\xi^k\kappa, (-1)^k, (-1)^k) \in \mathcal{H} : k = 0, 1, \dots, 7\}.$$

A.5 Notations used for selected twisted subgroups of $\mathcal{H} = S_5 \times S^1$

The following symbols are used for selected twisted subgroups of \mathcal{H} :

$$S_5 := S_5 \times \{1\},$$

$$\mathbb{Z}_5^{t_1} := \langle ((12345), \omega_5) \rangle,$$

$$D_6 := D_6 \times \{1\},$$

$$D_6^d := \langle ((12), 1), ((123), 1), ((45), -1) \rangle = \langle ((123)(45), -1), ((12), 1) \rangle,$$

$$\mathbb{Z}_6^{t_2} := \langle ((45), 1), ((123), \omega_3) \rangle = \langle ((123)(45), \omega_3) \rangle,$$

$$S_4 := S_4 \times \{1\},$$

$$D_4^d := \langle ((24), 1), ((35), 1), ((2345), -1) \rangle = \langle ((2345), -1), ((24), 1) \rangle,$$

$$\mathbb{Z}_4^{t_1} := \langle ((2345), \omega_4) \rangle.$$

Here $\omega_k := e^{\frac{2\pi i}{k}}$.

A.6 Notations used for selected twisted subgroups of $\mathcal{K} := \mathbb{Z}_5^{t_1} \times S^1$

In this case, the following symbols are used for selected twisted subgroups of \mathcal{K} :

$$\mathbb{Z}_5^{t_1} := \mathbb{Z}_5^{t_1} \times \{1\},$$

$$\mathbb{Z}_5^{t_1, t_1} := \langle ((12345), \omega_5, \omega_5) \rangle.$$

A.7 Notations used for selected twisted subgroups of $\mathcal{K} := D_6^d \times S^1$

For this group, the following symbols are used for selected twisted subgroups of \mathcal{K} :

$$\begin{aligned}
D_6^d &:= D_6^d \times \{1\}, \\
\mathbb{Z}_6^{t_3, t_1} &:= \langle ((125)(34), -1, \omega_6) \rangle, \\
D_2^{d, d} &:= \langle ((12), 1, 1), ((12)(34), -1, -1) \rangle, \\
D_2^{d, \hat{d}} &:= \langle ((34), -1, 1), ((12)(34), -1, -1) \rangle, \\
\mathbb{Z}_6^{t_3, t_2} &:= \langle ((125)(34), -1, \omega_3) \rangle, \\
D_2^d &:= D_2^d \times \{1\}, \\
D_2^{d, z} &:= \langle ((12)(34), -1, 1), ((12), 1, -1) \rangle, \\
D_6^{d, d} &:= \langle ((12), 1, 1), ((125), 1, 1), ((34), -1, -1) \rangle = \langle ((125)(34), -1, -1), ((12), 1, 1) \rangle.
\end{aligned}$$

A.8 Notations used for selected twisted subgroups of $\mathcal{K} := S_4 \times S^1$

For this group, the following symbols are used for selected twisted subgroups of \mathcal{K} :

$$\begin{aligned}
S_4 &:= S_4 \times \{1\} \times \{1\}, \\
\mathbb{Z}_4^{t_2} &:= \langle ((2345), 1, -1) \rangle, \\
D_4^d &:= \langle ((24), 1, 1), ((35), 1, 1), ((2345), 1, -1) \rangle = \langle ((2345), 1, -1), ((24), 1, 1) \rangle, \\
D_2^d &:= \langle ((24), 1, 1), ((24)(35), 1, -1) \rangle, \\
\mathbb{Z}_3^{t_1} &:= \langle ((234), 1, \omega_3) \rangle.
\end{aligned}$$

APPENDIX B
COMPUTATION OF THE NORMAL FORM

Let us consider the delay $\tau > 0$ in equation (4.1) as a bifurcation parameter, which is varied near the point $\tau_* = 2\pi/\omega_k$. The characteristic equation of the linearization of (4.1) at zero reads

$$\det(\lambda^2 \text{Id} + H_0 + K - Ke^{-\lambda\tau}) = 0. \quad (\text{B.1})$$

Assume that conditions (4.5), (4.6) hold and $K = \varepsilon D$ with a sufficiently small $\varepsilon > 0$. Then, as shown in the proof of Theorem 4.1.1, a pair of complex conjugate eigenvalues $\lambda_k(\tau), \bar{\lambda}_k(\tau)$ crosses the imaginary axis transversally at the points $\pm i\omega_k$ for $\tau_* = 2\pi/\omega_k$, while all the other eigenvalues have negative real parts.

We now use the multiple time scale method to compute the normal form of system (4.1) near the zero equilibrium $x = 0$ for τ close to τ_* . According to (4.3), we have the following third order expansion of equation (4.1):

$$\ddot{x} + H_0 x + L(x, x) + Q(x, x, x) = K(x(t - \tau) - x(t)) + o(\|x\|^3). \quad (\text{B.2})$$

We seek a uniform second-order approximate periodic solution in the form

$$x(t) = s x_1(T_0, T_2) + s^2 x_2(T_0, T_2) + s^3 x_3(T_0, T_2) + h.o.t. \quad (\text{B.3})$$

where $T_0 = t$, $T_2 = s^2 t$, and s is a nondimensional book keeping parameter; *h.o.t.* stays for higher order terms in s . Note that it is not necessary to relate the approximate solution with the time scale $T_1 = st$ because a second order approximation will require independence of T_1 in the solution (e.g. [110], page 166). Using the notation

$$\begin{aligned} \frac{d}{dt} &= \frac{\partial}{\partial T_0} + s^2 \frac{\partial}{\partial T_2} + \dots = \mathcal{D}_0 + s^2 \mathcal{D}_2 + h.o.t., \\ \frac{d^2}{dt^2} &= \frac{\partial^2}{\partial T_0^2} + 2s^2 \frac{\partial^2}{\partial T_0 \partial T_2} + \dots = \mathcal{D}_0^2 + 2s^2 \mathcal{D}_0 \mathcal{D}_2 + h.o.t. \end{aligned} \quad (\text{B.4})$$

for the time derivatives, from (B.3) one obtains

$$x(t - \tau) = x(T_0 - \tau, T_2 - s^2\tau) = \sum_{m=1}^3 s^m x_m(T_0 - \tau, T_2) - s^3 \tau \mathcal{D}_2 x_1(T_0 - \tau, T_2) + h.o.t.$$

Further, introducing the notation $\tau = \tau_* + s^2\delta$ where δ is the detuning parameter,

$$x(t - \tau) = \sum_{m=1}^3 s^m x_m(T_0 - \tau_*, T_2) - s^3 (\tau_* \mathcal{D}_2 - \delta \mathcal{D}_0) x_1(T_0 - \tau_*, T_2) + h.o.t. \quad (\text{B.5})$$

Now, substituting (B.3)–(B.5) into (B.2) and comparing the like powers of s up to the cubic terms yields the following equations, where for notational simplicity we omit the time scales of the variables except for the delayed ones:

$$\mathcal{D}_0^2 x_1 + (H_0 + K)x_1 - Kx_1(T_0 - \tau_*) = 0, \quad (\text{B.6})$$

$$\mathcal{D}_0^2 x_2 + (H_0 + K)x_2 + \frac{1}{2}L(x_1, x_1) - Kx_2(T_0 - \tau_*) = 0, \quad (\text{B.7})$$

$$\begin{aligned} \mathcal{D}_0^2 x_3 + 2\mathcal{D}_0 \mathcal{D}_2 x_1 + (H_0 + K)x_3 + L(x_1, x_2) + \frac{1}{6}Q(x_1, x_1, x_1) \\ = K(x_3(T_0 - \tau_*, T_2) - \tau_* \mathcal{D}_2 x_1(T_0 - \tau_*, T_2) - \delta \mathcal{D}_0 x_1(T_0 - \tau_*, T_2)). \end{aligned} \quad (\text{B.8})$$

Since $\tau = \tau_*$ is a Hopf bifurcation point for (B.2), the linearization (B.6) has a periodic solution of the form

$$x_1 = (A(T_2)e^{i\omega_k T_0} + \bar{A}(T_2)e^{-i\omega_k T_0})e_k, \quad (\text{B.9})$$

where the real eigenvector e_k corresponds to the eigenvalues $\pm i\omega_k$ of (B.1) for $\tau = \tau_* = 2\pi/\omega_k$. Substituting this expression in equation (B.7) and using $e^{i\omega_k \tau_*} = 1$, we obtain a particular solution

$$x_2 = a_k (A^2 e^{2i\omega_k T_0} + \bar{A}^2 e^{-2i\omega_k T_0}) + b_k A \bar{A}$$

with a_k, b_k defined by (4.4). Further, substituting the expressions for x_1 and x_2 into (B.8), we obtain

$$\begin{aligned}
& \mathcal{D}_0^2 x_3 + (H_0 + K)x_3 - Kx_3(T_0 - \tau_*, T_2) + 2i\omega_k(A'e^{i\omega_k T_0} - \bar{A}'e^{-i\omega_k T_0})e_k \\
& + L((Ae^{i\omega_k T_0} + \bar{A}e^{-i\omega_k T_0})e_k, a_k(A^2e^{2i\omega_k T_0} + \bar{A}^2e^{-2i\omega_k T_0}) + b_k A\bar{A}) \\
& + \frac{1}{6}Q(e_k, e_k, e_k)(A^3e^{3i\omega_k T_0} + \bar{A}^3e^{-3i\omega_k T_0} + 3A^2\bar{A}e^{i\omega_k T_0} + 3A\bar{A}^2e^{-i\omega_k T_0}) \\
& = -(\tau_*A'e^{i\omega_k T_0} + \tau_*\bar{A}'e^{-i\omega_k T_0} + i\omega_k\delta Ae^{i\omega_k T_0} - i\omega_k\delta\bar{A}e^{-i\omega_k T_0})Ke_k.
\end{aligned} \tag{B.10}$$

Note that the nonhomogeneous equation (B.10) has terms proportional to $e^{i\omega_k T_0}$, which sum to $\chi(T_2)e^{i\omega_k T_0}$ with

$$\chi = 2i\omega_k A'e_k + \left(L(e_k, a_k + b_k) + \frac{1}{2}Q(e_k, e_k, e_k)\right)A^2\bar{A} + \tau_*A'Ke_k + i\omega_k\delta AKe_k.$$

At the same time, $i\omega_k$ is an eigenvalue of the associated homogeneous equation. Since x_3 is a periodic solution of (B.10), it does not contain secular terms, which is only possible if the equation

$$(-\omega_k^2 \text{Id} + H_0 + K - Ke^{-i\omega_k \tau_*})\phi = (-\omega_k^2 \text{Id} + H_0)\phi = \chi$$

is solvable with respect to $\phi = \phi(T_2)$, where $\phi(T_2)e^{i\omega_k T_0}$ is the first harmonic in the Fourier expansion of x_3 . The solvability requires the orthogonality of χ with the eigenvector e_k of H_0 corresponding to the eigenvalue ω_k^2 :

$$\langle e_k, \text{Re } \chi \rangle = \langle e_k, \text{Im } \chi \rangle = 0.$$

Substituting the above expression for χ in these relations leads to the following equation

$$A' + \frac{i\omega_k\delta\langle e_k, Ke_k \rangle}{2i\omega_k + \tau_*\langle e_k, Ke_k \rangle}A + \frac{\langle e_k, L(e_k, a_k + b_k) + \frac{1}{2}Q(e_k, e_k, e_k) \rangle}{2i\omega_k + \tau_*\langle e_k, Ke_k \rangle}A^2\bar{A} = 0,$$

which is the normal form of the Hopf bifurcation for equation (4.1) with the parameter τ .

Using the notation (4.5), this is equivalent to

$$A' + \frac{i\omega_k\delta\langle e_k, Ke_k \rangle}{2i\omega_k + \tau_*\langle e_k, Ke_k \rangle}A + \frac{\xi_k}{2i\omega_k + \tau_*\langle e_k, Ke_k \rangle}A^2\bar{A} = 0. \tag{B.11}$$

The normal form (B.11) has a periodic orbit if and only if $\delta\xi_k < 0$. This orbit has the simple form $A = A_0 e^{i\omega_0 t}$ (a relative equilibrium). Computing A_0, ω_0 from (B.11) and using the relations (B.3) and (B.9), one obtains the asymptotic relationship between the amplitude $\|x\|_\infty$ of a small periodic orbit of (4.1) and its period T , which is equal to the delay:

$$T = \tau = \tau_* - \frac{\xi_k \pi}{4\omega_k^3} \|x\|_\infty^2 + o(\|x\|_\infty^2). \quad (\text{B.12})$$

Furthermore, if $\delta\langle e_k, Ke_k \rangle < 0$, then the periodic orbit of the normal form (B.11) is asymptotically stable and so is the periodic orbit $x(t)$ of (4.1). Due to $\delta\xi_k < 0$, this asymptotic stability condition is equivalent to (4.7) yielding the conclusion of Theorem 4.1.1.

Finally, equation (B.11) with $K = 0$ provides asymptotics of small periodic solutions of the uncontrolled system (4.2). In particular, the relationship (B.12) between the period and the amplitude holds, which justifies Remark 4.1.3.

REFERENCES

- [1] Alexander, J. C. and J. A. Yorke (1978). Global bifurcations of periodic orbits. *Amer. J. Math.* 100(2), 263–292.
- [2] Appelbe, B., D. Rachinskii, and A. Zhezherun (2008). Hopf bifurcation in a van der poltype oscillator with magnetic hysteresis. *Physica B: Condensed Matter* 403, 301–304.
- [3] Arkhipov, R., A. Amann, and A. Vladimirov (2015a). Pulse repetition-frequency multiplication in a coupled cavity passively mode-locked semiconductor lasers. *Applied Physics B* 118(4), 539–548.
- [4] Arkhipov, R., T. Habruseva, A. Pimenov, M. Radziunas, S. Hegarty, G. Huyet, and A. Vladimirov (2016). Semiconductor mode-locked lasers with coherent dual-mode optical injection: simulations, analysis, and experiment. *Journal of the Optical Society of America B* 33(3), 351–359.
- [5] Arkhipov, R., A. Pimenov, M. Radziunas, D. Rachinskii, A. G. Vladimirov, D. Arsenijevic, H. Schmeckeber, and D. Bimberg (2013). Hybrid mode-locking in semiconductor lasers: simulations, analysis and experiments. *IEEE Journal of Selected Topics in Quantum Electronics* 19, 1100208.
- [6] Arkhipov, R., A. Pimenov, M. Radziunas, D. Rachinskii, A. G. Vladimirov, D. Arsenijević, H. Schmeckeber, and D. Bimberg (2013). Hybrid mode locking in semiconductor lasers: simulations, analysis, and experiments. *IEEE Journal of Selected Topics in Quantum Electronics* 19(4), 1100208.
- [7] Arkhipov, R. M., A. Amann, and A. G. Vladimirov (2015b). Pulse repetition-frequency multiplication in a coupled cavity passively mode-locked semiconductor lasers. *Applied Physics B* 118, 539–548.
- [8] Arkhipov, R. M., T. Habruseva, A. Pimenov, M. Radziunas, G. Huyet, and A. G. Vladimirov (2016). Semiconductor mode-locked lasers with coherent dual mode optical injection: Simulations, analysis and experiment. *Journal of the Optical Society of America B* 33, 351–359.
- [9] Ashkenas, I. L., H. R. Jex, and D. T. McRuer (1964). Pilot-induced oscillations: their cause and analysis. Technical report, SYSTEMS TECHNOLOGY INC INGLEWOOD CA.
- [10] Balanov, Z., P. Kravets, W. Krawcewicz, and D. Rachinskii (2018). Equivariant degree method for analysis of hopf bifurcation of relative periodic solutions: Case study of a ring of oscillators. *Journal of Differential Equations* 265(9), 4530 – 4574.

- [11] Balanov, Z., P. Kravets, W. Krawcewicz, D. Rachinskii, and H. Wu (2018). Hopf bifurcation of relative periodic solutions in a system of five passively mode-locked lasers. *Journal of Nonlinear and Variational Analysis* 2(2), 233–262.
- [12] Balanov, Z. and W. Krawcewicz (2008). Symmetric hopf bifurcation: twisted degree approach. *Handbook of Differential Equations, Ordinary Differential Equations* 4, 1–131.
- [13] Balanov, Z., W. Krawcewicz, D. Rachinskii, and A. Zhezherun (2012). Hopf bifurcation in symmetric networks of coupled oscillators with hysteresis. *J. Dynam. Differential Equations* 24(4), 713–759.
- [14] Balanov, Z., W. Krawcewicz, and B. Rai (2003). Taylor–couette problem and related topics. *Nonlinear Analysis: Real World Applications* 4(4), 541–559.
- [15] Balanov, Z., W. Krawcewicz, S. Rybicki, and H. Steinlein (2010). A short treatise on the equivariant degree theory and its applications. *Journal of Fixed Point Theory and Applications* 8(1), 1–74.
- [16] Balanov, Z., W. Krawcewicz, and H. Steinlein (2006). *Applied equivariant degree*, Volume 1. American Institute of Mathematical Sciences Springfield.
- [17] Banerjee, S., B. Mukhopadhyay, and R. Bhattacharyya (2010). Effect of maturation and gestation delays in a stage structure predator prey model. *Journal of Applied Mathematics and Informatics* 28(5-6), 1379–1393.
- [18] Bélair, J. and M. C. Mackey (1989, Jul). Consumer memory and price fluctuations in commodity markets: An integrodifferential model. *Journal of Dynamics and Differential Equations* 1(3), 299–325.
- [19] Bellman, R. E. and K. L. Cooke (1963). *Differential-difference equations*. Rand Corporation.
- [20] Bellman, R. E. and J. M. Danskin (1954). *A survey of the mathematical theory of time-lag, retarded control, and hereditary processes*. Rand Corporation.
- [21] Borsuk, K. (1933). Drei sätze über die n-dimensionale euklidische sphäre. *Fundamenta Mathematicae* 20(1), 177–190.
- [22] Botez, D. and D. Scifres (2008). Diode laser arrays. In D. Botez and D. Scifres (Eds.), *Cambridge Studies in Modern Optics*. Cambridge University Press.
- [23] BOUCEKKINE, R., D. D. L. CROIX, and O. LICANDRO (2004). Modelling vintage structures with DDEs: Principles and applications. *Mathematical Population Studies* 11(3-4), 151–179.

- [24] Bredon, G. E. (1972). *Introduction to compact transformation groups*, Volume 46. Academic press.
- [25] Bröcker, T. and T. tom Dieck (2013). *Representations of compact Lie groups*, Volume 98. Springer Science & Business Media.
- [26] Brokate, M. and J. Sprekels (1994). *Hysteresis and phase transitions*. Springer.
- [27] Broucke, R. (1975). On relative periodic solutions of the planar general three-body problem. *Celestial mechanics* 12(4), 439–462.
- [28] Brouwer, L. E. J. (1911). Über abbildung von mannigfaltigkeiten. *Mathematische Annalen* 71(1), 97–115.
- [29] Carr, T. W., R. Haberman, and T. Erneux (2012). Delay-periodic solutions and their stability using averaging in delay-differential equations, with applications. *Physica D: Nonlinear Phenomena* 241(18), 1527–1531.
- [30] Carr, T. W., I. B. Schwartz, M. Y. Kim, and R. Roy (2006). Delayed-mutual coupling dynamics of lasers: scaling laws and resonances. *SIAM J. Dynamical Systems* 5, 699–725.
- [31] Chandrasekhar, S. (1969). *Ellipsoidal figures of equilibrium*, Volume 9. Yale University Press New Haven.
- [32] Chossat, P. and R. Lauterbach (2000). *Methods in equivariant bifurcations and dynamical systems*, Volume 15. World Scientific Publishing Co Inc.
- [33] Chow, S. N. and J. Mallet-Paret (1978). The Fuller index and global Hopf bifurcation. *J. Differential Equations* 29(1), 66–85.
- [34] Chow, S. N., J. Mallet-Paret, and J. A. Yorke (1978). Global Hopf bifurcation from a multiple eigenvalue. *Nonlinear Anal.* 2(6), 753–763.
- [35] Delfyett, P. J., S. Gee, M.-T. Choi, H. Izadpanah, W. Lee, S. Ozharar, F. Quinlan, and T. Yilmaz (2006). Optical frequency combs from semiconductor lasers and applications in ultrawideband signal processing and communications. *Journal of Lightwave Technology* 24(7), 2701–2719.
- [36] Dombovari, Z. and G. Stepan (2015). On the bistable zone of milling processes. *Philosophical Transactions of the Royal Society A: Mathematical, Physical and Engineering Sciences* 373(2051), 20140409.
- [37] Engelborghs, K., T. Luzyanina, and D. Roose (2002). Numerical bifurcation analysis of delay differential equations using DDE-BIFTOOL. *ACM Trans. Math. Software* 28(1), 1–21.

- [38] Engelborghs, K., T. Luzyanina, and G. Samaey (2001). Dde-biftool v. 2.00: a matlab package for bifurcation analysis of delay differential equations.
- [39] Erneux, T. (2009a). *Applied Delay Differential Equations*. Springer.
- [40] Erneux, T. (2009b). *Applied delay differential equations*, Volume 3. Springer Science & Business Media.
- [41] Erneux, T. and P. Mandel (1995). Minimal equations for antiphase dynamics in multimode lasers. *Physical Review A* 52, 4137–4144.
- [42] Faria, T. and L. T. Magalhães (1995). Normal forms for retarded functional-differential equations and applications to Bogdanov-Takens singularity. *J. Differential Equations* 122(2), 201–224.
- [43] Fiedler, B. (2006). *Global bifurcation of periodic solutions with symmetry*, Volume 1309. Springer.
- [44] Fiedler, B., V. Flunkert, P. Hövel, and E. Schöll (2010). Delay stabilization of periodic orbits in coupled oscillator systems. *Philosophical Transactions of the Royal Society of London A: Mathematical, Physical and Engineering Sciences* 368, 319–341.
- [45] Fiedler, B., V. Flunkert, P. Hövel, and E. Schöll (2010). Delay stabilization of periodic orbits in coupled oscillator systems. *Philosophical Transactions of the Royal Society of London A: Mathematical, Physical and Engineering Sciences* 368, 319–341.
- [46] Fiedler, B., S. Yanchuk, V. Flunkert, P. Hövel, H.-J. Wünsche, and E. Schöll (2008). Delay stabilization of rotating waves near fold bifurcation and application to all-optical control of a semiconductor laser. *Physical Review E* 77(6), 066207.
- [47] Fowler, A. C. (1982). An asymptotic analysis of the delayed logistic equation when the delay is large. *IMA Journal of Applied Mathematics* 28, 41–49.
- [48] Fowler, A. C. (2005). Asymptotic methods for delay equations. *Journal of Engineering Mathematics* 53, 271–290.
- [49] Fuller, F. B. (1967). An index of fixed point type for periodic orbits. *Amer. J. Math.* 89, 133–148.
- [50] Golubitsky, M. and I. Stewart (2003). *The symmetry perspective: from equilibrium to chaos in phase space and physical space*, Volume 200. Springer Science & Business Media.
- [51] Golubitsky, M., I. Stewart, et al. (2012). *Singularities and groups in bifurcation theory*, Volume 2. Springer Science & Business Media.

- [52] Gourley, S. A. and Y. Kuang (2004). A stage structured predator-prey model and its dependence on maturation delay and death rate. *Journal of Mathematical Biology* 49(2), 188–200.
- [53] Gradišek, J., M. Kalveram, T. Insperger, K. Weinert, G. Stpn, E. Govekar, and I. Grabec (2005). On stability prediction for milling. *International Journal of Machine Tools and Manufacture* 45(7), 769 – 781.
- [54] Griess, Jr., R. L. (1998). *Twelve sporadic groups*. Springer Monographs in Mathematics. Springer-Verlag, Berlin.
- [55] Grigorieva, E. V. and S. A. Kashchenko (1993). Complex temporal structures in models of a laser with optoelectronic delayed feedback. *Optics Communications* 102, 183–192.
- [56] Habruseva, T., S. P. Hegarty, A. G. Vladimirov, A. Pimenov, D. Rachinskii, N. Rebrova, E. A. Viktorov, and G. Huyet (2010). Bistable regimes in an optically injected mode-locked laser. *Optics Express* 20, 25572–25583.
- [57] Habruseva, T., S. P. Hegarty, A. G. Vladimirov, A. Pimenov, D. Rachinskii, N. Rebrova, E. A. Viktorov, and G. Huyet (2012). Bistable regimes in an optically injected mode-locked laser. *Optics express* 20(23), 25572–25583.
- [58] Hale, J. (1977). *Theory of functional differential equations* (Second ed.). Springer-Verlag, New York-Heidelberg. Applied Mathematical Sciences, Vol. 3.
- [59] Haus, H. (1975). Theory of mode locking with a slow saturable absorber. *IEEE Journal of Quantum Electronics* 11(9), 736–746.
- [60] Haus, H. A. (2000). Mode-locking of lasers. *IEEE Journal of Selected Topics in Quantum Electronics* 6(6), 1173–1185.
- [61] Henry, R., Z. Masoud, A. Nayfeh, and D. Mook (2001). Cargo pendulation reduction on ship-mounted cranes via boom-luff angle actuation. *Journal of Vibration and Control* 7(8), 1253–1264.
- [62] Hooton, E., Z. Balanov, W. Krawcewicz, and D. Rachinskii (2017a). Noninvasive stabilization of periodic orbits in O_4 -symmetrically coupled systems near a Hopf bifurcation point. *Internat. J. Bifur. Chaos Appl. Sci. Engrg.* 27(6), 1750087, 18.
- [63] Hooton, E., Z. Balanov, W. Krawcewicz, and D. Rachinskii (2017b). Sliding Hopf bifurcation in interval systems. *Discrete Contin. Dyn. Syst.* 37(7), 3545–3566.
- [64] Hooton, E., Q. Hu, P. Kravets, and D. Rachinskii (2018). Selective Pyragas control of Hamiltonian systems. *Discrete & Continuous Dynamical Systems - S* 12(7), 2019–2034.

- [65] Hooton, E., P. Kravets, and D. Rachinskii (2017). Restrictions to the use of time-delayed feedback control in symmetric settings. *Discrete & Continuous Dynamical Systems-B*, 859–871.
- [66] Hooton, E. W. and A. Amann (2012a). Analytical limitation for time-delayed feedback control in autonomous systems. *Physical Review Letters* 109(15), 154101.
- [67] Hooton, E. W. and A. Amann (2012b). Analytical limitation for time-delayed feedback control in autonomous systems. *Physical Review Letters* 109(15), 154101.
- [68] Ikeda, K. (1979). Multiple-valued stationary state and its instability of the transmitted light by a ring cavity system. *Optics Communications* 30(2), 257 – 261.
- [69] Ize, J. (2005). Equivariant degree. In *Handbook of topological fixed point theory*, pp. 301–337. Springer.
- [70] Ize, J. and A. Vignoli (2003). *Equivariant degree theory*, Volume 8. Walter de Gruyter.
- [71] Jaurigue, L., A. Pimenov, D. Rachinskii, E. Schöll, K. Lüdge, and A. G. Vladimirov (2015). Timing jitter of passively mode-locked semiconductor lasers subject to optical feedback: A semi-analytic approach. *Physical Review A* 92, 053807.
- [72] Jaurigue, L., A. Pimenov, D. Rachinskii, E. Schöll, K. Lüdge, and A. G. Vladimirov (2015). Timing jitter of passively-mode-locked semiconductor lasers subject to optical feedback: A semi-analytic approach. *Physical Review A* 92(5), 053807.
- [73] Jechow, A., M. Lichtner, R. Menzel, M. Radziunas, D. Skoczowsky, and A. G. Vladimirov (2009). Stripe-array diode-laser in an off-axis external cavity: Theory and experiment. *Optics Express* 17(22), 19599–19604.
- [74] Jiang, L. A., E. P. Ippen, and H. Yokoyama (2007). *Ultrahigh-Speed Optical Transmission Technology*. Springer.
- [75] Just, W., B. Fiedler, M. Georgi, V. Flunkert, P. Hövel, and E. Schöll (2007). Beyond the odd number limitation: a bifurcation analysis of time-delayed feedback control. *Physical Review E* 76, 026210.
- [76] Kaiser, R. and B. Hüttl (2007). Monolithic 40-ghz mode-locked mqw dbr lasers for high-speed optical communication systems. *IEEE Journal of Selected Topics in Quantum Electronics* 13(1), 125–135.
- [77] Kawakubo, K. (1991). *The theory of transformation groups*. Oxford University Press.
- [78] Keane, A., B. Krauskopf, and C. M. Postlethwaite (2017). Climate models with delay differential equations. *Chaos: An Interdisciplinary Journal of Nonlinear Science* 27(11), 114309.

- [79] Kevorkian, J. and J. D. Cole (1980). *Perturbation Methods in Applied Mathematics*. Springer.
- [80] Kevorkian, J. and J. D. Cole (1996). *Multiple scale and singular perturbation methods*, Volume 114 of *Applied Mathematical Sciences*. Springer-Verlag, New York.
- [81] Kielhöfer, H. (1992). Hopf bifurcation from a differentiable viewpoint. *J. Differential Equations* 97(2), 189–232.
- [82] Kozin, I., R. Roberts, and J. Tennyson (2000). Relative equilibria of D_2H^+ and H_2D^+ . *Molecular Physics* 98(5), 295–307.
- [83] Kozjakin, V. S. and M. A. Krasnosel'skii (1980). A method of parameter functionalization in the problem of bifurcation points. *Dokl. Akad. Nauk SSSR* 254(5), 1061–1064.
- [84] Krasnosel'skii, M. and A. Pokrovskii (1989). *Systems with hysteresis*. Springer.
- [85] Krasovskii, N. N. (1963). *Problems of the Theory of Stability of Motion*. (Russian), 1959 English translation: Stanford University Press.
- [86] Kravets, P., D. Rachinskii, and A. Vladimirov (2019). Periodic pulsating dynamics of slowfast delayed systems with a period close to the delay. *European Journal of Applied Mathematics* 30(1), 3962.
- [87] Krawcewicz, W. and J. Wu (1997). *Theory of degrees, with applications to bifurcations and differential equations*, Volume 17. Wiley-Interscience.
- [88] Krupa, M. (1990). Bifurcations of relative equilibria. *SIAM journal on mathematical analysis* 21(6), 1453–1486.
- [89] Kuang, Y. (1993). *Delay differential equations: with applications in population dynamics*, Volume 191. Academic press.
- [90] Kuramoto, M., N. Kitajima, H. Guo, Y. Furushima, M. Ikeda, and H. Yokoyama (2007). Two-photon fluorescence bioimaging with an all-semiconductor laser picosecond pulse source. *Optics Letters* 32(18), 2726–2728.
- [91] Kyrychko, Y. and S. Hogan (2010). On the use of delay equations in engineering applications. *Journal of Vibration and Control* 16(7-8), 943–960.
- [92] Lamb, J. S., I. Melbourne, and C. Wulff (2006). Hopf bifurcation from relative periodic solutions; secondary bifurcations from meandering spirals. *Journal of Difference Equations and Applications* 12(11), 1127–1145.
- [93] Lang, R. and K. Kobayashi (1980). External optical feedback effects on semiconductor injection laser properties. *IEEE journal of Quantum Electronics* 16(3), 347–355.

- [94] Lichtner, M., V. Z. Tronciu, and A. G. Vladimirov (2012). Theoretical investigation of striped and non-striped broad area lasers with off-axis feedback. *IEEE Journal of Quantum Electronics* 48(3), 353–360.
- [95] Lichtner, M., M. Wolfrum, and S. Yanchuk (2011). The spectrum of delay differential equations with large delay. *SIAM Journal on Mathematical Analysis* 43(2), 788–802.
- [96] Marsden, J. E. and M. McCracken (1976a). *The Hopf bifurcation and its applications*. Springer-Verlag, New York. With contributions by P. Chernoff, G. Childs, S. Chow, J. R. Dorroh, J. Guckenheimer, L. Howard, N. Kopell, O. Lanford, J. Mallet-Paret, G. Oster, O. Ruiz, S. Schechter, D. Schmidt and S. Smale, Applied Mathematical Sciences, Vol. 19.
- [97] Marsden, J. E. and M. McCracken (1976b). *The Hopf bifurcation and its applications*. Springer-Verlag, New York. Applied Mathematical Sciences, Vol. 19.
- [98] Marsden, J. E. and T. S. Ratiu (1995). Introduction to mechanics and symmetry. *Physics Today* 48(12), 65.
- [99] Masoud, Z. N., A. H. Nayfeh, and A. Al-Mousa (2003). Delayed position-feedback controller for the reduction of payload pendulations of rotary cranes. *Modal Analysis* 9(1-2), 257–277.
- [100] Masoud, Z. N., A. H. Nayfeh, and D. T. Mook (2004, Feb). Cargo pendulation reduction of ship-mounted cranes. *Nonlinear Dynamics* 35(3), 299–311.
- [101] Masoud, Z. N., A. H. Nayfeh, and N. A. Nayfeh (2005). Sway reduction on quay-side container cranes using delayed feedback controller: simulations and experiments. *Modal Analysis* 11(8), 1103–1122.
- [102] May, R. M. and R. M. Anderson (1978). Regulation and stability of host-parasite population interactions: Ii. destabilizing processes. *The Journal of Animal Ecology* 47(1), 249–267.
- [103] Mayergoyz, I. (2003). *Mathematical models of hysteresis and their applications*. Springer.
- [104] Meyer, K., G. Hall, and D. Offin (2008). *Introduction to Hamiltonian dynamical systems and the N-body problem*, Volume 90. Springer Science & Business Media.
- [105] Meyer, K. R. (1999). *Periodic solutions of the N-body problem*, Volume 1719. Springer Science & Business Media.
- [106] Mitchell, J. L. and T. W. Carr (2010). Oscillations in an intrahost model of plasmodium falciparum malaria due to cross-reactive immune response. *Bull. Mathematical Biology* 72, 590–610.

- [107] Montaldi, J. and R. Roberts (1999). Relative equilibria of molecules. *Journal of Nonlinear Science* 9(1), 53–88.
- [108] Myshkis, A. (1951). *Linear differential equations with lagged argument*. Goztekhnizdat, Moscow.
- [109] N., R. N. (1975). Kinetics of a solid-state laser with an additional moving mirror. *Soviet Journal of Quantum Electronics* 4(10), 1191–1193.
- [110] Nayfeh, A. H. (2000). *Perturbation methods*. Wiley Classics Library. Wiley-Interscience [John Wiley & Sons], New York. Reprint of the 1973 original.
- [111] New, G. H. C. (1974). Pulse evolution in mode-locked quasi-continuous lasers. *IEEE Journal of Quantum Electronics* 10(2), 115–124.
- [112] Nizette, M., D. Rachinskii, A. Vladimirov, and M. Wolfrum (2006a). Pulse interaction via gain and loss dynamics in passive mode locking. *Physica D: Nonlinear Phenomena* 218(1), 95–104.
- [113] Nizette, M., D. Rachinskii, A. Vladimirov, and M. Wolfrum (2006b). Pulse interaction via gain and loss dynamics in passive mode locking. *Physica D: Nonlinear Phenomena* 218(1), 95–104.
- [114] Orosz, G., B. Krauskopf, and R. E. Wilson (2005). Bifurcations and multiple traffic jams in a car-following model with reaction-time delay. *Physica D: Nonlinear Phenomena* 211(3-4), 277–293.
- [115] Orosz, G., R. E. Wilson, and B. Krauskopf (2004). Global bifurcation investigation of an optimal velocity traffic model with driver reaction time. *Physical Review E* 70(2), 026207.
- [116] Pekarsky, S. and J. E. Marsden (1998). Point vortices on a sphere: stability of relative equilibria. *Journal of Mathematical Physics* 39(11), 5894–5907.
- [117] Pérez-Chavela, E. and S. Rybicki (2013). Topological bifurcations of central configurations in the n-body problem. *Nonlinear Analysis: Real World Applications* 14(1), 690–698.
- [118] Pieroux, D. and T. Erneux (1996). Strongly pulsating lasers with delay. *Physical Review A* 53, 2765–2771.
- [119] Pieroux, D., T. Erneux, and K. Otsuka (1994). Minimal model of a class-b laser with delayed feedback: cascading branching of periodic solutions and period-doubling bifurcation. *Physical Review E* 50, 1822–1829.

- [120] Pimenov, A., T. Habruseva, D. Rachinskii, S. P. Hegarty, H. Guillaume, and A. G. Vladimirov (2014). Effect of dynamical instability on timing jitter in passively mode-locked quantum-dot lasers. *Optics Letters* 39, 6815–6818.
- [121] Pimenov, A., T. Habruseva, D. Rachinskii, S. P. Hegarty, G. Huyet, and A. G. Vladimirov (2014). Effect of dynamical instability on timing jitter in passively mode-locked quantum-dot lasers. *Optics Letters* 39(24), 6815–6818.
- [122] Pimenov, A., V. Z. Tronciu, U. Bandelow, and A. G. Vladimirov (2013). Dynamical regimes of a multistribe laser array with external off-axis feedback. *Journal of the Optical Society of America B* 30(6), 1606–1613.
- [123] Pimenov, A., E. A. Viktorov, S. P. Hegarty, T. Habruseva, G. Huyet, D. Rachinskii, and A. G. Vladimirov (2014). Bistability and hysteresis in an optically injected two-section semiconductor laser. *Physical Review E* 89(5), 052903.
- [124] Pimenov, A., E. A. Viktorov, S. P. Hegarty, T. Habruseva, G. Huyet, and A. G. Vladimirov (2014). Bistability and hysteresis in an optically injected two-section semiconductor laser. *Physical Review E* 89, 052903.
- [125] Puzyrev, D., A. Vladimirov, A. Pimenov, S. Gurevich, and S. Yanchuk (2017). Bound pulse trains in arrays of coupled spatially extended dynamical systems. *Phys. Rev. Lett.* 119, 163901.
- [126] Puzyrev, D., A. G. Vladimirov, S. V. Gurevich, and S. Yanchuk (2016). Modulational instability and zigzagging of dissipative solitons induced by delayed feedback. *Physical Review A* 93, 041801(R).
- [127] Pyragas, K. (1992a). Continuous control of chaos by self-controlling feedback. *Physics Letters A* 170, 421–428.
- [128] Pyragas, K. (1992b). Continuous control of chaos by self-controlling feedback. *Physics Letters A* 170, 421–428.
- [129] Pyragas, K. and A. Tamaševičius (1993). Experimental control of chaos by delayed self-controlling feedback. *Physics Letters A* 180(1-2), 99–102.
- [130] Rachinskii, D., A. Vladimirov, U. Bandelow, B. Hüttl, and R. Kaiser (2006). Q-switching instability in a mode-locked semiconductor laser. *JOSA B* 23(4), 663–670.
- [131] Rebrova, N., G. Huyet, D. Rachinskii, and A. G. Vladimirov (2011). Optically injected mode-locked laser. *Physical Review E* 83(6), 066202.
- [132] Rosenblum, M. G. and A. S. Pikovsky (2004, Mar). Controlling synchronization in an ensemble of globally coupled oscillators. *Phys. Rev. Lett.* 92, 114102.

- [133] Ruan, S. (2009). On nonlinear dynamics of predator-prey models with discrete delay. *Mathematical Modelling of Natural Phenomena* 4(02), 140–188.
- [134] Safonov, L. A., E. Tomer, V. V. Strygin, Y. Ashkenazy, and S. Havlin (2002). Multifractal chaotic attractors in a system of delay-differential equations modeling road traffic. *Chaos: An Interdisciplinary Journal of Nonlinear Science* 12(4), 1006–1014.
- [135] Schneider, I. (2013). Delayed feedback control of three diffusively coupled Stuart–Landau oscillators: a case study in equivariant Hopf bifurcation. *Philosophical Transactions of the Royal Society of London A: Mathematical, Physical and Engineering Sciences* 371, 20120472.
- [136] Schwartz, I. B. and H. L. Smith (1983). Infinite subharmonic bifurcation in an seir epidemic model. *J. Mathematical Biology* 18, 233–253.
- [137] Sieber, J., A. Gonzalez-Buelga, S. Neild, D. Wagg, and B. Krauskopf (2008). Experimental continuation of periodic orbits through a fold. *Physical review letters* 100(24), 244101.
- [138] Sivaramakrishnan, S. (2017). *Dynamics of passively coupled continuous wave and mode locked lasers*. PhD Thesis, The University of Michigan.
- [139] Slepneva, S., B. Kelleher, B. OShaughnessy, S. P. Hegarty, A. G. Vladimirov, and G. Huyet (2013). Dynamics of fourier domain mode-locked lasers. *Optics express* 21(16), 19240–19251.
- [140] Smith, H. L. (2011). *An introduction to delay differential equations with applications to the life sciences*, Volume 57. Springer New York.
- [141] Steinlein, H. (1985). Borsuk’s antipodal theorem and its generalizations and applications: A survey, méthodes topologiques en analyse non linéaire. *Sem. Math. Sup.* 95, 166–235.
- [142] STPN, G., T. INSPERGER, and R. SZALAI (2005). Delay, parametric excitation, and the nonlinear dynamics of cutting processes. *International Journal of Bifurcation and Chaos* 15(09), 2783–2798.
- [143] Sukow, D. W., M. E. Bleich, D. J. Gauthier, and J. E. Socolar (1997). Controlling chaos in a fast diode resonator using extended time-delay autosynchronization: Experimental observations and theoretical analysis. *Chaos: An Interdisciplinary Journal of Nonlinear Science* 7(4), 560–576.
- [144] Szalai, R. and G. Stépán (2006). Lobes and lenses in the stability chart of interrupted turning. *Journal of computational and nonlinear dynamics* 1(3), 205–211.

- [145] Szalai, R., G. Stpn, and S. J. Hogan (2004). Global dynamics of low immersion high-speed milling. *Chaos: An Interdisciplinary Journal of Nonlinear Science* 14(4), 1069–1077.
- [146] Taylor, M. L. and T. W. Carr (2009). An sir epidemic model with partial temporary immunity modeled with delay. *J. Mathematical Biology* 59, 841–880.
- [147] Tlidi, M., A. Vladimirov, D. Pieroux, and D. Turaev (2009). Spontaneous motion of cavity solitons induced by a delayed feedback. *Physical review letters* 103(10), 103904.
- [148] tom Dieck, T. (1987). *Transformation groups*, Volume 8. Walter de Gruyter.
- [149] Tuckerman, L. S. and D. Barkley (1990). Bifurcation analysis of the Eckhaus instability. *Physica D* 46, 57–86.
- [150] Vanderbauwhede, A., M. Krupa, and M. Golubitsky (1987). Secondary bifurcations in symmetric systems. In *Proc. Equadiff Conference*, Volume 118, pp. 709–716. Lect. Notes in Pure & Appl. Math.
- [151] Villermanx, E. (1994). Pulsed dynamics of fountains. *Nature* 371(6492), 24–25.
- [152] Villermanx, E. (1995, Dec). Memory-induced low frequency oscillations in closed convection boxes. *Phys. Rev. Lett.* 75, 4618–4621.
- [153] Visintin, A. (1994). *Differential models of hysteresis*. Springer.
- [154] Vladimirov, A. G., G. Kozyreff, and P. Mandel (2003). Synchronization of weakly stable oscillators and semiconductor laser arrays. *EPL (Europhysics Letters)* 61(5), 613.
- [155] Vladimirov, A. G., D. Rachinskii, and M. Wolfrum (2012). Modeling of passively mode-locked semiconductor lasers. In K. Lüdge (Ed.), *Nonlinear Laser Dynamics: From Quantum Dots to Cryptography*, Chapter VIII, pp. 189–222. John Wiley & Sons.
- [156] Vladimirov, A. G. and D. Turaev (2005). Model for passive mode locking in semiconductor lasers. *Physical Review A* 72(3), 033808.
- [157] Vladimirov, A. G., D. Turaev, and G. Kozyreff (2004a). Delay differential equations for mode-locked semiconductor lasers. *Optics Letters* 29(11), 1221–1223.
- [158] Vladimirov, A. G., D. Turaev, and G. Kozyreff (2004b). Delay differential equations for mode-locked semiconductor lasers. *Optics Letters* 29(11), 1221–1223.
- [159] Vladimirov, A. G. and D. V. Turaev (2004). A new model for a mode-locked semiconductor laser. *Radiophysics and Quantum Electronics* 47(10-11), 769–776.

- [160] Vladimirov, A. G., M. Wolfrum, G. Fiol, D. Arsenijevic, D. Bimberg, E. Viktorov, P. Mandel, and D. Rachinskii (2010). Locking characteristics of a 40-ghz hybrid mode-locked monolithic quantum dot laser. In *SPIE Photonics Europe*, pp. 77200Y–77200Y. International Society for Optics and Photonics.
- [161] Volterra, V. (1926). Variazioni e fluttuazioni del numero d’individui in specie animali conviventi. *Memoria della Reale Accademia Nazionale dei Lincei* 2, 31–113.
- [162] Volterra, V. (1931). *Leçons sur la théorie mathématique de la lutte pour la vie*, Volume 7. Gauthier-Villars.
- [163] Wulff, C. and M. Roberts (2002). Hamiltonian systems near relative periodic orbits. *SIAM Journal on Applied Dynamical Systems* 1(1), 1–43.
- [164] Xu, R., M. A. J. Chaplain, and F. A. Davidson (2004). Persistence and stability of a stage-structured predator-prey model with time delays. *Applied Mathematics and Computation* 150, 259–277.
- [165] Yanchuk, S., K. R. Schneider, and L. Recke (2004). Dynamics of two mutually coupled semiconductor lasers: instantaneous coupling limit. *Physical Review E* 69(5), 056221.
- [166] Yanchuk, S. and J. Sieber (2013). Relative equilibria and relative periodic solutions in systems with time-delay and S^1 symmetry. *arXiv preprint arXiv:1306.3327*.
- [167] Yanchuk, S. and M. Wolfrum (2006). Eckhaus instability in systems with large delay. *Physical Review Letters* 6, 220201.
- [168] Yanchuk, S. and M. Wolfrum (2010). A multiple time scale approach to the stability of external cavity modes in the lang-kobayashi system using the limit of large delay. *SIAM Journal on Applied Dynamical Systems* 9(2), 519–535.

BIOGRAPHICAL SKETCH

Pavel Kravets was born in 1991 in Samara, Russia. In 2012, he graduated from Samara State Aerospace University (SSAU) and received a BS *cum laude* in Applied Mathematics and Computer Science. In 2014, he also received a MS *cum laude* in Applied Mathematics and Computer Science from SSAU. The same year Pavel joined a PhD program in Mathematics at The University of Texas in Dallas where he successfully passed qualifying exam in 2016 and started working under the supervision of Professor Dmitry Rachinskiy. Pavel's research interests include Dynamical Systems, Differential Equations and Applied Mathematical Modeling.

CURRICULUM VITAE

Pavel Kravetc

• Education

- 2019 **PhD**, Mathematics, University of Texas at Dallas, Texas, USA
- MS**, Applied Mathematics and Computer Science, Samara State Aerospace University, Russia
- 2014 Thesis: "Hopf bifurcation in three-dimensional epidemiological model", advisor Dr. Vladimir Sobolev, hsablem@gmail.com
- BS**, Applied Mathematics and Computer Science, Samara State Aerospace University, Russia
- 2012 Thesis: "On one model of enzyme substrate inhibition", advisor Dr. Vladimir Sobolev, hsablem@gmail.com

• Fields of Interest

Mathematical Modeling, Applied Dynamical Systems, Nonsmooth Dynamics, Symmetries, Delay Differential Equations, Stabilization, Control

• Publications

- [1] Z. Balanov, P. Kravetc, W. Krawcewicz, and D. Rachinskii. Equivariant degree method for analysis of hopf bifurcation of relative periodic solutions: Case study of a ring of oscillators. *Journal of Differential Equations*, 265(9):4530 – 4574, 2018. <https://doi.org/10.1016/j.jde.2018.06.014>.
- [2] Z. Balanov, P. Kravetc, W. Krawcewicz, D. Rachinskii, and H. Wu. Hopf bifurcation of relative periodic solutions in a system of five passively mode-locked lasers. *Journal of Nonlinear and Variational Analysis*, 2(2):233–262, 2018. <https://doi.org/10.23952/jnva.2.2018.2.10>.
- [3] N. Begun, P. Kravetc, and D. Rachinskii. Chaos in saw map. *International Journal of Bifurcation and Chaos*, 29(02):1930005, 2019. <https://doi.org/10.1142/S0218127419300052>.
- [4] O. Gendelman, P. Kravetc, and D. Rachinskii. Mixed global dynamics of forced vibro-impact oscillator with Coulomb friction. *Chaos: An Interdisciplinary Journal of Nonlinear Science*, Submitted. arXiv preprint <https://arxiv.org/abs/1903.06231>.
- [5] E. Hooton, Q. Hu, P. Kravetc, and D. Rachinskii. Selective Pyragas control of Hamiltonian systems. *Discrete & Continuous Dynamical Systems - S*, 12(7):2019–2034, 2018. <https://doi.org/10.3934/dcdss.2019130>.
- [6] E. Hooton, P. Kravetc, and D. Rachinskii. Restrictions to the use of time-delayed feedback control in symmetric settings. *Discrete & Continuous Dynamical Systems - B*, 23:543, 2018. <https://doi.org/10.3934/dcdsb.2017207>.

- [7] P. Kravets, D. Rachinskii, and A. Vladimirov. Periodic pulsating dynamics of slowfast delayed systems with a period close to the delay. *European Journal of Applied Mathematics*, page 124, 2017. <https://doi.org/10.1017/S0956792517000377>.

• Conferences

- talk **Periodic solutions in systems of delay-differential equations with symmetries**, *August 13-14, 2018*, Advanced Summer School on Continuation Methods for Nonlinear Problems, University of Illinois at Urbana-Champaign
- poster **Periodic solutions of delay-differential equations with applications to lasers, population dynamics and control**, *July 15-19, 2018*, Summer School in Applied Mathematics: The complex math of the real world, Technion, Israel Institute of Technology
- talk **Relative periodic solutions in systems of coupled lasers**, *June 12-15, 2017*, International Conference on Topological Nonlinear Analysis, University of Guangzhou
- talk **Traveling waves in a chain of excitable switches**, *June 6-10, 2016*, School/Workshop on Applicable Theory of Switched Systems, The University of Texas at Dallas
- poster **Formation of pulses through a cascade of Hopf bifurcations in population models with delay**, *November 6-8, 2015*, TexAMP 2015, The University of Texas at Dallas

• Awards

- 2017 **Outside Teaching Assistant of the Year**, Department of Mathematical Sciences, The University of Texas at Dallas

• Work Experience

- Software Engineer**, NetCracker Corp., Samara, Russia
www.netcracker.com
September 2011 – November 2012 NetCracker Corporation is an international company that develops OSS/BSS systems for first-tier providers such as Sprint, Deutsche Telekom and others. My duties included bug fixing and various development tasks for one interlayer module which provides business logic for order processing.
- Software Engineer**, SEC Smart Solutions, Samara, Russia
www.smartsolutions-123.ru
February 2013 – June 2014 Design and development of distributed train scheduling system for Russian Railways. My duties included implementation of complex algorithms for schedule optimization and developing both back-end and front-end of the system.

• Teaching Experience

Teaching Assistant, Department of Mathematical Sciences, UTD

Fall 2014 MATH 2420 Differential Equations with Applications
Spring 2015 MATH 2419 Calculus II (Honors and Cohort)
Fall 2015 MATH 2417 Calculus I
Fall 2015 MATH 4341 Topology (grading)
Spring 2016 MATH 2419 Calculus II (Honors and Cohort)
Spring 2016 MATH 2312 Precalculus (grading)
Summer 2016 MATH 2420 Differential Equations with Applications
Fall 2016 MATH 2417 Calculus I Honors
Spring 2017 MATH 1325 Applied Calculus (grading)
Spring 2018 MATH 6302 Functional Analysis I (grading)
Spring 2019 MATH 2418 Linear Algebra (2 sections including Honors)
Summer 2019 MATH 2418 Linear Algebra

Teaching Associate, Department of Mathematical Sciences, UTD

Fall 2016 MATH 2313 Precalculus
Spring 2017 MATH 1325 Applied Calculus I
Fall 2017 MATH 1326 Applied Calculus II
Spring 2018 MATH 2414 Integral Calculus
Fall 2018 MATH 1314 College Algebra

• Misc

membership **SIAM**, Society of Industrial and Applied Mathematics, UT Dallas and SMU Student Chapter

group leader **Mathematical Sciences Department Teaching Assistants Training Workshop**, The University of Texas at Dallas, August 14-18, 2017